Two-Body Correlations in Nuclear Systems

H. Müther

Institut für Theoretische Physik,
Universität Tübingen, Tübingen, Germany

A. Polls

Departament d'Estructura i Constituents de la Matèria
Universitat de Barcelona, E-08028 Barcelona, Spain

February 8, 2008

Abstract

Correlations in the nuclear wave-function beyond the mean-field or Hartree-Fock approximation are very important to describe basic properties of nuclear structure. Various approaches to account for such correlations are described and compared to each other. This includes the hole-line expansion, the coupled cluster or "exponential S" approach, the self-consistent evaluation of Greens functions, variational approaches using correlated basis functions and recent developments employing quantum Monte-Carlo techniques. Details of these correlations are explored and their sensitivity to the underlying nucleon-nucleon interaction. Special attention is paid to the attempts to investigate these correlations in exclusive nucleon knock-out experiments induced by electron scattering. Another important issue of nuclear structure physics is the role of relativistic effects as contained in phenomenological mean field models. The sensitivity of various nuclear structure observables on these relativistic features are investigated. The report includes the discussion of nuclear matter as well as finite nuclei.

1   Introduction

One of the central challenges of theoretical nuclear physics is the attempt to describe the basic properties of nuclear systems in terms of a realistic nucleon-nucleon (NN) interaction. Such an attempt typically contains two major steps. In the first step one has to consider a specific model for the NN interaction. This could be a model which is inspired by the quantum-chromo-dynamics[1], a meson-exchange or One-Boson-Exchange model[2, 3] or a purely phenomenological ansatz in terms of two-body spin-isospin operators multiplied by local potential functions[4, 5]. Such models are considered as a realistic description of the NN interaction, if the adjustment of parameters within the model yields a good fit to the NN scattering data at energies below the threshold for pion production as well as energy and other observables of the deuteron.

After the definition of the nuclear hamiltonian, the second step implies the solution of the many-body problem of A nucleons interacting in terms of such a realistic two-body NN interaction. The simplest approach to this many-body problem of interacting fermions one could think of would be the mean field or Hartree-Fock approximation. This procedure yields

very good results for the bulk properties of nuclei, binding energies and radii, if one employs simple phenomenological NN forces like e.g. the Skyrme forces, which are adjusted to describe such nuclear structure data[6]. However, employing realistic NN interactions the Hartree-Fock approximation fails very badly: it leads to unbound nuclei[7].

This failure of the Hartree-Fock approximation is a consequence of the strong short-range components of a realistic NN interaction, which are necessary to describe the NN data. The Hartree-Fock wavefunction describes the nucleus as a system of nucleons moving independent from each other in a mean field derived from the average interaction with all other nucleons. This implies that the wavefunction contains large amplitudes of configurations, in which two nucleons are so close to each other, that they are exposed to the very repulsive components of the NN interaction at short distances. The hard-core potentials[8], which were very popular in the sixties, describe these components in terms of an infinitely repulsive core for relative distances smaller than the radius of this hard core of about $0.4\ fm$. In this case a Hartree-Fock calculation would even yield an infinite repulsive energy. Modern models for the NN interaction, in particular the meson-exchange models which lead to non-local NN interactions, contain softer cores. Nevertheless, a careful treatment of two-body short range correlations beyond the mean field approximation is indispensable to describe the structure of nuclei in terms of realistic NN interactions. The same is true for the correlations which are induced by the strong tensor components in the NN interaction, which mainly originate from the pion exchange contributions.

Various different tools have been developed to account for such correlation effects. Below we will describe some of these methods including the Brueckner hole-line expansion[9, 10, 11], the coupled cluster or "exponential S" approach[12, 13], the self-consistent evaluation of Greens functions[14], variational approaches using correlated basis functions[15, 16, 17] and recent developments employing quantum Monte-Carlo techniques[18, 19].

Using such methods one obtains correlated many-body wave functions, which are rather sensitive to the NN interaction under consideration. Therefore the question arises which kind of experimental observables might be considered to investigate details of these correlations. The hope is that different predictions derived from the various model of the NN interaction will allow to distinguish between the various model for the NN interaction at short distances. Therefore, finally such nuclear structure studies will help to explore the details of the strong baryon baryon interaction at short distances.

What is the effect of correlations on the nuclear wave function? In order to discuss this question let us consider for the moment a system of infinite nuclear matter. The mean field or Hartree-Fock wave function of nuclear matter corresponds to the Slater determinant of plane wave states, in which all single-particle states with momenta below the Fermi momentum k_F are occupied. Correlations on top of this Hartree-Fock state will yield a depletion of single-particle states with momenta k below k_F and a non-vanishing occupation of states with high momentum. From this consideration one may think that the study of high-momentum components in the single-particle wave functions of nuclear states might be an ideal tool to explore correlation effects in the nuclear wave function. Therefore it has been suggested to study these high-momentum components by means of exclusive single nucleon knock-out experiments like $(e, e'N)$ with the $(A - 1)$ nucleus remaining in the ground state or other well defined state[20, 21]. However, a detailed analysis of the spectral function for such knock-out experiments shows that the expected high-momentum components in the nuclear wavefunction could only be observed at high missing energies, i.e. with an excitation energy of the residual target nucleus well above the threshold for the emission of a secondary nucleon[22, 23, 24]. Therefore one expects exclusive two-nucleon knock-out experiments like (γ, NN) or $(e, e'NN)$[25, 26] to be more sensitive to the effects of correlations. Details for the analysis of such nucleon knock-out experiments induced

by inelastic electron scattering will be given below.

Up to this point we merely discussed the nuclear system within the framework of the non-relativistic quantum many-body theory. At first sight this seems to be well justified since the binding energies of nuclei with single-particle potentials of -50 MeV or so, are very small on the scale of the nucleon rest mass. It has already been discussed, however, that the short-range components of the NN interaction are very strong with large repulsive components, which are compensated by strong attractive ones. Within the meson-exchange model for the NN interaction the repulsive components are generated by the exchange of the ω, a vector meson, while the attractive parts are described in terms of the exchange of a scalar particle, the σ meson[2]. This σ meson does not represent a meson in the usual sense but its exchange is used to describe the correlated two-pion exchange without and with intermediate excitation of the interacting nucleons[27, 28]. Calculating the nucleon self energies from such a meson exchange model within a Hartree approximation, one finds that the ω exchange yields a component Σ_0, which transforms under a Lorentz transformation like the time-like component of a vector, while the scalar meson exchange yields a contribution Σ_s, which transforms like a scalar. Inserting this self energy into the Dirac equation for a nucleon in the medium of nuclear matter leads to binding effects which are as small as the -50 MeV discussed above. This small binding effect, however, results from a strong cancellation between the repulsive Σ_0 and the attractive Σ_s component. The attractive scalar component Σ_s leads to Dirac spinors for the nucleons in the nuclear medium, which contain a small component significantly enhanced as compared to the Dirac spinor of a free nucleon. This effect is often described in terms of an effective Dirac mass m^* for the nucleon, which can be of the order of 600 MeV in nuclear matter around saturation density.

This modification of the Dirac spinors in the nuclear medium requires a self-consistent evaluation of the matrix elements of the meson exchange interaction. Within the phenomenological $\sigma - \omega$ or Walecka model of nuclear physics[29, 30] it is this self-consistency, which provides the saturation of nuclear matter. This relativistic effect, however, is also observed in Dirac-Brueckner-Hartree-Fock studies, which are based on realistic NN interactions[31, 32, 33, 34]. Including these relativistic features improves the predictions for the saturation point of nuclear matter as well as the bulk properties of finite nuclei significantly[35, 36, 37, 38]. The question is: Are there other observables, which are sensitive to the enhancement of the small component of the nucleon Dirac spinors in the nuclear medium?

The calculation scheme discussed so far, determine the interaction of two nucleons in the vacuum in a first step and then solve the many-body problem of nucleons interacting by such realistic potentials in a second step, is of course based on the picture that nucleons are elementary particles with properties, which are not affected by the presence of other nucleons in the nuclear medium. One knows, of course, that this is a rather simplified picture: nucleons are built out of quarks and their properties might very well be influenced by the surrounding medium. A cartoon of this feature is displayed in Fig. 1. So the question is, how important are the sub-nucleonic degrees of freedom, must we expect a change of the nucleon properties in the nuclear medium? At low energies it might be sufficient to account for the internal structure of the nucleons by considering the possibility that the nucleon may get excited to the $\Delta(3,3)$ excitation at 1232 MeV. It has been demonstrated[39] that the process of two interacting nucleons, which polarize each other to such isobar excitations are an important ingredient to the medium range attraction of the NN interaction. Attempts have been made to account for such isobar excitations also in microscopic studies of nuclear structure[40, 41].

Furthermore, not only the basic properties of the nucleons, their mass or electromagnetic form-factor might be affected by the nuclear medium, also the masses and thereby the propagation of the mesons might be modified as well[42, 43, 44]. This will have consequences for the
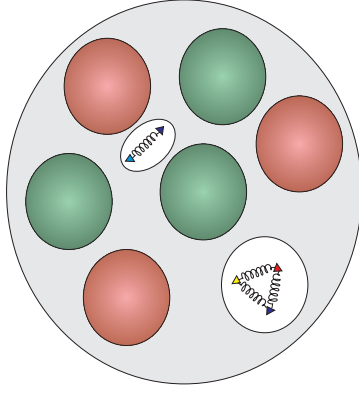
Figure 1: Cartoon of a nucleus, displaying the size of the nucleons as compared to the typical distance to nearest neighbors. Also indicated are the internal structure of nucleons and mesons.
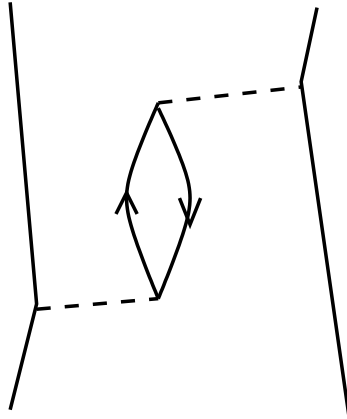

Figure 2: Two nucleons interacting in a nuclear medium, see discussion in the text.

meson-exchange model of the NN interaction. For example, a lowering of the meson masses in the nuclear medium as compared to the vacuum would lead to a larger range of the corresponding meson exchange interaction terms, which should lead to different results in the nuclear structure calculation.

In studying such features of sub-nucleonic degrees of freedom, however, one should be careful to avoid the mixing of different points of view on the same process. As an example, let us consider a process like the one indicated by the diagram in Fig. 2: Two nucleons, represented by the two upward going lines, interact with each other by the exchange of e.g. a pion, which is represented by the dashed line. Propagating in a nuclear medium between these two nucleons, the pion may interact with a third nucleon leading to an intermediate particle-hole excitation of the nuclear system. Such processes might be considered as a modification of the pion propagator in the nuclear medium, which could be characterized by a modification of the effective pion mass inside a nucleus. The process displayed in Fig. 2, however, will also be included in any many-body calculation based on two-nucleon interactions, which accounts for three-nucleon correlations or includes effects of ring diagrams. Therefore effects which one may identify with a modification of meson propagators are accounted for in an approach, which does not even

mention any mesonic degrees of freedom.

The pion re-scattering process displayed in Fig. 2 may also lead to an excitation of the intermediate nucleon to e.g. the Δ resonance. Again such terms might be considered as a modification of the meson propagator. Such terms would also be accounted for in a many-body theory based on baryon - baryon interactions, like e.g. the Argonne V28[45], which includes the Δ degrees of freedom explicitly. Within the framework of a many-body theory which does not account for such Δ excitations, such a process might be taken into account by means of a three-nucleon interaction. This example has been given to demonstrate the model dependence of three-body forces or statements about the relevance of mesonic degrees of freedom. The approaches which we will discuss throughout this review, are all based on realistic NN interactions and try to solve the many-body problem as good as possible. It is the aim to study how far such an approach, which ignores all sub-nucleonic degrees of freedom, can predict the properties of nuclear systems at zero temperature and without external pressure. Remaining discrepancies between theoretical prediction and empirical data can then bet attributed to the necessity to account for sub-nucleonic degrees of freedom, explicitly.

Such many-body calculations can then also be used to obtain predictions for nuclear matter under extreme conditions like in neutron stars, supernova explosions[46] or in central heavy ion collisions. They yield a prediction for the equation of state of nuclear matter at high densities and/or high temperatures which is free of any parameters. The success or failure of such theoretical calculations in predicting the properties of normal nuclear matter from the NN interactions of two nucleons in the vacuum can be used to judge the reliability of these predictions for nuclear matter at extreme conditions.

Nuclear systems provide an intriguing and challenging object for the development of quantum many-body theories. The underlying NN interaction is non-trivial: It contains a rich operator structure with strong tensor components and is in general non-local. The interacting particles must be considered as quasiparticle and the inclusion of internal degrees of freedom might get important. An extension of the many-body theory to account for relativistic effects might be necessary. Empirical data are available and should be reproduced for finite systems with particle numbers ranging from $A = 2$ to infinite nuclear matter. For other systems of condensed matter or Fermi liquids, like electron gas or liquid Helium 3, reliable data on finite samples are difficult to obtain but of high interest. Therefore nuclei are an ideal testing ground for many-body theory for finite systems in particular. The experience collected here should be rather useful in the study of other systems.

After this introduction, we will present an outline of some many-body approaches which are used in nuclear physics. This includes the Brueckner - Bethe hole-line expansion, the coupled cluster or "exponential S" approach, the self-consistent evaluation of Greens functions, variational approaches using correlated Jastrow-type basis functions and variational and quantum Monte Carlo techniques. A short review on the status of realistic NN interactions and on the differences between those models will be given in the first part of section 3. This section 3 also contains the discussion of results for bulk properties of infinite nuclear matter and finite nuclei. As an example on experimental efforts to explore the effects of correlations in detail, we will report on the analysis of inelastic electron scattering in section 4. The section 5 describes attempts to extend the many-body theory to account for relativistic features as well as the sensitivity of some observables to these relativistic effects.
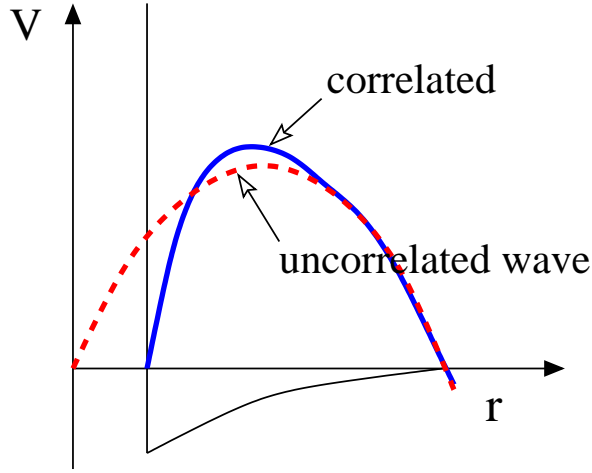
2   Many-Body Approaches

Figure 3: Schematic picture of a NN interaction with hard core and its effect on the correlated NN wave function $\Psi(r)$.

2.1 *Hole - Line Expansion*

As it has been discussed already above one problem of nuclear structure calculations based on realistic NN interactions is to deal with the strong short-range components contained in all such interactions. This problem is evident in particular when so-called hard-core potentials are employed, which are infinite for relative distances smaller than the radius of the hard core r_c. The matrix elements of such a potential V evaluated for an uncorrelated two-body wave function $\Phi(r)$ diverges since $\Phi(r)$ is different from zero also for relative distances r smaller than the hard-core radius r_c (see the schematic picture in Fig. 3. A way out of this problem is to account for the two-body correlations induced by the NN interaction in the correlated wave function $\Psi(r)$ or by defining an effective operator, which acting on the uncorrelated wave function $\Phi(r)$ yields the same result as the bare interaction V acting on $\Psi(r)$. This concept is well known for example in dealing with the scattering matrix T, which is defined by

$$< \Phi|T|\Phi >=< \Phi|V|\Psi > \ . \tag{1}$$

As it is indicated in the schematic Fig. 3, the correlations tend to enhance the amplitude of the correlated wave function Ψ relative to the uncorrelated one at distances r for which the interaction is attractive. A reduction of the amplitude is to be expected for small distances for which $V(r)$ is repulsive. From this discussion we see that the correlation effects tend to make the matrix elements of T more attractive than those of the bare potential V. For two nucleons in the vacuum the T matrix can be determined by solving a Lippmann-Schwinger equation

$$
\begin{aligned}
T|\Phi > &= V\left\{|\Phi > +\frac{1}{\omega - H_0 + i\epsilon}V|\Psi >\right\} \\
&= \left\{V + V\frac{1}{\omega - H_0 + i\epsilon}T\right\}|\Phi > \ .
\end{aligned} \tag{2}
$$

In these equations the starting energy ω stands for the energy of the two interacting nucleons and H_0 represents the operator for the nucleons in the intermediate state without residual interaction, i.e. the kinetic energy.

This concept of an effective operator accounting for correlation effects in the wave function is one way to present the Brueckner-Bethe-Goldstone (BBG) approach to the many-body problem.

To show the features of the BBG approach, we consider the nuclear hamiltonian, a sum of the kinetic energy t_{kin} and the two-body interaction V, and introduce an appropriate single-particle potential U

$$H = H_0 + H_1, \qquad H_0 = t_{kin} + U, \qquad H_1 = V - U. \tag{3}$$

The eigenstates of H_0 for A particles, i.e. Slater determinants build from the corresponding single-particle wavefunctions, provide a basis of the Hilbert-space for the A nucleon problem

$$H_0 \Phi_i(1, \dots, A) = E_i^0 \Phi_i(1, \dots, A), \tag{4}$$

with E_i^0 the sum of the single particle energies. This basis Φ_i is used to split the Hilbert-space into a model space and the rest. If one is interested in the ground-state properties of closed shell nuclei like ^{16}O this model space could be defined by a single Slater determinant. If one is interested in the states of open shell nuclei at low energies, this model space could consist out of those functions Φ_i which represent a typical set of basis states for a shell-model configuration mixing calculation[47]. The concept of a model space, however, can also be considered for the system of infinite nuclear matter. One may choose the model space to contain all Slater determinants, which can be constructed by considering occupied states with momenta below a model space momentum k_M. If this momentum k_M is equal to the Fermi momentum of a free Fermi gas k_F of the density considered, the model space reduces just to this model wave function[48]. With this choice for a model space one can define projection operators $\mathcal{P}$ and $\mathcal{Q}$, which project onto the model space and on the rest of the A-nucleon Hilbert space, respectively. It is the aim to derive an effective hamiltonian H_{eff}, which is defined within the model space, with eigenvalues E_i identical to the eigenvalues of the original hamiltonian H and eigenvectors, which are just the projection of the exact eigenvectors Ψ_i of H on the model space. This implies that

$$\mathcal{P} H_{eff} \mathcal{P} \Psi_i = E_i \mathcal{P} \Psi_i. \tag{5}$$

With this separation of the Hilbert-space into a model space and a rest also the treatment of correlations is separated: There are correlations which can be represented by degrees of freedom within this model space. They are treated explicitly and accounted for by the diagonalization of the effective hamiltonian H_{eff} (see Eq. (5)) within the model-space. This will typically be correlations which are described in terms of single-particle excitations around the Fermi energy with low excitation energy, small momentum transfers and therefore of longer range. These long range correlations are quite sensitive to the shell structure of finite systems and will therefore be different for nuclear matter and specific finite nuclei. The correlations, which cannot be represented by the mixing of configurations within the model space are treated by means of the effective operator. Such correlations include excitations up to states high above the Fermi surface. This implies large excitation energies and high momentum transfers, which means correlations of short range.

Several expansions have been formulated for this effective hamiltonian. There are the energy-dependent expansions of Feshbach [49] and of Bloch and Horowitz [50]. They correspond to the Brillouin - Wigner perturbation expansion and therefore yield an effective hamiltonian which depends on the exact energy to be calculated. To get rid of this energy-dependence in the case of multi-dimensional degenerate model-spaces one has to consider the so-called folded diagram expansion, which has been formulated e.g. by Brandow [51] and Kuo, Lee and Ratcliff [52]. Using this folded-diagram formulation, the effective hamiltonian could be written as

$$H_{eff} = H_0 + H_1 + \left\{ H_1 \frac{\mathcal{Q}}{E^0 - H_0} H_{eff} + \text{folded diagrams} \right\}_{\text{linked}}, \tag{6}$$

with E^0 referring to the eigenvalue of H_0 for the state in the model space considered.
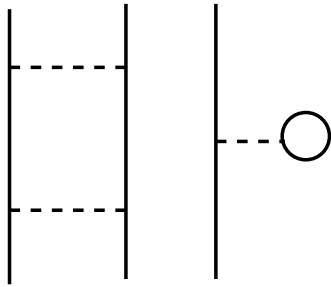
Figure 4: Example of an unlinked diagram, which should be ignored in the expansion of H_{eff} in Eq. (6)

Note that in this expansion one only needs to consider the contribution of the so-called linked diagrams. This implies that contributions like the one characterized by the diagram in Fig. 4 can be ignored. Such unlinked contributions contain products of matrix elements of H_1 (the two-body parts are represented by the dashed lines in Fig. 4), which are completely unlinked in the sense that the summation over single-particle quantum numbers of the states attached to the matrix elements of H_1 are completely disconnected. Translated into the representation of diagrams this means that the corresponding diagram can be separated into two pieces without cutting a solid or dashed line, representing the propagation of a nucleon and an interaction, respectively. This restriction to linked diagram contribution is of particular importance for systems with many particles, like e.g. infinite nuclear matter. Unlinked contributions, which represent a combination of processes which are independent from each other, diverge in the limit of particle number to infinity. Details on the definition and on techniques to evaluate the contribution of folded diagrams can be found in [51, 52, 53, 54, 55]. Folded diagrams do not occur if the model space is of dimension one, an assumption, which is most commonly made in calculating ground-state properties of closed shell nuclei or infinite nuclear matter.

From the expansion in Eq. (6) it is obvious that H_{eff} will not only contain one-body and two-body operators but, in general, also operators involving three and more nucleons. If, however, we restrict the discussion to the evaluation of ground-state properties and consider only the effective two-body operators in H_{eff}, the expansion is reduced to the summation of ladder diagrams and one obtains the Bethe-Goldstone equation

$$G(\omega) = V + V \frac{Q}{\omega - h_{12}} G \,, \tag{7}$$

which defines an effective NN interactions of two nucleons. Note that the projection operator on many-body states $\mathcal{Q}$ outside the model space in (6) has been replaced by the Pauli operator Q, which is a two-body operator defined by

$$Q|ij> = \begin{cases} |ij> & \text{if i and j are single-particle unoccupied in } \Phi \\ 0 & \text{else} \end{cases} \,, \tag{8}$$

with Φ referring to the Slater-determinant defining the model-space. The energy denominator in (7) corresponds to the excitation energy of the intermediate two-particle two-hole state, i.e. it is the sum of the single-particle energies for the interacting nucleons in states below the Fermi energy, expressed by the starting energy ω minus the energy of the two nucleons in the intermediate states above the Fermi energy, denoted by the operator h_{12}. (See also the graphical representation in Fig. 5)

The Bethe-Goldstone equation (7) is quite similar to the Lippmann-Schwinger Eq. (2) for the scattering matrix T. The only differences are the Pauli operator Q and the energy denominator which in (7) is defined in terms of single-particle energies of the many-body system instead of the kinetic energies in Eq. (2). Therefore the solution of the Bethe-Goldstone equation, the G-matrix, corresponds to an effective interaction between two nucleons, which accounts for correlation effects in the nuclear medium. Similar to Eq. (1) one can define for each product wave function of two uncorrelated single-particle wave functions $|\phi_{\alpha\beta} >$ a correlated wave function $|\psi_{\alpha\beta} >$ by

$$
\begin{aligned}
G|\phi_{\alpha\beta} > &= V|\psi_{\alpha\beta} > \\
&= V\left\{1 + \frac{Q}{\omega - h_{12}}G\right\}|\phi_{\alpha\beta} >,
\end{aligned}
\tag{9}
$$

which implies that the correlated wave function $|\psi_{\alpha\beta} >$ can be identified with

$$
|\psi_{\alpha\beta} >= |\phi_{\alpha\beta} > + \frac{Q}{\omega - h_{12}}G|\phi_{\alpha\beta} >
\tag{10}
$$

The second term on the right hand side of this equation, the difference between the correlated and uncorrelated wave function, is called the defect function. If the uncorrelated state refers to two single-particle states α and β below the Fermi surface, the difference between the starting energy $\omega = \epsilon_\alpha + \epsilon_\beta$ (ϵ_α denoting the single-particle energies of H_0) and the eigenvalue of h_{12} is negative for all intermediate states, which are restricted to two-particle states above the Fermi surface. This means that the summation or integration over intermediate particle states does not meet any pole in the propagators of (9) or (10). This implies that the matrix elements of G are real. There exist not phase shifts between the uncorrelated and the correlated wave function, the defect function vanishes for large relative distances. This vanishing of the defect function at large r is called the healing property, the correlated wave functions "heals" to the uncorrelated one at large r.

One of the main points of the Brueckner-Bethe-Goldstone approach to the many-body system is to evaluate the contributions to the effective hamiltonian H_{eff} in Eq. (6) not in a perturbation expansion in which the contributions are ordered with respect to the numbers of bare interaction V terms, but in terms of the G-matrix.

Up to this point we have not specified yet, how to choose the unperturbed hamiltonian H_0 or the single-particle potential U in Eq. (3). The aim is of course to choose H_0 such that the Slater determinant Φ defining the model space is close to the exact wavefunction for the ground-state. Therefore it seems quite natural to define the single-particle potential U in analogy to the Hartree-Fock definition with the bare interaction V replaced by the corresponding G-matrix. To be more precise, the Brueckner-Hartree-Fock (BHF) definition of U is given by

$$
< \alpha|U|\beta >= \begin{cases} \sum_{\nu \leq F} < \alpha\nu|\frac{1}{2}\left(G(\omega_{\alpha\nu}) + G(\omega_{\beta\nu})\right)|\beta\nu >, & \text{if } \alpha \text{ and } \beta \leq F \\ \sum_{\nu \leq F} < \alpha\nu|G(\omega_{\alpha\nu})|\beta\nu >, & \text{if } \alpha \leq F \text{ and } \beta > F \\ 0 & \text{if } \alpha \text{ and } \beta > F, \end{cases}
\tag{11}
$$

In this definition $\alpha \leq F$ refers to single-particle states α below the Fermi surface and the starting energies in calculating G are defined by $\omega_{\alpha h} = \epsilon_\alpha + \epsilon_h$ using the single-particle energies

$$
\epsilon_\alpha =< \alpha|t_{kin} + U|\alpha > .
\tag{12}
$$

For matrix elements of U involving hole states states, i.e. $< \alpha|U|\beta >$ with α and/or $\beta \leq F$, it can be shown by a theorem of Bethe, Brandow and Petschek (BBP)[56], that the on-shell
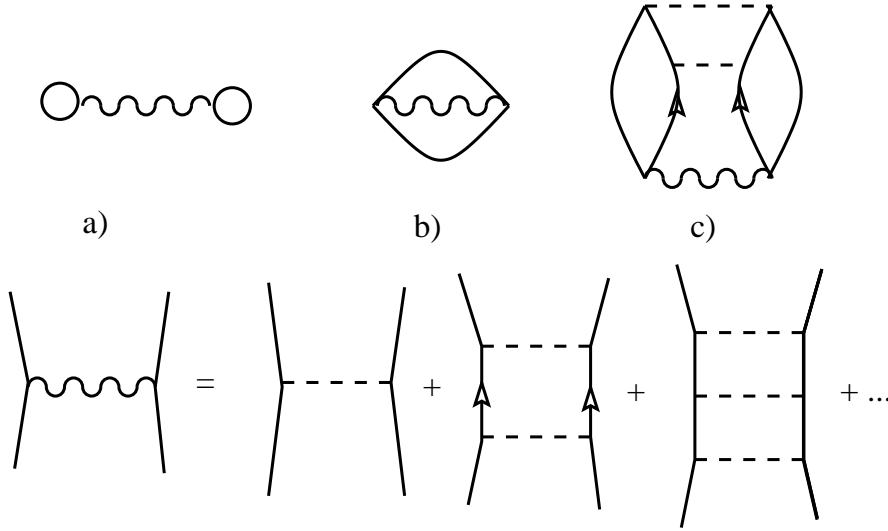
Figure 5: The upper half of this figure displays Goldstone diagrams, which are are included in the calculation of the ground-state energy within the BHF approximation (13). Diagram a) corresponds to the direct, b) to the Fock-exchange contribution. The wiggly lines represent the G matrix and the lower half of the figure visualizes the Bethe-Goldstone Eq. (7) demonstrating that the G interaction line represents the sum of all particle-particle ladder diagrams. This implies that e.g. the Goldstone diagram displayed in c) is redundant as it is contained already in a).

definition of the starting energy in the BHF choice for U (11) yields an exact cancellation of many diagrams of higher order in G. The BBP theorem cannot be applied to the particle-particle matrix elements of U (α and $\beta > F$). Therefore the choice $U = 0$ for particle states, the so-called conventional choice, has been favored in many BHF calculations.

Looking at the Eqs. (7), (11) and (12), which define the BHF approach, one can see that these equations request the solution of a self-consistency problem: in order to solve the Bethe-Goldstone equation (7) one has to know the single-particle states $|\alpha >$ and single-particle energies ϵ_α, to define the Pauli operator Q and starting energies, respectively. On the other hand, one should know the G-matrix already to determine the single-particle states and energies by diagonalizing $t_{kin} + U$. This self-consistency requirement goes beyond the usual self-consistency requirement, which request the knowledge of the hole states to define U. A self-consistent solution of the BHF equations can be obtained by solving the Bethe-Goldstone equation and the Hartree-Fock equation in an iteration scheme. After the self-consistency has been achieved, it is easy to calculate the total energy by

$$E_{BHF} = \frac{1}{2} \sum_{\nu \leq F} t_\nu + \epsilon_\nu \ , \tag{13}$$

the sum of single-particle energies ϵ_ν and the expectation value of the kinetic energy t_ν for the single-particle wave functions of the hole states. Goldstone diagrams representing this approximation for the energy are displayed in Fig. 5. Results for other observables like e.g. the radius of the mass or charge-distribution are usually determined by simply calculating the expectation value of the corresponding operator for the model space Slater determinant Φ. Strictly speaking one should derive an effective operator also for such observables, which account for the restriction of the complete Hilbert space to the model space.

The optimal choice of H_0 to be used for the particle states in the BHF definition of U, and consequently also the h_{12} in the Bethe-Goldstone equation, has widely been discussed in particular for the case of nuclear matter calculations [57, 48]. Good arguments have been presented to favor a single-particle spectrum which is continuous at the Fermi surface and therefore contains an attractive potential for the low-lying particle states [48] or all particle states [57]. The answer to the questions, which is the optimal choice, can only be obtained by evaluating the contributions of higher order correction and their sensitivity to the choice of U.

So before we can answer the question, how to choose U in an optimal way, we should discuss, how to go beyond the BHF approximation, which is also often called the lowest order Brueckner theory. The total energy is calculated in the BHF approximation (see Eq. (13)) by taking into account the contribution of all ladder diagrams with any number of intermediate two-particle states, which are summed up in the G-matrix. This means that all diagrams with two hole lines are taken into account. The first step beyond this two-hole line approach would be to include the contributions of all linked diagrams with three hole lines. This ordering with respect to the number of hole lines, which is the basic assumption of the hole line expansion, can be justified with the following argument: Linked diagrams including n hole lines describe processes, in which n nucleons are interacting in a coherent way. This means that all n nucleons should be within a volume that they can all interact with each other. If the range of the strong interaction r_V is smaller than the average distance to the next neighbor d_N, the probability that $n + 1$ nucleons are found within a volume of mutual interaction is smaller than the corresponding probability for n nucleons by a factor $(r_V/d_N)^3$. In nuclear matter around saturation density, the average distance to the next neighbor d_N is around 1.8 fm, which is larger than range of the strong short-range components of the NN interaction (the radius of a hard core is around 0.4 fm, the range for the exchange of an ω meson, $\hbar/\mu c$, corresponds to 0.26 fm), however, comparable to the range of the pion exchange (1.45 fm). It is obvious that this hole line expansion should work at small densities, but may fail at large densities, at which the assumption, r_V small compared to d_N, is not justified. The convergence of the hole-line expansion will be discussed in section 3 below.

The inclusion of all two-hole line contributions requires the solution of the two-body problem in the nuclear medium, as expressed by the Bethe-Goldstone equation. For the inclusion of all three-hole lines one has to solve the three-body problem in the nuclear medium, which corresponds to solving the Bethe-Fadeev equations[58] (see also diagrams in Fig. 6). Techniques and details how to solve the Bethe-Fadeev equations have been described by Day[59]. Numerical solutions for the three-hole line contributions in nuclear matter have recently been presented by Song et al.[60, 61].

Various techniques have been developed to solve the BHF equations, i.e. the Bethe-Goldstone equation in particular for nuclear matter and finite nuclei. As an example for a standard solution in infinite nuclear matter we would like to refer to the work of Haftel and Tabakin[62]. A description, how to solve the Bethe-Goldstone equation for finite systems, including a FORTRAN program, can be found in [63].

2.2 *Coupled Cluster Method*

A very detailed description of the coupled cluster Method (CCM), which has been introduced more than 40 years ago by Coester and Kümmel[64, 65] can be found in [12]. More recently a review on this approach has been given by Bishop [13]. Also in the CCM or "Exponential S" approach one starts assuming an appropriate Slater determinant Φ as a first approximation for the exact eigenstate of Ψ for the A-particle system. If the overlap $< \Psi|\Phi >$ is different from
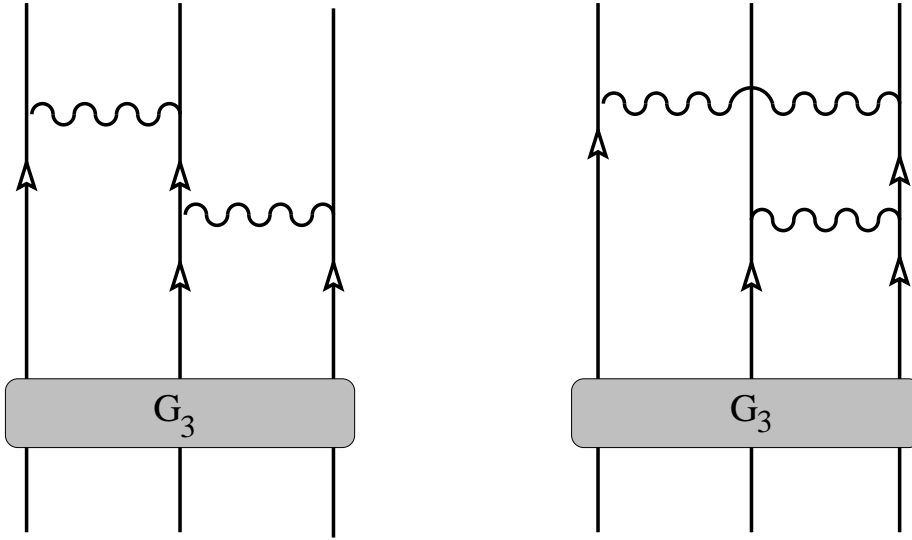
Figure 6: Three-particle ladder diagrams to be included in the Bethe-Fadeev equation.

zero, one can always consider the "Exponential S" ansatz

$$\Psi = e^S \Phi \tag{14}$$

with S an operator of the form

$$S = \sum_{n=1}^{A} S_n \tag{15}$$

where S_n is an n-particle operator which can be written

$$S_n = \frac{1}{(n!)^2} \sum_{\substack{\nu_1 \ldots \nu_n \\ \rho_1 \ldots \rho_n}} < \rho_1 \ldots \rho_n |S_n| \nu_1 \ldots \nu_n > a_{\rho_1}^\dagger \ldots a_{\rho_n}^\dagger a_{\nu_n} \ldots a_{\nu_1} \tag{16}$$

Here and in the following $a_\alpha^\dagger$ (a_α) stand for creation (annihilation) operators for nucleons in a state α with α a single-particle state of the basis, which also defines the Slater determinant Φ. We will use labels $\nu_1 \ldots \nu_n$ to refer to hole states, i.e. single particle states which are occupied in the model state Φ and indices $\rho_1 \ldots \rho_n$ to denote particle states, i.e. states above the Fermi surface of Φ. Expanding the exponential in (14) one obtains

$$\Psi = \left(1 + S_1 + \frac{1}{2}S_1^2 + S_2 + \frac{1}{6}S_1^3 + S_2 S_1 + S_3 \ldots \right) \Phi. \tag{17}$$

So exact eigenstates of the hamiltonian Ψ is written as a sum of the reference state Φ, one-particle on-hole (S_1) excitations relative to Φ, two-particle two-hole ($1/2S_1^2 + S_2$) and so on up to A-particle A-hole excitations. Therefore it is obvious that the ansatz (14) is sufficient, but one may ask the question, why we are using the exponential form of the ansatz and not simply write

$$\begin{aligned} \Psi &= (1 + F_1 + F_2 + F_3 \ldots) \Phi \\ &= (1 + F) \Phi, \end{aligned} \tag{18}$$

where F_n contains all n-particle n-hole contributions, which implies

$$
\begin{aligned}
F_1 &= S_1 \\
F_2 &= \frac{1}{2}S_1^2 + S_2 \\
F_3 &= \frac{1}{6}S_1^3 + S_2 S_1 + S_3
\end{aligned}
\tag{19}
$$

If the two expansions are treated including all terms up to $n = A$ both expansions lead to the exact result. The question is, which approach is more appropriate if one has to truncate the expansion and consider terms F_i or S_i only up to an order $i \leq n$ with n smaller than the total particle number A.

A first answer on the question why the "exponential S" ansatz (14) is preferable to the parametrisation (18) can be given by Thouless theorem[66]: If we restrict the "exponential S" ansatz including only terms up to $n = 1$, the Thouless theorem says that the ansatz (14) includes all Slater determinants which are not orthogonal to Φ. Therefore the solution of the CCM method in the S_1 approximation would correspond to the Hartree-Fock approach. On the other hand, however, the F_1 approach, i.e. ignore all contributions of F_i with $i = 2 \ldots A$ in (18), is more restrictive and more sensitive to the choice of the initial state Φ.

A more convincing argument, however, can be found by considering the fact that e.g. F_2 will contain two-particle two-hole excitation which are unrelated and completely independent from each other. Just from statistical arguments it is clear that such unlinked contributions will become more and more important if the size of the system, or the particle number gets large. This problem can be seen by inspecting the set of equations, which determine the amplitudes F_i. To derive these equations one considers the Schrödinger equation

$$
H|\Psi> = E|\Psi>
\tag{20}
$$

assumes the ansatz (18) and projects from the left with $<\Phi|$, $<\Phi|a_\nu^\dagger a_\rho$, $<\Phi|a_{\nu_1}^\dagger a_{\nu_2}^\dagger a_{\rho_2} a_{\rho_1}$ and so on. This yields

$$
\begin{aligned}
E &= <\Phi|H(1+F)|\Phi> \\
E <\rho|F_1|\nu> &= <\Phi|a_\nu^\dagger a_\rho H(1+F)|\Phi> \\
E <\rho_1 \rho_2|F_2|\nu_1 \nu_2> &= <\Phi|a_{\nu_2}^\dagger a_{\rho_2} a_{\rho_1} H(1+F)|\Phi>
\end{aligned}
\tag{21}
$$

One finds that all left-hand sides of these equations contain the energy, which is an extensive quantity, i.e. it grows proportional to the particle number A. Therefore also the right-hand side of these equations must be extensive, which is a reflection of the fact that these equations contain unlinked terms.

The "exponential S" ansatz provides a way out of this problem. This can be seen already from Eqs. (19), in which e.g. F_2 is rewritten in terms of unlinked contributions S_1^2 and a linked term S_2. To demonstrate this feature we consider the equations which determine the amplitudes S_n. To do this we consider the Schrödinger equation in the form

$$
e^{-S}He^{S}|\Phi> = e^{-S}E|\Psi> = E|\Phi>
\tag{22}
$$

and project it from the left with $<\Phi|$, which yields

$$
\begin{aligned}
E &= <\Phi|e^{-S}He^{S}|\Phi> = <\Phi|He^{S}|\Phi> \\
&= <\Phi|H\left(1 + S_1 + \frac{1}{2}S_1^2 + S_2\right)|\Phi>
\end{aligned}
\tag{23}
$$

13

Note that in the first line we have used the fact $S^\dagger|\Phi> = 0$, which is obvious from the definitions of the S_n in (16). The other equations are obtained by multiplying (22) from the left with $<\Phi|a^\dagger_\nu a_\rho$, $<\Phi|a^\dagger_{\nu_1}a^\dagger_{\nu_2}a_{\rho_2}a_{\rho_1}$ etc. which yields

$$
\begin{aligned}
<\Phi|a^\dagger_\nu a_\rho e^{-S}He^S|\Phi> &= 0 \\
<\Phi|a^\dagger_{\nu_1}a^\dagger_{\nu_2}a_{\rho_2}a_{\rho_1}e^{-S}He^S|\Phi> &= 0
\end{aligned}
\tag{24}
$$

and so on. Note that these equations do not contain the extensive quantity E as the corresponding Eqs. (21) for the F_l.

The fact, that the Eqs. (24) do not contain extensive quantities, growing with A, is only a hint that the matrix elements contained in these equations do not contain terms, which correspond to unlinked diagrams. In order to proof this feature, one has to consider the evaluation of the matrix elements more in detail. For that purpose we consider the expansion

$$
e^{-S}He^S = H + [H,S] + \frac{1}{2!}\left[[H,S],S\right] + \frac{1}{3!}\left[[[H,S],S],S\right] + \dots
\tag{25}
$$

As an example for such commutator expression let us consider the commutator between the operator of kinetic energy with S_1

$$
\begin{aligned}
[t_{kin},S_1] &= \sum_{\alpha\beta\rho\nu} <\alpha|t_{kin}|\beta><\rho|S_1|\nu> \left[a^\dagger_\alpha a_\beta, a^\dagger_\rho a_\nu\right] \tag{26} \\
&= \sum_{\alpha\nu}\left\{\sum_\rho <\alpha|t_{kin}|\rho><\rho|S_1|\nu> a^\dagger_\alpha a_\nu\right\} - \sum_{\beta\rho}\left\{\sum_\nu <\nu|t_{kin}|\beta><\rho|S_1|\nu> a^\dagger_\rho a_\beta\right\}
\end{aligned}
$$

Each commutator removes one $a^\dagger$ and one a operator from the operator product, and links single-particle labels of two amplitudes together. Translated into the language of diagrams such a link means that there is an internal line, a single-particle propagator, connecting the operator symbols of t_{kin} and S_1. The components of S commute with each other since they all contain creation operator for particle states and annihilation operators for hole states in Φ. Therefore links produced by the commutators in (25) can only occur between the hamiltonian H and S. This implies that the expansion in (25) is finite: if e.g. the hamiltonian contains one- and two-body operators only, there will only be up to four nested commutators on the right hand side. Furthermore we see that the left-hand sides of Eqs. 24) correspond to matrix elements of a linked operator product between the unperturbed model ground-state Φ as ket- and n-particle n-hole states relative to Φ as bra-state.

In order to obtain explicit equations for the amplitudes S_n one introduces the so-called n-particle subsystem amplitudes Ψ_n defined by

$$
<x_1\dots x_n|\Psi_n|\nu_1\dots\nu_n> = <\Phi|a^\dagger_{\nu_1}\dots a^\dagger_{\nu_n}a_{x_n}\dots a_{x_1}|\Psi> .
\tag{27}
$$

So this subsystem amplitudes correspond to the overlap of the exact A-particle wave function Ψ with an n-particle n-hole excitation of the reference state Φ. Note, however, that the label x_i does not necessarily refer to quantum numbers of a single-particle state in Φ, it may also refer to coordinates of a nucleon in the usual space or in momentum space. As an example we consider explicitly

$$
\begin{aligned}
<x_1|\Psi_1|\nu_1> &= <x_1|\nu_1> + <x_1|S_1|\nu_1> \\
<x_1x_2|\Psi_2|\nu_1\nu_2> &= \mathcal{A}\{<x_1|\Psi_1|\nu_1><x_2|\Psi_1|\nu_2>\} + <x_1x_2|S_2|\nu_1\nu_2>
\end{aligned}
\tag{28}
$$

If we consider x_1 to represent coordinate, we see that the single-particle amplitude contains the uncorrelated wave function of the hole state $<x_1|\nu_1>$ and possible corrections defined by

S_1. In a similar way Ψ_2 contains the anti-symmetrized ($\mathcal{A}$ represents the operator of antisymmetrisation of the indices ν_i) product of the Ψ_1 plus corrections due to S_2 This would imply that $< x_1 x_2 | S_2 | \nu_1 \nu_2 >$ plays a role similar to the defect function in (10). For the three- and more-particle amplitudes it is convenient to introduce also[67]

$$
\begin{aligned}
< x_1 x_2 \rho | \chi_3^{(12)} | \nu_1 \nu_2 \nu_3 > \ &= \ < x_1 x_2 \rho | \Psi_3 | \nu_1 \nu_2 \nu_3 > - \mathcal{A} \{ < \rho | \Psi_1 | \nu_3 > < x_1 x_2 | S_2 | \nu_1 \nu_2 > \} \\
&= \ \mathcal{A} \{ < x_2 | \Psi_1 | \nu_2 > < x_1 \rho | S_2 | \nu_1 \nu_3 > \} \\
&\quad + \mathcal{A} \{ < x_1 | \Psi_1 | \nu_1 > < x_2 \rho | S_2 | \nu_2 \nu_3 > \} \\
&\quad + < x_1 x_2 \rho | S_3 | \nu_1 \nu_2 \nu_3 > \ .
\end{aligned}
\tag{29}
$$

Furthermore we can define a single-particle potential for hole states ν by

$$
< x | U | \nu > = \sum_{\nu' \leq F} < x \nu' | V \Psi_2 | \nu \nu' > \ .
\tag{30}
$$

If we identify Ψ_2 with a correlated two-particle wave function like in (10), the product $V \Psi_2$ plays the same role than the G matrix in the hole-line expansion and the single-particle potential of (30) can directly be compared with the definition of the single-particle potential (11) in the BHF approach.

Using all these definitions the one-particle, Hartree-Fock like equation, determining S_1 or Ψ_1 can be written

$$
\begin{aligned}
< x_1 | t_{kin,1} \Psi_1 | \nu_1 > &+ \sum_{\nu' \leq F} < x_1 \nu' | t_{kin,2} S_2 | \nu_1 \nu' > \\
+ < x_1 | U | \nu_1 > &+ \sum_{\nu \nu' \leq F} < x_1 \nu \nu' | V_{23} \chi_3^{(23)} | \nu_1 \nu \nu' > \ = \ \sum_{\nu \leq F} < x_1 | \Psi_1 | \nu > h_{\nu \nu_1}
\end{aligned}
\tag{31}
$$

with $h_{\nu \nu_1}$ the matrix elements for single-particle energy between hole states

$$
h_{\nu \nu_1} = < \nu | t_{kin,1} \Psi_1 \nu_1 > + < \nu | U | \nu_1 >
\tag{32}
$$

The indices $1, 2$ in these equation shall denote that operators of kinetic energy and the two-body interaction V act on the corresponding single-particle states in the ket-vector.

The corresponding equation for the two-body amplitudes, determining S_2 or Ψ_2 can be written (omitting some corrections proportional to S_1)

$$
\begin{aligned}
< x_1 x_2 | Q(t_{kin,1} + t_{kin,2}) S_2 | \nu_1 \nu_2 > \ &- \ \sum_{\nu \leq F} (< x_1 x_2 | S_2 | \nu \nu_2 > h_{\nu \nu_1} + < x_1 x_2 | S_2 | \nu_1 \nu > h_{\nu \nu_2}) \\
+ < x_1 x_2 | Q V_{12} S_2 | \nu_1 \nu_2 > \ &= \ - < x_1 x_2 | V_{12} | \nu_1 \nu_2 > - < x_1 x_2 | S_2 P V_{12} \Psi_2 | \nu_1 \nu_2 > \\
&\quad - \sum_{\nu \leq F} < x_1 x_2 \nu | Q V_{13} \chi_3^{(13)} + Q V_{23} \chi_3^{(23)} | \nu_1 \nu_2 \nu > \\
&\quad - \frac{1}{2} \sum_{\nu \nu' \leq F} < x_1 x_2 \nu \nu' | Q V_{34} \chi_4^{(34)} | \nu_1 \nu_2 \nu \nu' > \ .
\end{aligned}
\tag{33}
$$

Here Q refers again to the Pauli operator for two-particle states, which we have defined already in (8). From these two equations (31) and (33) we can observe some general features of the problem to determine the amplitudes S_n. The different equations are coupled. If we restrict our considerations to two-body interaction terms only, the n-body equation, which should provide S_n requires the knowledge of S_{n+1} and S_{n+2}. If the hamiltonian would also contain a three-body interaction, S_{n+3} would be needed as well. In order to solve the one-body equation (31) which will determine S_1 or Ψ_1, one should know the amplitudes S_2 and S_3, which are hidden in U, Ψ_2
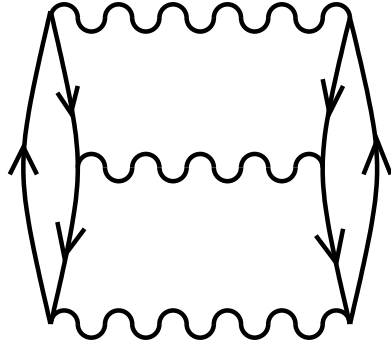
Figure 7: Hole-hole ladder diagram included in CCM SUB2 approximation

and χ_3, respectively. For the two-body equation (33) the information on S_3 and S_4 (contained in χ_4) is needed.

This implies that one has to truncate the hierarchy of this set of equations by assuming in the so-called "SUBn" approximation that all amplitudes S_i with $i > n$ are assumed to be zero. As a first example we will consider the SUB2 approximation and compare it to the BHF approach discussed in the preceeding subsection. The SUB2 assumption implies that we ignore the last term on the left-hand side of Eq. (31) (χ_3) and the last two terms in Eq. (33). If for the moment we furthermore assume that

$$h_{\nu\mu} = \epsilon_\nu \delta_{\nu\mu} \tag{34}$$

is diagonal and neglect the matrix elements of $S_2 P V_{12} \Psi_2$ we can rewrite Eq. (33) into

$$Q\left(\epsilon_{\nu_1} + \epsilon_{\nu_2} - (t_{kin,1} + t_{kin,2})\right) S_2 |\nu_1\nu_2> = QV\Psi_2|\nu_1\nu_2> \tag{35}$$

which corresponds to

$$S_2|\nu_1\nu_2> = \frac{Q}{\epsilon_{\nu_1} + \epsilon_{\nu_2} - (t_{kin,1} + t_{kin,2})} V\Psi_2|\nu_1\nu_2> \ . \tag{36}$$

Comparing with Eq. (10) we may identify

$$
\begin{aligned}
G|\phi_{\nu_1\nu_2}> &\longleftrightarrow V\Psi_2|\nu_1\nu_2> \\
\frac{Q}{\omega - h_{12}} G|\phi_{\nu_1\nu_2}> &\longleftrightarrow S_2|\nu_1\nu_2> ,
\end{aligned} \tag{37}
$$

where the last line identifies the so-called defect functions in the two approaches. With this identification we also see that the single-particle equation (31) corresponds to the single-particle equation if we ignore the term $t_{kin,2}S_2$ in that equation.

The main difference between the Coupled Cluster Method (CCM) SUB2 approach and the BHF approximation is the inclusion of the $S_2 P V_{12} \Psi_2$ in the two-body Eq. (33) as compared to the Bethe-Goldstone equation (7). In terms of diagrams this means that the energy calculated in the CCM SUB2 approach also includes hole-hole scattering diagrams like the one displayed in Fig. 7. This means that the hole-hole ladders are treated on the same level as the particle-particle ladders. This should be of particular importance if the phase space of hole-hole states, which can be reached by the two-body interaction is as large as the corresponding space of particle-particle configurations. As we will see in the discussion of results in chapter 3, for

realistic interactions in nuclear physics, the particle-particle ladders are dominant as compared to the hole-hole ladders. Therefore the differences between the results of CCM SUB2 and BHF calculations are usually small. Note that particle-particle and hole-hole ladders are also often referred to as particle-particle hole-hole ring diagrams, which are included in a pphh RPA calculation[68, 69, 70]

Within the framework of the CCM approach one does not have any choice for the auxiliary potential U as it was the case in the BHF approach. From the comparison of the two approaches discussed above (see Eq. (37)) one finds that the CCM SUB2 approach is rather close to the BHF assuming the conventional choice for the particle state-spectrum in the Bethe-Goldstone equation, which means that h_{12} is replace by the sum of the kinetic energies. All corrections to the CCM SUB2 approach occur due to the inclusion of the three-body and higher order terms.

In order to discuss the effects of the three-body amplitude on the calculated energies, we write the equation for χ_3[71]

$$
\begin{aligned}
< x_1 x_2 x_3 | \chi_3^{(12)} | \nu_1 \nu_2 \nu_3 > \ = \ & \mathcal{A} \{ < x_3 x_1 | S_2 | \nu_2 \nu_1 > < x_2 | \Psi_1 | \nu_2 > \\
& + < x_2 x_3 | S_2 | \nu_2 \nu_3 > < x_1 | \Psi_1 | \nu_1 > \} \\
& + \sum_{y_i} < x_1 x_2 x_3 | \frac{Q_3}{e_3} | y_2 y_3 y_1 > < y_1 y_2 y_3 | G_{12} \chi_3^{(12)} | \nu_1 \nu_2 \nu_3 > \\
& + \sum_{y_i} < x_1 x_2 x_3 | \frac{Q_3}{e_3} | y_2 y_3 y_1 > < y_3 y_1 y_2 | G_{12} \chi_3^{(12)} | \nu_1 \nu_2 \nu_3 > \ (38)
\end{aligned}
$$

In this equation we have identified $V \Psi_2$ with G according to (37). Q_3 denotes the Pauli operator for three-particle states and the energy denominator e_3 is defined by

$$
e_3 = \epsilon_{\nu_1} + \epsilon_{\nu_2} + \epsilon_{\nu_3} - (t_{kin1} + t_{kin2} + t_{kin3}) \ . \tag{39}
$$

The resulting amplitudes χ_3 multiplied with V enter into the one-body (31) as well as two-body Eq. (33). The contribution to the binding energy E originating from these contributions is of third and higher order in G. The Goldstone diagrams representing the contributions of third order (omitting exchange diagrams) are displayed in Fig. 8. The diagram of Fig. 8a is a particle-hole ring diagram. The summation of all ph ring diagram contributions can be obtained by calculating the correlation energy arising from particle-hole RPA calculations. The diagram displayed in Fig. 8b is a contribution, which within the BHF approach one would try to cancel by an appropriate definition of the single-particle spectrum U for particle states. This indicates again that U should be chosen to minimize the effects of three- and four-body terms.

If one would like to evaluate the amplitudes $< x_1 \ldots x_n | S_n | \nu_1 \ldots \nu_n >$ in the real space representation, which means that x_i refer to the usual coordinates of the nucleons, the basic equations (31) and (33) must be considered as differential equations. This is particularly useful if the NN interaction V is described in terms of local potential terms[67, 71]. For non-local potentials it is me more convenient to use momentum space representation. In this case the equations lead to inhomogeneous integral equations[72]. The CCM equations have also been solved in a Hilbert space, which is spanned by a basis of appropriate oscillator functions[73], which leads to a solution of a coupled system of nonlinear equations.

If the amplitude S_i have been determined, it is easy to evaluate the energy according to (23). Knowing S_i we also have the information on the exact wave function (not normalized). An efficient evaluation of observables different from the energy can be done using the following considerations. As an example we consider the single-particle density matrix

$$
d_{\beta \alpha} = \frac{< \Psi | a_\beta^\dagger a_\alpha | \Psi >}{< \Psi | \Psi >} \tag{40}
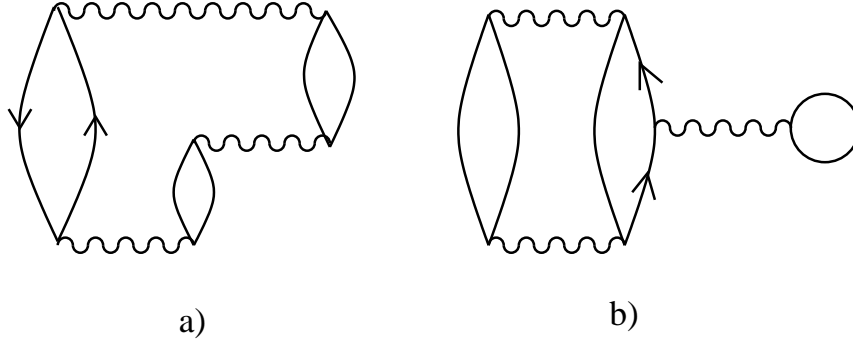$$

Figure 8: Lowest order contributions originating from the inclusion of three-body terms in the CCM. The diagram shown in the left part (a) is a particle-hole ring diagram, while the one displayed in (b) contains a bubble insertion into a particle line, which one would like to compensate by an appropriate choice of the single-particle potential for particle states.

One can rewrite this expression into

$$
\begin{aligned}
d_{\beta\alpha} &= \frac{<\Phi|e^{S^\dagger}a_\beta^\dagger a_\alpha e^S|\Phi>}{<\Phi|e^{S^\dagger}e^S|\Phi>} \\
&= \frac{<\Phi|e^{S^\dagger}e^S e^{-S}a_\beta^\dagger a_\alpha e^S|\Phi>}{<\Phi|e^{S^\dagger}e^S|\Phi>} \\
&= <\Phi|e^{-S}a_\beta^\dagger a_\alpha e^S|\Phi> + \sum_n \frac{<\Phi|e^{S^\dagger}e^S X_n^\dagger|\Phi><\Phi|X_n e^{-S}a_\beta^\dagger a_\alpha e^S|\Phi>}{<\Phi|e^{S^\dagger}e^S|\Phi>}
\end{aligned} \tag{41}
$$

The last line has been obtained by inserting the unity operator

$$
|\Phi><\Phi| + \sum_n X_n^\dagger|\Phi><Phi|X_n \tag{42}
$$

with the n-particle n-hole operator

$$
X_n^\dagger = \frac{1}{(n!)^2} \sum_{\rho_i>F,\nu_i\leq F} a_{\rho_1}^\dagger \ldots a_{\rho_n}^\dagger a_{\nu_n} \ldots a_{\nu_1} . \tag{43}
$$

Since $X_n^\dagger$ commutes with S, the expression (41) can be rewritten into

$$
d_{\beta\alpha} = <\Phi|e^{-S}a_\beta^\dagger a_\alpha e^S|\Phi> + \sum_n <\Phi|X_n e^{-S}a_\beta^\dagger a_\alpha e^S|\Phi> \frac{<\Psi|X_n^\dagger|\Psi>}{<\Psi|\Psi>} . \tag{44}
$$

The matrix elements of operators like $e^{-S}a_\beta^\dagger a_\alpha e^S$ can be calculated employing an expansion similar to the expansion in (25). The factors of the form $<\Psi|X_n^\dagger|\Psi> / <\Psi|\Psi>$, on the other hand correspond to the matrix elements of the n-body density operator, which brings us back to the starting point in (40). This means that the final matrix elements can be calculated in an iterative scheme[73, 74].

2.3   *Many-Body Theory in Terms of Green's Functions*

The two-body approaches discussed so far, the hole-line expansion as well as the CCM, are essentially restricted to the evaluation of ground-state properties. The Green's function approach,

which will shortly be introduced in this section also yields results for dynamic properties like e.g. the single-particle spectral function which is closely related to the cross section of particle knock-out and pick-up reactions. It is based on the time-dependent perturbation expansion and also assumes a separation of the total hamiltonian into an single-particle part H_0 and a perturbation H_1 as introduced in (3). A more detailed description can be found e.g. in the textbooks of Fetter and Walecka[75], Negele and Orland[76] or in the book by Mattuck[77], which particularly provides a rather intuitive interpretation of the Feynman diagrams. A very comprehensive description of the main features has been presented by Mahaux and Sartor[78]. Introductions are also given in various review articles[14, 46].

The expectation value of any operator O is calculated in the so-called interaction picture as

$$< \Psi^{\mathrm{I}}(t)|O_{\mathrm{I}}(t)|\Psi^{\mathrm{I}}(t) > , \tag{45}$$

where the time-dependent operator $O_{\mathrm{I}}(t)$ in the interaction picture is related to the operator O in the usual Schrödinger picture by

$$O_{\mathrm{I}}(t) = e^{iH_0 t} O e^{-iH_0 t} . \tag{46}$$

and the time-dependence of the state $|\Psi^{\mathrm{I}}(t) >$ can be derived from

$$i\frac{\partial}{\partial t}|\Psi^{\mathrm{I}}(t) >= H_{1\mathrm{I}}(t)|\Psi^{I}(t) > . \tag{47}$$

If we introduce the evolution operator in the interaction scheme $U_{\mathrm{I}}(t, t_0)$ by

$$|\Psi^{\mathrm{I}}(t) >= U_{\mathrm{I}}(t, t_0)|\Psi^{\mathrm{I}}(t_0) > , \tag{48}$$

the equation of motion for the state $|\Psi^{\mathrm{I}} >$ (47) can be rewritten into a differential equation for the evolution operator

$$i\frac{\partial}{\partial t}U_{\mathrm{I}}(t, t_0) = H_{1\mathrm{I}}(t)U_{\mathrm{I}}(t, t_0) . \tag{49}$$

This equation can be transformed into an integral equation

$$U_{\mathrm{I}}(t, t_0) = U_{\mathrm{I}}(t_0, t_0) - i \int_{t_0}^{t} dt_1\, H_{1\mathrm{I}}(t_1)U_{\mathrm{I}}(t_1, t_0) . \tag{50}$$

Using the fact that $U_{\mathrm{I}}(t_0, t_0)$ is identical to the unit operator $\hat{1}$, we can iterate this integral equation to a perturbative expansion in powers of $H_{1\mathrm{I}}$:

$$\begin{aligned}
U_{\mathrm{I}}(t, t_0) &= \hat{1} + (-i) \int_{t_0}^{t} dt_1\, H_{1\mathrm{I}}(t_1) \\
&\quad + (-i)^2 \int_{t_0}^{t} dt_1\, H_{1\mathrm{I}}(t_1) \int_{t_0}^{t_1} dt_2\, H_{1\mathrm{I}}(t_2) + \ldots
\end{aligned} \tag{51}$$

The integration variables used on the left-hand side are nested in a rather inconvenient way. Therefore one rewrites the term of order n in this expansion using

$$\int_{t_0}^{t} dt_1\, H_{1\mathrm{I}}(t_1) \ldots \int_{t_0}^{t_{n-1}} dt_n\, H_{1\mathrm{I}}(t_n) = \frac{1}{n!} \int_{t_0}^{t} dt_1 \ldots \int_{t_0}^{t} t_n\, \mathcal{T}\left(H_{1\mathrm{I}}(t_1) \ldots H_{1\mathrm{I}}(t_n)\right) \tag{52}$$

with the time ordering or chronological operator $\mathcal{T}$, which is defined for two operators by

$$\mathcal{T}\left(A(t_1)B(t_2)\right) = \begin{cases} A(t_1)B(t_2), & \text{if } t_1 \geq t_2, \\ (-1)^m B(t_2)A(t_1), & \text{otherwise.} \end{cases} \tag{53}$$

19

Here m is the number of exchanges of fermion creation and annihilation operators contained in A and B, which are needed to bring A and B into chronological order. Note that for our present purpose (52) the factor $(-1)^m$ is always equal to 1, as the number of fermion operators defining H_{1I} is even. The definition of $\mathcal{T}$ in (53) for two operators is easily extended to n operators. Applying (52) to the expansion of the time evolution operator in (51), one gets

$$U_{\mathrm{I}}(t, t_0) = \sum_{n=0}^{\infty} \frac{(-i)^n}{n!} \int_{t_0}^{t} dt_1 \dots \int_{t_0}^{t} dt_n \, \mathcal{T} \left(H_{1\mathrm{I}}(t_1) \dots H_{1\mathrm{I}}(t_n) \right) \tag{54}$$

In order to arrive at a perturbation expansion for the calculation of matrix elements, one assumes that the perturbation H_1 is "switched off" at times $t = -\infty$ and $t = +\infty$ and can be switched on in an adiabatic way for times $t \approx 0$. This can be achieved by a time-dependent hamiltonian of the form

$$H_\alpha(t) = H_0 + e^{-\alpha|t|} H_1 \tag{55}$$

where α is a small positive number that becomes infinitesimal in the adiabatic limit. This procedure implies that the eigenstates of the hamiltonian H_α are identical to the eigenstates of the unperturbed hamiltonian H_0 at times $|t| = \infty$ and should evolve to the corresponding eigenstates of the total H at $t \approx 0$ if we use the time evolution operator $U_{\mathrm{I}\alpha}(t, t')$ for the hamiltonian H_α. If we denote the (nondegenerate) ground state of H_0 by Φ_0, which is independent of time in the interaction picture, this means that we obtain an eigenstate of the exact H at time $t = 0$ by

$$|\Psi_0(t = 0)> = \lim_{\alpha \to 0} U_{\mathrm{I}\alpha}(0, -\infty)|\Phi_0 > . \tag{56}$$

It has been shown by Gell-Mann and Low[79] that Ψ_0 is indeed an exact eigenstate of H if the perturbation expansion converges.

In order to calculate matrix elements we now consider the Heisenberg scheme. In this representation, which corresponds to the interaction scheme with $H_0 = H$, the wave function is time-independent and identical to $\Psi_0(t = 0)$ and the time-dependence is completely assigned to the operators $O_H(t)$ which are defined as in (46), replacing H_o by H. This means that a matrix element of an operator O can be calculated as

$$\begin{aligned}
\frac{< \Psi_0|O_H(t)|\Psi_0 >}{< \Psi_0|\Psi_0 >} &= \lim_{\alpha \to 0} \frac{< \Phi_0|U_{\mathrm{I}\alpha}(\infty, 0)O_H(t)U_{\mathrm{I}\alpha}(0, -\infty)|\Phi_0 >}{< \Phi_0|U_{\mathrm{I}\alpha}(\infty, 0)U_{\mathrm{I}\alpha}(0, -\infty)|\Phi_0 >} \\
&= \lim_{\alpha \to 0} \frac{< \Phi_0|U_{\mathrm{I}\alpha}(\infty, t)O_\mathrm{I}(t)U_{\mathrm{I}\alpha}(t, -\infty)|\Phi_0 >}{< \Phi_0|U_{\mathrm{I}\alpha}(\infty, -\infty)|\Phi_0 >} .
\end{aligned} \tag{57}$$

Using the explicit representation of the time evolution operator in (54) one can furthermore show (see, e.g.[75]) that the matrix element for any time-ordered product of two Heisenberg operators can be calculated as

$$\begin{aligned}
\frac{< \Psi_0|\mathcal{T} \left(A_\mathrm{H}(t)B_\mathrm{H}(t') \right)|\Psi_0 >}{< \Psi_0|\Psi_0 >} &= \lim_{\alpha \to 0} \Bigg[\frac{1}{< \Psi_0|\Psi_0 >} \sum_{n=0}^{\infty} \frac{(-i)^n}{n!} \int_{-\infty}^{\infty} dt_1 \dots \int_{-\infty}^{\infty} dt_n \, e^{-\alpha(|t_1| + \dots |t_n|)} \\
&\quad \times < \Phi_0|\mathcal{T} \left(V_\mathrm{I}(t_1) \dots V_\mathrm{I}(t_n)A_\mathrm{I}(t)B_\mathrm{I}(t') \right)|\Phi_0 > \Bigg] ,
\end{aligned} \tag{58}$$

which means that one has to evaluate matrix elements of time-ordered products of operators in the interaction scheme for the ground state of the unperturbed hamiltonian Φ_0.

The operators in these matrix elements are time-ordered. Therefore we can apply Wick's theorem[80] to evaluate them. In the following we will shortly review this scheme and illustrate how the various contributions are visualized in terms of Feynman diagrams.

First we recall that the operator for the residual interaction H_1 as well as any other operator can be expressed in terms of the basic single-particle creation $(a_i^\dagger)$ and annihilation operators (a_i). It is easy to verify that these operators in the interaction scheme are given by

$$
\begin{aligned}
a_{\mathrm{I}j}(t) &= a_j \exp\left(-i\epsilon_j t\right), \\
a_{\mathrm{I}j}^\dagger(t) &= a_j^\dagger \exp\left(+i\epsilon_j t\right),
\end{aligned}
\tag{59}
$$

with ϵ_j the single-particle energies defining the unperturbed hamiltonian H_0 The ground state for this unperturbed hamiltonian, Φ_0, is given by a Slater determinant in which all single-particle states i with an energy ϵ_i below the Fermi energy ϵ_{F} are occupied. The Fermi energy separates hole-states ($\epsilon_\nu \leq \epsilon_{\mathrm{F}}$, occupied in the unperturbed ground state) from particle states ($\epsilon_\rho > \epsilon_{\mathrm{F}}$, unoccupied in the unperturbed ground state). If $M, N, O, P, \ldots$ represent creation or annihilation operators, in the Schrödinger or in the interaction picture, one can define the normal product of such operators by

$$
\mathcal{N}\left(MNOP\ldots\right) = (-1)^\gamma OP\ldots MN\ldots
\tag{60}
$$

where the sequence of operators on the right-hand side of this equation is such that all creation operators for particle states $(a_\rho^\dagger)$ and annihilation operators for hole states (a_ν) are moved to the left (O, P), whereas all creation operators for hole states $(a_\nu^\dagger)$ and annihilation operators for particle states (a_ρ) are moved to the right (M, N) and γ counts the number of exchanges of these operators required to obtain the normal ordering. This normal ordering guarantees that the matrix element of such an ordered product calculated for the unperturbed state Φ_0 vanishes:

$$
<\Phi_0|\mathcal{N}\left(MNOP\ldots\right)|\Phi_0> = 0.
\tag{61}
$$

Furthermore we define a "contraction" of two operators, using the chronological operator of (53) for two such operators M, N in the interaction scheme, as

$$
\begin{aligned}
\underbrace{MN} &= <\Phi_0|\mathcal{T}\left(MN\right) - \mathcal{N}\left(MN\right)|\Phi_0> \\
&= <\Phi_0|\mathcal{T}\left(MN\right)|\Phi_0>,
\end{aligned}
\tag{62}
$$

which is just a complex number given by

$$
\underbrace{a_{\mathrm{I}j}(t)a_{\mathrm{I}k}^\dagger(t')} = \begin{cases}
\delta_{jk}e^{-i\epsilon_j(t-t')} & \text{if } j \text{ is a particle state and } t > t', \\
-\delta_{jk}e^{-i\epsilon_j(t-t')} & \text{if } j \text{ is a hole state and } t' > t, \\
0 & \text{otherwise,}
\end{cases}
\tag{63}
$$

$$
\underbrace{a_{\mathrm{I}k}^\dagger(t')a_{\mathrm{I}j}(t)} = -\underbrace{a_{\mathrm{I}j}(t)a_{\mathrm{I}k}^\dagger(t')}.
\tag{64}
$$

Using Wick's theorem it is easy to show that matrix elements of time-ordered products calculated for the unperturbed ground state Φ_0 as in (58) can be calculated as a sum of all terms in which the single-particle operators are pairwise contracted, which means that each pair is replaced by the corresponding value for the contraction (63).

The use of Feynman diagrams provides an easy control of all the contributions. To demonstrate this, we consider as an example the matrix element occurring in the first-order term of (58)

$$
\frac{1}{2}\sum_{i,j,k,l} <ij|V|kl><\Phi_0|\mathcal{T}\left(a_{\mathrm{I}i}^\dagger(t_1)a_{\mathrm{I}j}^\dagger(t_1)a_{\mathrm{I}l}(t_1)a_{\mathrm{I}k}(t_1)a_{\mathrm{I}\alpha}(t)a_{\mathrm{I}\beta}^\dagger(t')\right)|\Phi_0>,
\tag{65}
$$

where we have made the substitution $A_{\mathrm{I}} \to a_{\mathrm{I}\alpha}$, $B_{\mathrm{I}} \to a_{\mathrm{I}\beta}^\dagger$, and used the explicit representation of V. For this example we will furthermore assume that $t' < t_1 < t$. As before the operator of
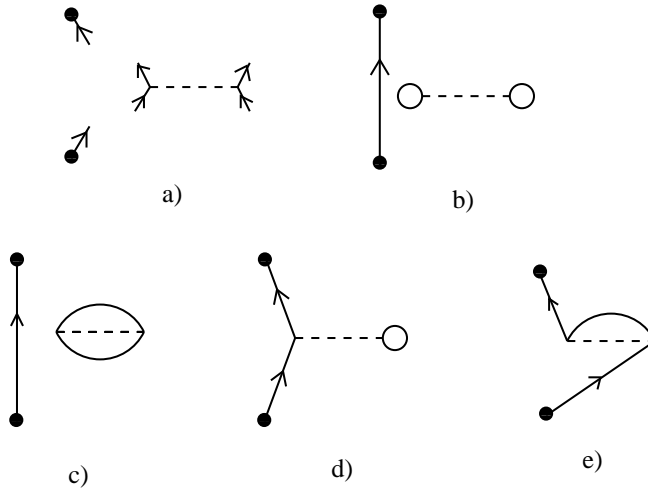
Figure 9: Building blocks for Feynman diagrams **(a)** and completely contracted contributions as discussed in the text.

the residual interaction is represented in the Feynman diagram by a horizontal dashed line, with an outgoing and incoming arrow at each end. The outgoing arrows refer to creation operators contained in V $(a_{Ii}^\dagger, a_{Ij}^\dagger)$ in our notation, and the incoming ones refer to annihilation operators. The external operators are represented by a dot with an ingoing and an outgoing arrow for the annihilation and creation operator, respectively. These objects are displayed in Fig. 9a. With the assumption that the vertical axis represents a time axis the objects are ordered according to the choice of our example: $t' < t_1 < t$.

Any contraction implies that two of the lines with arrows must be paired. In the graphical representation this is achieved by connecting them. Looking at the contractions which yield results different from zero (see (63)–(64)), one finds that only those pairs of lines in which the arrows point into the same direction must be connected. Furthermore we can distinguish connected lines with an arrow pointing upwards, which refers to a particle state, i.e., the corresponding summation indices in (65) can be restricted to particle states, whereas connected lines with an arrow pointing downwards refer to hole lines.

All diagrams representing the completely contracted terms of the expression shown in (65) are displayed in Fig. 9b)–e). Note that we show only those diagrams that are topologically distinct in the sense that a diagram obtained from another one by just mirroring the ends of an interaction line is not displayed again. Recalling Wick's theorem, it is evident that all non-vanishing contributions to the perturbation calculation of the nth-order term in the matrix element of a time-ordered product of operators in (58) can be obtained in the following way.

- Draw n interaction lines (dashed lines in Fig. 9) and mark on the creation and annihilation operators for the external operators to be calculated (dots in Fig. 9).

- Construct all diagrams by connecting the "arrows" linked to these basic building blocks according to the rules given in the example of Fig. 9.

- Keep in mind that all possible time orderings of the interaction vertices relative to the external operators must be considered (see time integrations in (58)).

- Each of the resulting diagrams represents a non-vanishing contribution to the evaluation of (58) and there exist well-established Feynman rules that translate the contribution of the diagram into a calculable expression (see, e.g.[77]).

- Consider only the contribution of linked diagrams. The linked cluster theorem, which has already been discussed in sections 2.1 and 2.2 also holds for this case (see e.g.[75]). For the example displayed in Fig. 9 this implies that only the contributions of the linked diagrams displayed in Fig. 9d) and e) have to be taken into account.

Up to this point the diagrams have been used only as a kind of book-keeping tool to identify all non-vanishing contributions in the perturbation expansion. However, we have seen already that each connecting line in those diagrams represents a contraction, and a line with an arrow pointing upwards stands for [see (62)]

$$\underbrace{a_{\mathrm{I}j}(t)a_{\mathrm{I}k}^\dagger(t')} =< \Phi_0|\mathcal{T}\left(a_{\mathrm{I}j}(t)a_{\mathrm{I}k}^\dagger(t')\right)|\Phi_0 >, \tag{66}$$

with the creation of a particle taking place before the annihilation $(t > t')$. This means that we can ignore the operator $\mathcal{T}$ and rewrite this contraction as

$$\begin{aligned} < \Phi_0|a_{\mathrm{I}j}(t)a_{\mathrm{I}k}^\dagger(t')|\Phi_0 > &= \sum_\beta < \Phi_0|a_{\mathrm{I}j}(t)|\beta >< \beta|a_{\mathrm{I}k}^\dagger(t')|\Phi_0 > \\ &= \delta_{jk}e^{-i\epsilon_j(t-t')} \quad \text{for } j \text{ a particle state.} \end{aligned} \tag{67}$$

In the first line of this equation we have inserted a summation over a complete set of states $|\beta >$ with one particle in addition to the number of fermions in $|\Phi_0 >$, in order to show that this contraction describes the product of a probability amplitude to create a particle at a time t', producing a state β and the probability that it is annihilated at the later time t reproducing the unperturbed ground state Φ_0. In the second line of this equation we have copied the result for the contraction from (63) that such a propagation of a particle on top of the unperturbed state is only possible if $j = k$ refers to a state above the Fermi energy, in order not to violate the Pauli principle.

In a similar way one can convince oneself that a line with an arrow pointing down represents the propagation of a hole state, i.e., a particle must be removed first from a state h below the Fermi energy before it is put back at a later time. With this interpretation of the contractions visualized in the diagrams one can easily interpret the Feynman diagrams in terms of time-dependent processes.

The single-particle Green's function can be considered as a special example of an expectation value for the time-ordered product of two operators calculated for the exact ground-state in (58). It is defined by

$$ig(\alpha t, \beta t') =< \Psi_0|\mathcal{T}\left(a_{\mathrm{H}\alpha}(t)a_{\mathrm{H}\beta}^\dagger(t')\right)|\Psi_0 > . \tag{68}$$

Note that here and in the following we have dropped the denominator $< \Psi_0|\Psi_0 >$, assuming that the exact ground state is properly normalized. The creation and annihilation operators in the Heisenberg representation are defined in an appropriate basis, characterized by quantum numbers α and β. If we assume that α refers to a position $\vec{r'}$ and β to a position $\vec{r}$ of the considered fermion in r space, the single-particle Green's function $ig(\vec{r'}t', \vec{r}t)$ describes the propagation of this fermion from the space-time point $(\vec{r}t)$ to $(\vec{r'}t')$. In contrast to the discussion of the contractions in the previous section, in this case the propagation is with respect to the exact ground state and the complete hamiltonian.

For a system that is invariant under translation, such as the infinite nuclear or neutron matter, which we want to consider, the appropriate set of basis states is that of the momentum eigenstates; the Green's function is diagonal in this representation. Rewriting the effect of the chronological operator $\mathcal{T}$ defined in (53) in terms of step functions $\Theta(t - t')$, we find that the

Green's function is given as

$$
\begin{aligned}
ig(k, t - t') &= \Theta(t - t') < \Psi_0 | a_{\mathrm{H}k}(t) a_{\mathrm{H}k}^\dagger(t') | \Psi_0 > -\Theta(t' - t) < \Psi_0 | a_{\mathrm{H}k}^\dagger(t') a_{\mathrm{H}k}(t) | \Psi_0 > \\
&= \Theta(t - t') \sum_\gamma e^{-i(E_\gamma^{(A+1)} - E_0^A)(t - t')} \left| < \Psi_\gamma^{(A+1)} | a_k^\dagger | \Psi_0 > \right|^2 \\
&\quad - \Theta(t' - t) \sum_\delta e^{-i(E_0^A - E_\delta^{(A-1)})(t - t')} \left| < \Psi_\delta^{(A-1)} | a_k | \Psi_0 > . \right|^2
\end{aligned} \tag{69}
$$

To arrive at the second part of this equation we have inserted a complete set of eigenstates for the system with $A + 1$ particles ($\Psi_\gamma^{(A+1)}$) and $A - 1$ particles ($\Psi_\delta^{(A-1)}$), as appropriate, and replaced the hamiltonian in the exponential functions of the definition for the Heisenberg operators by the corresponding eigenvalues. This means that the energies E_0^A, $E_\gamma^{(A+1)}$, and $E_\delta^{(A-1)}$ refer to the exact energies for the ground state of our reference system, and the exact energies of eigenstates with $A + 1$ and $A - 1$ particles, respectively. Note that the step function can be represented by its integral form:

$$
\Theta(t) = -\lim_{\eta \to 0} \frac{1}{2\pi i} \int_{-\infty}^{\infty} d\omega \frac{e^{-i\omega t}}{\omega + i\eta} . \tag{70}
$$

Thus the Fourier transformed Green's function, transforming the time difference $t - t'$ to an energy variable ω, can be written as

$$
g(k, \omega) = \lim_{\eta \to 0} \left(\sum_\gamma \frac{\left| < \Psi_\gamma^{(A+1)} | a_k^\dagger | \Psi_0 > \right|^2}{\omega - \left(E_\gamma^{(A+1)} - E_0^A \right) + i\eta} + \sum_\delta \frac{\left| < \Psi_\delta^{(A-1)} | a_k | \Psi_0 > \right|^2}{\omega - \left(E_0^A - E_\delta^{(A-1)} \right) - i\eta} \right) . \tag{71}
$$

This is the so-called spectral or Lehmann representation of the single-particle Green's function[81]. Inspecting this equation one finds that the single-particle Green's function is represented in terms of quantities that are measurable. It shows poles at energies that correspond to energies of the system with one particle added ($A + 1$) and one particle removed ($A - 1$) relative to the energy of the ground state for the reference system. The residua of these poles are given by the spectroscopic factors, i.e., the probabilities of adding and removing one particle with momentum k to produce the specific state γ (δ) of the residual system. The infinitesimal quantity η shifts those poles below the Fermi energy (the states of the $A - 1$ system) to slightly above the real axis and those above the Fermi energy (the states of the $A + 1$ system) to slightly below the real axis.

In our spectral representation of the single-particle Green's function (71) we assumed that the spectra of the many-body system are defined in terms of discrete energies $E_\gamma^{(A+1)}$. This is true of course only for systems confined to a finite space. For infinite systems, the energy spectra are continuous and it is more appropriate to introduce the so-called hole and particle spectral functions defined by

$$
\begin{aligned}
S_{\mathrm{h}}(k, \omega) &= \frac{1}{\pi} \mathrm{Im} g(k, \omega), \quad \text{for } \omega \leq \epsilon_{\mathrm{F}} \\
&= \sum_\gamma \left| < \Psi_\gamma^{(A-1)} | a_k | \Psi_0 > \right|^2 \delta \left(\omega - (E_0^A - E_\gamma^{(A-1)}) \right) , \\
S_{\mathrm{p}}(k, \omega) &= \frac{1}{\pi} \mathrm{Im} g(k, \omega), \quad \text{for } \omega > \epsilon_{\mathrm{F}} \\
&= \sum_\gamma \left| < \Psi_\gamma^{(A+1)} | a_k^\dagger | \Psi_0 > \right|^2 \delta \left(\omega - (E_\gamma^{(A+1)} - E_0^A) \right)
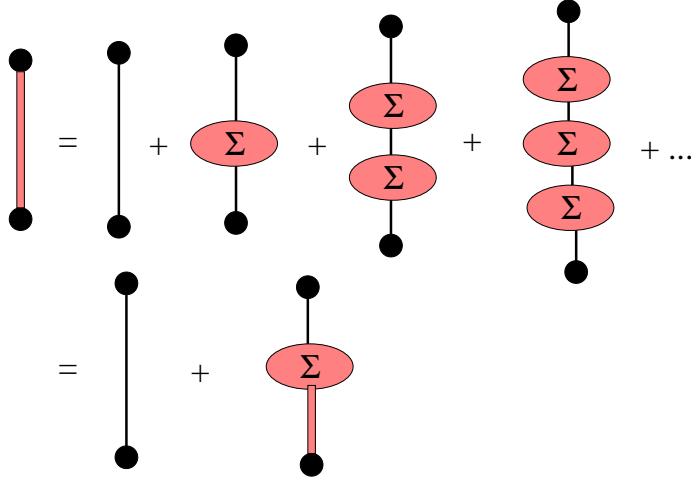\end{aligned} \tag{72}
$$

Figure 10: Classifying the diagrams for the single-particle Green's function in terms of the mass operator Σ and graphical representation of the Dyson equation(78). The thick line represents the "dressed" single-particle Green's function while the thin lines stand for the unperturbed Green's function g_0.

where we have made reference to the case of discrete spectra in the second and fourth lines. These definitions imply that the single-particle Green's function is given in terms of the spectral functions by

$$g(k,\omega) = \lim_{\eta \to 0} \left(\int_{-\infty}^{\epsilon_F} d\omega' \frac{S_h(k,\omega')}{\omega - \omega' - i\eta} + \int_{\epsilon_F}^{\infty} d\omega' \frac{S_p(k,\omega')}{\omega - \omega' + i\eta} \right) . \tag{73}$$

The single-particle Green's function or the spectral functions defining the single-particle Green's function can be used to evaluate observables of the system. As a first example we mention the momentum distribution or momentum density

$$n(k) \ = <\Psi_0|a_k^\dagger a_k|\Psi_0> = \int_{-\infty}^{\epsilon_F} d\omega \, S_h(k,\omega) . \tag{74}$$

The single-particle Green's function allows the evaluation of the expectation value for any single-particle operator O. If we return to the non-diagonal nomenclature used, e.g., in (68) and generalize the definition of spectral functions in a corresponding way, such a calculation is performed via

$$<\Psi_0|O|\Psi_0> = \sum_{\alpha,\beta} \int_{-\infty}^{\epsilon_F} d\omega \, S_h(\alpha\beta,\omega) <\alpha|O|\beta> , \tag{75}$$

with $<\alpha|O|\beta>$ denoting the single-particle matrix element calculated in the basis $\alpha, \beta \dots$. Furthermore, if the interaction between the fermions is a two-body interaction, one can even calculate the energy of the correlated ground state via

$$\begin{aligned} E_0^A &= <\Psi_0|H|\Psi_0> \\ &= \frac{1}{2} \sum_{\alpha,\beta} \int_{-\infty}^{\epsilon_F} d\omega \, S_h(\alpha\beta,\omega) \left(<\alpha|T_{\text{kin}}|\beta> + \omega \delta_{\alpha,\beta} \right) , \end{aligned} \tag{76}$$

with T_{kin} representing the single-particle operator for the kinetic energy.

What remains to be discussed are the tools and approximations used to determine the single-particle Green's function. For that purpose we consider the single-particle Green's function for
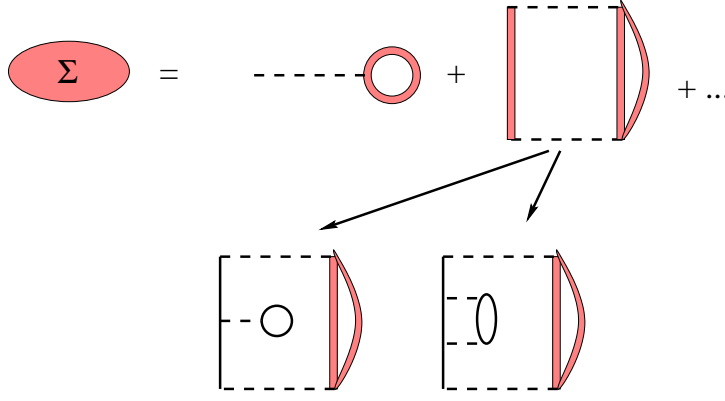
Figure 11: Diagrams contributing to the self-energy Σ. Note that the thick connecting lines represent "dressed" single-particle Green's functions. This means that expanding e.g. the rightmost diagram in the upper line yields among other the terms displayed in the lower part of the figure.

the unperturbed hamiltonian

$$g_0(\alpha\beta, \omega) = \delta_{\alpha\beta} \left\{ \frac{\Theta(\epsilon_\alpha - \epsilon_F)}{\omega - \epsilon_\alpha + i\eta} + \frac{\Theta(\epsilon_F - \epsilon_\alpha)}{\omega - \epsilon_\alpha^{HF} - i\eta} \right\} . \tag{77}$$

and classify all linked diagrams contributing to the expansion for the final, "dressed" single-particle Green's function following the diagrammatic representation in the upper part of Fig. 10. In this figure we group all Feynman diagrams into parts, which are irreducible with respect to the single-particle Green's function (represented by the ellipses Σ) and single-particle Green's function g_0 connecting these irreducible parts. The irreducible self-energy or mass operator Σ contains all diagrams of any order in the interaction H_1 or V, without an intermediate state, which is just a single-particle Green's function. Examples of such contributions are displayed in Fig. 11. Note that here we do not distinguish between particle- and hole-propagation, since the unperturbed Green's function g_0 (see Eq. (77)) as well as the resulting Green's function contains both contributions.

The series displayed in the upper part of Fig. 10 represents the Dyson equation and can be written

$$
\begin{aligned}
g(\alpha\beta, \omega) &= g_0(\alpha\beta, \omega) + \sum_{\gamma\delta} g_0(\alpha\gamma, \omega)\Sigma_{\gamma\delta}(\omega)\Big[g_0(\delta\beta, \omega) \\
&\quad + \sum_{\mu\nu} g_0(\delta\mu, \omega)\Sigma_{\mu\nu}(\omega)g_0(\nu\beta, \omega) + \ldots\Big] \\
&= g_0(\alpha\beta, \omega) + \sum_{\gamma\delta} g_0(\alpha\gamma, \omega)\Sigma_{\gamma\delta}(\omega)g(\delta\beta, \omega) .
\end{aligned}
\tag{78}
$$

Examples of diagrams to be included in the definition of the self-energy are displayed in Fig. 11. The diagram of first order in the interaction V is again the Hartree-Fock contribution. Note that it is defined in terms of the dressed Green's function, which is expressed by the fact that the loop connected to the V interaction line is drawn as a thick line representing the dressed Green's function. This reflects the problem of finding a self-consistent solution of the Hartree-Fock equations. The structure of the single-particle Green's function is identical to the unperturbed one, defined in (77). The only difference is that Hartree-Fock wave functions and energies should be used.

If, however, one goes beyond the Hartree-Fock approximation by including diagrams of higher order in the definition of the self-energy Σ, like e.g. the second term displayed in Fig. 11, the problem of a self-consistent determination of the Green's function gets much more involved. To demonstrate this feature let us consider as a first step this diagram of second order in V, replacing the dressed single-particle Green's functions by the corresponding Hartree-Fock Green's function g_0. This means that the intermediate states in that diagram are given in terms of intermediate 2-particle 1-hole (2p1h) and 2-hole 1-particle (2h1p) states. The corresponding expressions for the self-energy are given by

$$\Sigma_{\alpha\beta}^{(2p1h)}\omega) \;=\; \frac{1}{2} \sum_{\nu<F} \sum_{\rho_1,\rho_2>F} \frac{< \alpha\nu|V|\rho_1\rho_2 >< \rho_1\rho_2|V|\beta\nu >}{\omega - (\epsilon_{\rho_1} + \epsilon_{\rho_2} - \epsilon_\nu) + i\eta} , \tag{79}$$

and

$$\Sigma_{\alpha\beta}^{(2h1p)}(\omega) \;=\; \frac{1}{2} \sum_{\rho>F} \sum_{\nu_1,\nu_2<F} \frac{< \alpha\rho|V|\nu_1\nu_2 >< \nu_1\nu_2|V|\beta\rho >}{\omega - (\epsilon_{\nu_1} + \epsilon_{\nu_2} - \epsilon_\rho)\, i\eta} . \tag{80}$$

If we insert the sum of these two contributions into the Dyson equation (78), we obtain a single-particle Green's function, which exhibits a much richer pole-structure. In fact assuming a discretized space of single-particle states (as we have done also in Eqs. (79) and (80)) one can rewrite the Dyson equation into an eigenvalue problem[82]

$$
\begin{pmatrix}
\epsilon_1 & \dots & 0 & a_{11} & \dots & a_{1P} & A_{11} & \dots & A_{1Q} \\
 & \ddots & & \vdots & & \vdots & \vdots & & \vdots \\
0 & \dots & \epsilon_N & a_{N1} & \dots & a_{NP} & A_{N1} & \dots & A_{NQ} \\
a_{11} & \dots & a_{N1} & e_1 & & & 0 & & \\
\vdots & & \vdots & & \ddots & & & & \\
a_{1P} & \dots & a_{NP} & 0 & & e_P & & & 0 \\
A_{11} & \dots & A_{N1} & & & & E_1 & & \\
\vdots & & \vdots & & & & & \ddots & \\
A_{1Q} & \dots & A_{NQ} & 0 & \dots & 0 & & \dots & E_Q
\end{pmatrix}
\begin{pmatrix}
X_{0,k_1}^n \\
\vdots \\
X_{0,k_N}^n \\
X_1^n \\
\vdots \\
X_P^n \\
Y_1^n \\
\vdots \\
Y_Q^n
\end{pmatrix}
= \omega_n
\begin{pmatrix}
X_{0,k_1}^n \\
\vdots \\
X_{0,k_N}^n \\
X_1^n \\
\vdots \\
X_P^n \\
Y_1^n \\
\vdots \\
Y_Q^n
\end{pmatrix} , \tag{81}
$$

The matrix to be diagonalized contains the Hartree-Fock single-particle energies and the coupling to the P different $2p1h$ configurations, which is described in terms of

$$a_{\alpha i} =< \alpha\nu|V|\rho_1\rho_2 > \tag{82}$$

and Q different $2h1p$ configurations, for which we have introduced the abbreviation

$$A_{\alpha i} =< \alpha\rho|V|\nu_1\nu_2 > . \tag{83}$$

As long as we are still ignoring any residual interaction between the various $2p1h$ and $2h1p$ configurations the corresponding parts of the matrix in (81) are diagonal with elements defined by e_i (E_j) for $2p1h$ $(2h1p)$

$$
\begin{aligned}
e_i &= \epsilon_{\rho_1} + \epsilon_{\rho_2} - \epsilon_\nu \\
E_j &= \epsilon_{\nu_1} + \epsilon_{\nu_2} - \epsilon_\rho ,
\end{aligned}
\tag{84}
$$

where as before the indices ρ_i and ν_i refer to particle and hole states, respectively.
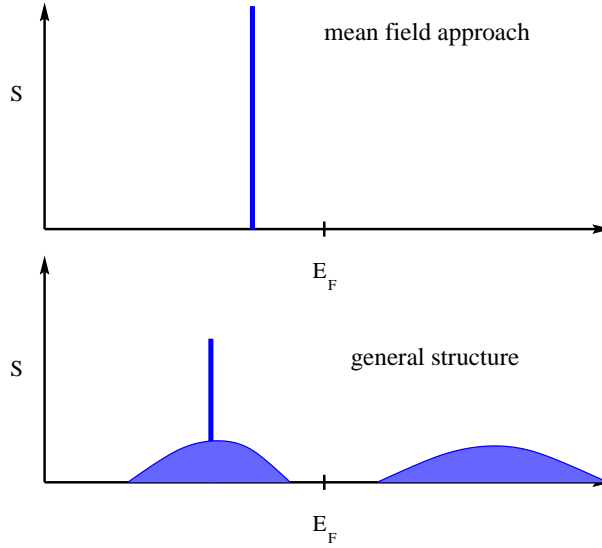
Figure 12: Schematic picture of the spectral function in the mean field approach (upper part) and the general case.

Solving the eigenvalue problem (Eq. (81)) one gets as a result the single-particle Green's function in the Lehmann representation in the discrete basis of the box defined as in (71). The eigenvalues ω_n define the position of the poles of the Green's function

$$
\begin{aligned}
\omega_n &= \left(E_\gamma^{(A+1)} - E_0^A \right) && \text{for} \quad \omega_n > E_F \\
\omega_n &= \left(E_0^A - E_\delta^{(A-1)} \right) && \text{for} \quad \omega_n < E_F
\end{aligned}
\tag{85}
$$

with E_F the Fermi energy for the A-nucleon system. The corresponding spectroscopic amplitudes are given by

$$
\begin{aligned}
< \Psi_0^A | a_{k_i} | \Psi_n^{A+1} > &= X_{0,k_i}^n && for \quad \omega_n > E_F \\
< \Psi_0^A | a_{k_i}^\dagger | \Psi_n^{A-1} > &= X_{0,k_i}^n && for \quad \omega_n < E_F
\end{aligned}
\tag{86}
$$

This multiplicity of the poles is a consequence of going beyond the mean-field approximation. Within the Hartree-Fock or independent particle approach, one can either remove a particle from the orbit j (if this is an orbit below the Fermi energy) or add a particle into this orbit (if j is a state above the Fermi energy). The spectroscopic factor is always one. This is reflected in the mean field approximation to the single-particle Green's function by the feature, that it exhibits for each orbit j exactly one pole with a spectroscopic factor of one. In the approach which we are discussing now this spectroscopic strength gets redistributed as indicated in the schematic picture of Fig. 12. The single-particle peak with strength one in the mean field approach gets reduced to a quasi-particle peak in the spectral function with a strength Z, which is smaller than one. Part of the strength gets redistributed into removal or hole-strength, which is predominantly due to the coupling to $2h1p$ configurations. Another part, however, is shifted to energies above E_F and therefore represents a spectroscopic amplitude for adding a particle. This implies of course that occupation numbers for the various orbits (see (74)) will in general be different from zero and one. Also it is not guaranteed any longer that the total particle number will be conserved, i.e. identical to A the one of the unperturbed state

$$
\int_0^\infty dk\, n(k) \quad \overset{?}{=} A
\tag{87}
$$

28

In order to obtain an approach, which is particle-number conserving, one has to go beyond the approximation which we have discussed sofar and calculate the Green's function in a self-consistent way. General rules for calculational schemes of Green's functions, which conserve symmetries like the property of a fixed particle number have been developed by Baym and Kadanov[83]. For our present purpose it is sufficient to say that one has to evaluate the self-energy Σ, which enters the Dyson equation (78) in a self-consistent way in sofar that the resulting Green's function should be used in the calculation of Σ. This self-consistency requirement is displayed in terms of diagrams in the lower part of Fig. 11.

The realization of this self-consistency requirement has to face a serious problem: Calculating the self-energy Σ in terms of Hartree-Fock Green's functions led to a dressed Green's function which exhibits $L+P+Q$ poles, where L stands for the number of Hartree-Fock states of a given symmetry and P and Q refer to the number of $2p1h$ and $2h1p$ states of this symmetry, respectively. In a next step towards a self-consistent solution, one may consider these Green's functions with $L+P+Q$ poles already in the calculation of the self-energy. This means that one also accounts for coupling to $3p2h$, $3h2p$, $4p3h$ etc. configurations. This implies that the number of poles in the Green's function resulting from this next iteration step will dramatically increase. This "inflation of poles" in the single-particle Green's function can be handled very easily by means of the so-called "BAsis GEnerated by Lanczos" (BAGEL) scheme[82, 84, 85]. In this scheme on represents the Green's function in terms of a few "characteristic" poles in the Lehmann representation. The number of these poles can be kept fixed in the iteration scheme, leading to self-consistency. These pole are determined by solving the eigenvalue Eq. (81) by means of the Lanczos scheme, starting with the single-particle states as appropriate initial vectors. Another possibility is to keep track of the distribution of the spectral strength in a purely numerical way. Corresponding calculations have been performed by van Neck et al. [86] assuming a model-space of finite dimension.

Up to this point we only discussed the determination of the single-particle Green's function assuming an expansion for the self-energy, which is self-consistent in terms of the Green's function but perturbative in terms of the interaction V. From the discussion in the preceeding section we know already that two-body correlations should be included in a non-perturbative way, which means that one should consider all ladder diagrams, when one is calculating e.g. the self-energy Σ. How can this be achieved within the framework of the Green's function approach?

For that purpose one should solve a Dyson equation for the two-particle Green's function. The Lehmann representation of the two-particle Green's function is given in terms of energies and states of the systems with A and $A \pm 2$ particles

$$
\begin{aligned}
g^{II}(\alpha\beta,\gamma\delta;\Omega) \;=\; & \sum_n \frac{<\Psi_0^A|a_\beta a_\alpha|\Psi_n^{A+2}><\Psi_n^{A+2}|a_\gamma^\dagger a_\delta^\dagger|\Psi_0^A>}{\Omega - (E_n^{A+2} - E_0^A) + i\eta} \\
& - \sum_m \frac{<\Psi_0^A|a_\gamma^\dagger a_\delta^\dagger|\Psi_m^{A-2}><\Psi_m^{A-2}|a_\beta a_\alpha|\Psi_0^A>}{\Omega - (E_0^A - E_m^{A-2}) - i\eta} \; .
\end{aligned}
\tag{88}
$$

The result for the noninteracting product of dressed propagators, including the exchange contribution reads

$$
\begin{aligned}
g_f^{II}(\alpha\beta,\gamma\delta;\Omega) \;=\; & i\int \frac{d\omega}{2\pi} \left\{ g(\alpha,\gamma;\omega)g(\beta,\delta;\Omega-\omega) - g(\alpha,\delta;\omega)g(\beta,\gamma;\Omega-\omega) \right\} \\
=\; & \sum_{m,m'} \frac{<\Psi_0^A|a_\alpha|\Psi_m^{A+1}><\Psi_m^{A+1}|a_\gamma^\dagger|\Psi_0^A><\Psi_0^A|a_\beta|\Psi_{m'}^{A+1}><\Psi_{m'}^{A+1}|a_\delta^\dagger|\Psi_0^A>}{\Omega - \{(E_m^{A+1} - E_0^A) + (E_{m'}^{A+1} - E_0^A)\} + i\eta} \\
& - \sum_{n,n'} \frac{<\Psi_0^A|a_\gamma^\dagger|\Psi_n^{A-1}><\Psi_n^{A-1}|a_\alpha|\Psi_0^A><\Psi_0^A|a_\delta^\dagger|\Psi_{n'}^{A-1}><\Psi_{n'}^{A-1}|a_\beta|\Psi_0^A>}{\Omega - \{(E_0^A - E_n^{A-1}) + (E_0^A - E_{n'}^{A-1})\} + i\eta}
\end{aligned}
$$

$$-(\gamma \longleftrightarrow \delta) \tag{89}$$

The integration in the first line of this equation can be performed by employing the Lehmann representation for the single-particle Green's functions. The ladder approximation to the two-particle propagator (88) is then given by:

$$
\begin{aligned}
g_L^{II}(\alpha\beta, \gamma\delta; \Omega) &= g_f^{II}(\alpha\beta, \gamma\delta; \Omega) \\
&+ \frac{1}{4} \sum_{\epsilon\eta\theta\zeta} g_f^{II}(\alpha\beta, \epsilon\eta; \Omega) < \epsilon\eta|V|\theta\zeta > g_L^{II}(\theta\zeta, \gamma\delta; \Omega).
\end{aligned} \tag{90}
$$

This ladder approximation for the two-particle Green's function can then be used to define the self-energy Σ in a non-perturbative way[14]. The Dyson equations (90) and (78) for the two-body and one-body Green's function have to be solved in a self-consistent manner, this procedure has been named Self-Consistent Green Function formalism (SCGF) and has been extensively discussed in Ref. [14].

2.4 *Variational Method and Correlated Basis Function*

An efficient way to handle the correlations induced by the NN-interaction is to embody them, from the very beginning, in a trial wave function Ψ_T, which describes the system of A nucleons

$$\Psi_T(1, ..., A) = F(1, ..., A)\Phi_{MF}(1, ..., A), \tag{91}$$

where Φ_{MF} is a mean field wave function corresponding to the uncorrelated system and the operator F is intended to take care of the dynamical correlations.

Once a trial wave function is defined, the variational principle ensures that if we are capable to calculate the expectation value of the nuclear hamiltonian

$$\frac{\langle \Psi_T \mid H \mid \Psi_T \rangle}{\langle \Psi_T \mid \Psi_T \rangle} = E_T, \tag{92}$$

then E_T will be an upperbound to the ground state energy, E_0. Parameters in the variational wave function are varied to minimize E_T and the best Ψ_T can then be used to evaluate other observables of interest. Obviously, for the method to be efficient, the trial wave function must give a good representation of the real ground state many-body wave function. Although conceptually it looks very simple, the evaluation of the expectation value is by no means an easy task and very sophisticated algorithms which require large computer capabilities have been devised during the last years.

Therefore the ingredients for a variational calculation are the hamiltonian and the wave function. In addition, one requires an efficient machinery to evaluate the expectation value. By the definition of the trial wave function, which is given in configuration space, the variational method is tailored for a non-relativistic framework where the only constituents are the nucleons, interacting through a local NN interaction with no energy or momentum dependence. A realistic interaction based on the exchange of mesons between the nucleons would be naturally given in momentum space, being non-local and energy dependent [2, 3]. There are, however, realistic interactions which are specially suitable for variational calculations [5, 4].

Following these guidelines, one can write a realistic nuclear hamiltonian in the form:

$$H = -\frac{\hbar^2}{2m} \sum_i \nabla_i^2 + \sum_{i<j} V_{ij} \tag{93}$$

where the two-body potential V_{ij} has a local operatorial structure, i.e. is given by the sum of functions depending on the relative distance between the nucleons and spin-isospin operators build according to invariance requirements. Although we devote a full section to discuss different modern realistic potentials, it is convenient at this point to make some comments on the potentials usually employed in variational calculations. For instance, the Argonne V_{14}[4] NN potential is given by the sum of 14 isoscalar terms

$$V_{ij} = \sum_{p=1,14} V_p(r_{ij})O_{ij}^p, \tag{94}$$

with

$$O_{ij}^{p=1,14} = \left[1, \vec{\sigma}_i \cdot \vec{\sigma}_j, S_{ij}, \mathbf{L} \cdot \mathbf{S}, \mathbf{L}^2, \mathbf{L}^2 \vec{\sigma}_i \cdot \vec{\sigma}_j, (\mathbf{L} \cdot \mathbf{S})^2\right] \otimes \left[1, \vec{\tau}_i \cdot \vec{\tau}_j\right], \tag{95}$$

Here

$$S_{ij} = 3(\vec{\sigma}_i \cdot \hat{r}_{ij})(\vec{\sigma}_j \cdot \hat{r}_{ij}) - \vec{\sigma}_i \cdot \vec{\sigma}_j \tag{96}$$

is the usual tensor operator, $\mathbf{L}$ is the relative orbital angular momentum , and $\mathbf{S}$ is the total spin of the pair.

The radial components of the potential contain a long range part which is given by a static nonrelativistic reduction of the one pion exchange potential (OPE) which contributes only to the $(\vec{\sigma}_i \cdot \vec{\sigma}_j)(\vec{\tau}_i \cdot \vec{\tau}_j)$ and $S_{ij}(\vec{\tau}_i \cdot \vec{\tau}_j)$. The intermediate and short range parts are given in terms of a physically plausible parameterization with a reasonable number of adjustable parameters.

However, these accurate NN potentials do not satisfactorily reproduce the nuclear matter saturation point and underbind nuclei with $A > 2$ [15]. As discussed in the introduction, a possible reason for that is the existence of three body forces which can have different origins. We will come back to the problem of three body forces, but here it is important to keep in mind that the nuclear hamiltonian can certainly have an additional term with three body forces. Usually the recent realistic variational calculations include also a three body force in the nuclear hamiltonian, which is constructed in largely phenomenological fashion with parameters determined to reproduce the saturation of nuclear matter and the correct binding energy for $A = 3, 4$ nuclei.[87]

There is also an updated version of the Argonne potential which breaks charge independence and charge symmetry and contains some additional isotensor and isovector components, responsible for the breaking of the isospin symmetries. This version of the two-body Argonne potential contains in total 43 parameters and an operatorial structure up to 18 operators, it is known as the Argonne v_{18} NN potential [89].

Once the realistic hamiltonian has been defined, which for the time being we suppose to have only two body forces, we need an ansatz for the variational wave function. At this point, we should appeal to the physical intuition and sense in order to choose an appropriate trial wave function for the system under consideration. In the nuclear case, i.e. for nuclei and for nuclear matter around saturation, the density is small enough to assume that two body correlations will be the most relevant ones. A form of $F(1, 2, ..., A)$ that has shown to be suitable for nuclear systems is

$$F(1, ..., A) = S \left[\prod_{i<j} F_2(i, j)\right] \tag{97}$$

i.e. a symmetrized product of two-body correlation operators, $F_2(i, j)$. The natural choice is to allow the two-body correlation operator to have a similar structure as the two-body NN interaction. In recent calculations, the ansatz for the two body correlation operator F contains the same set of operators as in Eq. (95) except the quadratic terms in the relative angular momentum,

$$F_2(i, j) = \sum_{m=1,8} f^{(m)}(r_{ij})O_{i,j}^{(m)}, \tag{98}$$

31

where the sum runs up to the spin-orbit components in Eq. (95).

When the components of the correlation operator with $m \geq 2$ are disregarded, one recovers the well known Jastrow correlation function [90] , which has been largely used in the context of quantum liquids [91] and also in nuclear physics for simple semi-realistic interactions [92].

The mean field wave function $\Phi_{MF}(1, .., A)$ is a Slater determinant of single particle wave functions, $\varphi_\alpha(i)$, where subscript α stands for the set of quantum numbers characterizing the single particle state, and (i) indicates the spatial and spin-isospin variables of particle (i). Those single particle wave functions are obtained by some mean field (MF) potential, which can be completely arbitrary. In the particular case of symmetric and spin and isospin saturated nuclear matter, the mean field wave function is a Slater determinant of plane waves:

$$\Phi_{MF}(1, 2, ..., A) = Det_{ij} \left[exp(i\mathbf{k}_i \cdot \mathbf{r}_j) \chi_i^S(j) \chi_i^T(j) \right], \tag{99}$$

with all single particle momentum states $\mathbf{k}_i$ occupied up to the Fermi momentum $k_F = (6\pi^2 \rho/d2)^{1/3}$, where d is the spin-isospin degeneracy of each particle level, $d = 4$ for nuclear matter and $d = 2$ for neutron matter. $\chi_i^S(j)$ and $\chi_i^T(j)$ are the spin and isospin functions. The mean field wave function (Φ_{MF}) is intended to carry the correct quantum statistics and any of the required symmetries of the system. As the mean field wave function has already the correct antisymmetric character, the correlation operator requires the presence of a symmetrizer operator S (Eq. (97)) to preserve the correct symmetry behavior of the trial wave function. Obviously in the case that the different two-body correlations commute with each other, as it would be the case for a simple Jastrow correlation, the presence of the symmetrizer is superfluous.

Besides being symmetric in all the variables, the correlation operator possesses the cluster decomposition property, namely that upon separating one subgroup of particles $(1, 2, ..., n)$ far from the rest $(n + 1, n + 2, ..., A)$, the operator $F(1, 2, ..., A)$ decomposes into a product

$$F(1, ..., A) = F^{(n)}(1, ..., n) F^{A-n}(n + 1, ..., A). \tag{100}$$

According to the clusterization property, the scalar component $f^{(p=1)}(r)$ in (98) heals to unity when r is large whereas $f^{(p \neq 1)}(r) \to 0$.

A realistic trial wave function is expected to give an upperbound very near to the ground state energy and a wave function close to the ground state wave function. The radial correlation functions $f^{(m)}(r)$ are determined by minimizing the energy, E_T. However, the minimization of the expectation value of the hamiltonian respect to arbitrary variations of $f^{(m)}(r)$

$$\frac{\delta}{\delta f^{(m)}} \frac{\langle \Psi_T \mid H \mid \Psi_T \rangle}{\langle \Psi_T \mid \Psi_T \rangle} = 0 \tag{101}$$

is a highly prohibitive job in the nuclear case. In practice, the correlations are either parameterized and the parameters fixed by minimization or they are generated by solving a set of coupled differential equations obtained by minimizing the energy obtained in a two-body cluster expansion.

Once the hamiltonian and the trial wave function are defined, one should be able to calculate the expectation value. The most efficient techniques are Fermi-Hyper-Netted- Chain (FHNC) theory and Variational Monte Carlo (VMC) method (to be discussed in the next sub-section). FHNC is an integral equation method that sums up series of clusters diagrams associated with the distribution functions of the many-body wave function. The method is suitable for infinite homogeneous systems as well as for finite, inhomogeneous systems. In fact, the expectation value of the hamiltonian (or any other operator) is written in terms of n-body densities,

$$\rho_1 = \frac{\langle \Psi_T \mid \sum_i \delta(\mathbf{r} - \mathbf{r}_i) \mid \Psi_T \rangle}{\langle \Psi_T \mid \Psi_T \rangle}, \tag{102}$$

$$\rho_2^{(p)}(1,2) = \frac{\langle \Psi_T \mid \sum_{i \neq j} \delta(\mathbf{r}_i - \mathbf{r}_1)\delta(\mathbf{r}_j - \mathbf{r}_2)O_{ij}^p \mid \Psi_T \rangle}{\langle \Psi_T \mid \Psi_T \rangle}. \tag{103}$$

The densities are then cluster expanded in terms of dynamical correlations $h(r) = \left[f^{(1)}(r) \right]^2 - 1$, products $f^{(1)}(r)f^{(p \geq 2)}(r)$, and statistical correlations, $\rho_0(i,j) = \sum_\alpha \phi_\alpha^\dagger(i)\phi_\alpha(j)$, associated to the exchanges in the mean field wave function. The terms of the resulting expansions are usually called cluster terms and are characterized by integrals containing a given number of correlations, and exchange functions joining the correlated particles. In the early calculations, the expansion was stopped at low orders [90, 94, 95, 96]. A great progress in the summation of the cluster expansion was achieved by realizing that the cluster terms are conveniently represented by cluster diagrams [97, 98] and by paying attention to the enormous amount of cancelations between the different terms of the cluster expansion. A crucial step towards the summation was the proper classification of the different cluster terms, i.e. diagrams. Finally, a close set of equations for Fermi systems represented by a wave function containing two-body Jastrow factor were derived [99, 100]. In this way, the uncertainties associated to a low order expansion were removed to a large extent. The restriction of the FHNC equations to Bose systems is equivalent to the earlier HNC equations used to calculate distribution functions in the context of classical theory of liquids [101].

Rules for constructing the different topological diagrams and derive the FHNC equations to sum up the different sets of diagrams have been given several times in the literature, here we refer the reader to two recent reviews of Fabrocini and Fantoni where they give in a very clear and pedagogical way the derivation of the FHNC equations for both, state independent and state depedent correlations, homogeneous and inhomogeneous systems[17, 93]. A review which contains an extensive analysis on the different low order cluster expansions and a very detailed derivation of the FHNC equations with special attention to the different treatment of the exchange terms [99, 100] is the one of Clark in an earlier volume of this series [92]. In that review one can also find results for nuclear matter with simple semi-phenomenological potentials that do not require the full operatorial structure of the two-body correlations.

For brevity, here we only illustrate the main ideas of the HNC summations by considering the case of a system of bosons, interacting through a potential that depends only on the distance between the particles. This example corresponds to a realistic situation in the context of Condensed Matter, i.e. to liquid ^{4}He at zero temperature. In that case the inter-atomic potential is much simpler than the NN interaction, in the sense that it depends only of the distance between the atoms. However, as in the NN interaction, it has a strong repulsion at short distances and weak atraction at medium and large distances. A good representation of the interatomic potential is given by the Lennard-Jones potential,

$$V(r) = 4\epsilon \left[\left(\frac{\sigma}{r} \right)^{12} - \left(\frac{\sigma}{r} \right)^6 \right], \tag{104}$$

where $\epsilon = 10.22$ Kelvin (K) ($1eV \sim 11000K$) and $\sigma = 2.556$ Angstrøm define the energy and length scales, respectively. In that case, the non interacting system would be described by a wave function with all atoms in the state of zero momentum, i.e. there is a macroscopic occupation of a single particle quantum state. This phenomenon is known as Bose-Einstein condensation. When the interactions is turned on, the correlations induced by the interaction lead to atoms in states with momentum different from zero. However, the liquid ^{4}He still shows a condensate fraction, i.e. a ratio between the number of atoms in the zero momentum state and the total number of atoms, of around 10%.
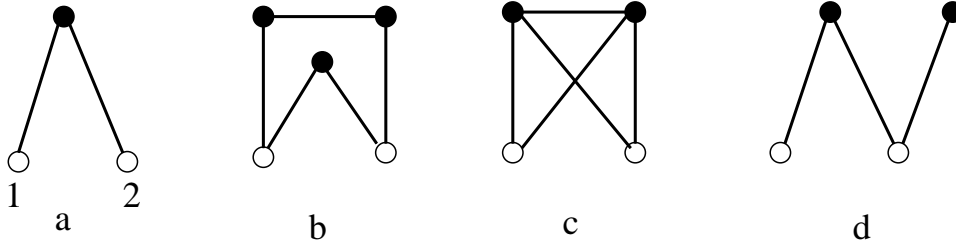
Figure 13: Different HNC diagrams which appear in the calculation of the distribution function, $g(r_{12})$

A convenient trial wave function to describe this system is given by a Jastrow wave function:

$$\Psi(1, 2, ...A) = F(1, 2, ..., A) = \prod_{i<j} f(r_{ij}), \qquad (105)$$

a product of two body correlations depending only on the distance between the particles. We work in the thermodynamical limit, allowing $N \to \infty$ and the volume $\Omega \to \infty$ but keeping the density $\rho = N/\Omega$ constant. In this limit, the energy per particle is given by:

$$e(\rho) = \frac{1}{2}\rho \int d^3r\, g(r) \left[V(r) - \frac{\hbar^2}{2m_4}\nabla^2 \ln\, f(r) \right] \qquad (106)$$

where $g(r)$ is the distribution function:

$$g(r) \equiv \frac{\rho_2^{(1)}(1, 2)}{\rho^2} = \frac{A(A-1)}{\rho^2}\frac{\int |\Psi|^2\, d^3r_3...d^3r_A}{\int |\Psi|^2\, d^3r_1...d^3r_A} \qquad (107)$$

which gives the probability to find two particles separated by a distance r, and is normalized such that

$$\rho \int d^3r[g(r) - 1] = -1. \qquad (108)$$

This condition can be used as an accuracy check of the approximations implemented in the calculation of $g(r)$. In this way, the problem to calculate the energy per particle is now translated in into the calculation of the distribution function. Now, the numerator and the denominator of Eq. (107) are expanded in powers of the correlation interaction, defined as $h(r) = [f(r)]^2 - 1$,

$$g(r) = \frac{A(A-1)}{\rho^2}\frac{f^2(r_{12})\, \int d^3r_3...d^3r_A\, (1 + \sum h(r_{ij}) + \sum h\, h + ...)}{\int d^3r_1...d^3r_A\, (1 + \sum h(r_{ij}) + ...)} \qquad (109)$$

The terms of the resulting expansion are characterized by integrals containing a given number of functions h. Now it is very useful to introduce a diagrammatic notation. This allows to classify the integrals according to their diagrammatic representation. The cluster diagrams are built employing the following simple rules: Their basic blocks are points and solid lines. Points (vertices) represent the coordinate $\mathbf{r}_i$ of a generic i-particle. Solid points (internal points) imply integration over the coordinates times a factor ρ, circles (external points) refer to particles labeled 1 and 2, and we do not integrate over their coordinates. Solid lines are correlation factors and can not be superimposed. Notice that in the diagrams of the denominator, all vertices are solid points.

In Fig. 13 we give several examples of diagrams appearing in the numerator of Eq. (109), for which the expressions are given by

$$Diagram(a) = \rho \int d^3r_3 h(r_{13}) h(r_{23}) , \qquad (110)$$

$$Diagram(b) = \rho \int d^3r_3 d^3r_4 d^3r_5 h(r_{13}) h(r_{14}) h(r_{23}) h(r_{24}), \qquad (111)$$

and

$$Diagram(c) = \rho^2 \int d^3r_3 d^3r_4 h(r_{13}) h(r_{14}) h(r_{34}) h(r_{24}) h(r_{23}). \qquad (112)$$

Cluster diagrams may be linked or unlinked. Unlinked diagrams have at least two parts with no common points. They can not be drawn without separating the pen from the paper. The linked diagrams can be classified in reducible and irreducible diagrams. The reducible diagrams are those which can be factorized in a product of two or more irreducible diagrams such that one of them contains the two external points. Diagram (d) of Fig. 13 is a reducible diagram. In the infinite systems the reducibility is closely connected to the translationally invariance character of the correlations. The irreducible diagrams are then classified into: *Nodal* (N), *Composite* (X) and the remaining ones called *elementary*. The *nodal* diagrams have at least one node, that is an internal point such that all ways of going from one 1 to 2 (the two external points) should go through it. The composite diagrams are those having two or more (12)-sub-diagrams. Where and (ij)-sub-diagram is a part of the diagram connected to the rest only through the points i and j. Diagrams a,b,c and d of Fig. 13 are examples of nodal, composite, elementary and reducible, respectively. There are two mathematical operations related to the construction of diagrams: the convolution product linked to the construction of nodal diagrams

$$(a(r_{1i}) \mid b(r_{i2})) = \rho \int d^3r_i a(r_{1i}) b(r_{i2}) \qquad (113)$$

and the algebraic product $(a(r_{ij}) b(r_{ij}))$ for the composite diagrams.

In evaluating the distribution function Eq. (109) one can take advantage of a lot of cancellations between the different terms. The expansion is linked and in addition in the thermodynamical limit, for the specific case of bosons, is irreducible up to terms of the order $1/N$. For homogeneous Fermi systems with Jastrow correlations, the expansion is fully irreducible. However, for state dependent correlations the cluster expansion is not irreducible, i.e. one should consider vertex corrections. In case of finite systems, both for fermions and bosons the cluster expansion is not irreducible [93].

The irreducible diagrams are summed up by means of the HNC equation, which allows for an iterative process to sum the nodal ($N(r)$) and composite ($X(r)$) diagrams once the sum of the elementary diagrams ($E(r)$) is given. The HNC equation is a non-linear integral equation relating the function $N(r)$ and $X(r)$

$$(X(r_{1i}) \mid N(r_{i2})) = N(r_{12}) - (X(r_{1i}) \mid X(r_{i2})), \qquad (114)$$

i.e., doing the convolution product (associated to the construction of nodal diagrams) of X(r) and N(r) we get all nodal diagrams except the ones corresponding to $(X(r_{1i}) \mid X(r_{i2}))$. This equation can be written also in momentum space as

$$\tilde{N}(k) = \frac{\tilde{X}(k)^2}{1 - \tilde{X}(k)} \qquad (115)$$

where the Fourier transform of a given function $a(r)$ is defined as

$$\tilde{a}(r) = \rho \int d^3r e^{i\vec{k}\cdot\vec{r}} a(r). \qquad (116)$$

35

The composite diagrams are given by

$$X(r) = f^2(r)e^{N(r)+E(r)} - 1 - N(r), \tag{117}$$

while the distribution function is expressed as

$$g(r) = f^2(r)e^{N(r)+E(r)} = 1 + X(r) + N(r) \tag{118}$$

The HNC integral equation (Eq. (115)) suggests an iterative process to calculate $g(r)$. At the first iteration , $X(r) = h(r)$, then the HNC equation is used to construct the first chain of diagrams. After a Fourier transformation to r-space, the resulting function $N(r)$ is used to define the new $X(r)$ (Eq. (117)). The number of diagrams summed in this way grows tremendously and in a few iterations one reaches convergence. However, there is a problem with the elementary diagrams, entering in the definition of $X(r)$, i.e. the HNC iterative process sums up all nodal and composite diagrams , once the sum of the elementary diagrams is known. In this sense, the function $E(r)$ is an input for solving the HNC equation. There is no exact method to compute this function and approximations are necessary. The simplest option, is to take $E(r) = 0$, known as HNC/0. Actually, this approximation is appropriate for nuclear systems, where the density is not very high.

The Fourier transform of the radial distribution function defines the static structure function $S(k)$,

$$S(k) = 1 \ + \ \rho \int d^3r \, [g(r) - 1] \tag{119}$$

which in the case of quantum liquids is experimentally accessible by means of elastic neutron scattering against the liquids [102]. The condition of Eq. (108), implies $S(0^+) = 0$ at zero temperature. When $k \to \infty$ then $S(k) \to 1$.

A two body correlation appropriate for the Lennard-Jones potential which has been largely used in the literature of quantum liquids is the McMillan form

$$f(r) = e^{-\frac{1}{2}\left[\frac{b\sigma}{r}\right]^5}. \tag{120}$$

This correlation function together with the corresponding distribution function are shown in Fig. 14 at the ^{4}He saturation density $\rho_0 = 0.365\sigma^{-3}$ in the HNC/0 approximation (i.e. by neglecting the elementary diagrams). The correlation function (Eq. (120)) avoids the configurations where the two particles are close enough to feel the strong repulsion of the potential. Finally, the distribution function has a hole at the origin, and the probability to find two particles at short distances is strongly depleted. The system minimizes its energy by favoring distances between the particles (maximum of g(r)) near to the maximum depth of the potential. At the same time, the "holes" in the wave function yield an increment of the kinetic energy, which was zero in the uncorrelated system. At the end, there is a delicate balance between the potential and the kinetic energy which results in the binding energy of the ^{4}He atoms to be $-7.17K$ at the saturation density, while the kinetic energy and the potential energy are $T \sim 14K$ and $V \sim 21K$. These arguments of the short range correlations apply equally well to the nuclear case, and as we will discuss below, the final binding energy is also a delicate balance between potential and kinetic energy. The short range correlations are responsible for an increment of the kinetic energy with respect to the kinetic energy of the uncorrelated system, which in the case of nuclear matter is given by $3\hbar^2 k_F^2/10m$, the average kinetic energy of the underlying free Fermi sea. Before leaving this example completely it is worth to mention that the HNC theory can treat at the same time short- and long-range correlations consistently
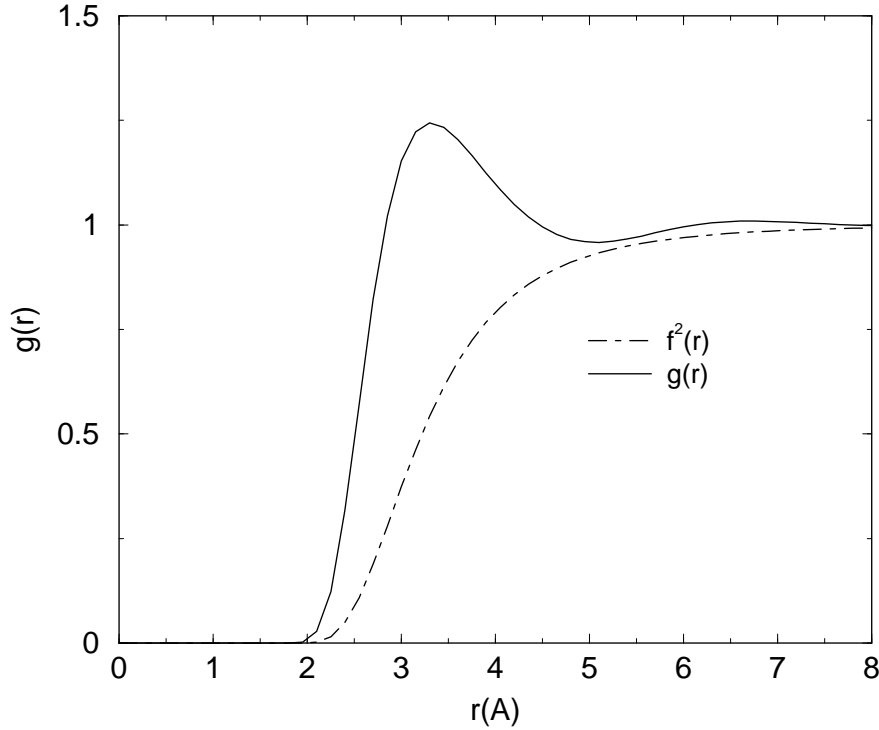
Figure 14: Two body correlation function (dot-dashed line) and the corresponding $g(r)$ calculated in HNC/0 at the experimental saturation density of liquid ^{4}He

[103], when instead of just using a short-range correlation function, one considers the optimal correlation, solution of

$$\frac{\delta}{\delta f} \frac{\langle \Psi_T \mid H \mid \Psi_T \rangle}{\langle \Psi_T \mid \Psi_T \rangle} = 0 \tag{121}$$

This optimal correlation has a long range behavior , that translates in the right limit of $S(k)$ at low k, $S(k) \sim \hbar k / 2m v_s$, being m the mass of the atoms and v_s the speed of sound. This behavior reflects the phonon nature of the low energy spectrum of an interacting boson system.

In the case of Fermi systems, the anti-symmetrization implied by the Pauli principle, incorporates statistical correlations to the cluster expansions, i.e. to the diagrams. In the case of homogeneous systems, the statistical correlations are accounted for by the Slater function $l(k_F r_{ij})$,

$$\rho_0(i,j) = l(x = k_F r_{ij}) = \frac{3}{x^3} \left[\sin(x) - x \, \cos(x) \right] \tag{122}$$

This Slater function, defines the distribution function for a free Fermi sea,

$$g(r) = 1 - \frac{1}{d} l^2(k_F r). \tag{123}$$

To take care of all topological different diagrams, we need to introduce new nodal and composite functions, which are related by a system of coupled non-linear integral equations (FHNC) [99, 100]. Once the FHNC equations are solved one can easily calculate the energy. The presence of the symmetrizer in the correlation operator and the non-commutativity of the operators involved in the correlations makes it very difficult to sum up all the contributions in the case of state dependent correlations. Actually, no scheme has been devised so far, which keeps track of all possible terms. A complete FHNC summation is possible only for the

Jastrow component. However, partial classes of diagrams containing operatorial correlations may exactly be summed by the Single Operator Chain approximation (FHNC/SOC)[104]. The FHNC/SOC integral equations sum all the nodal diagrams containing only one operatorial correlation per internal side, in addition to all the Jastrow correlated clusters. By computing its leading corrections, the estimated accuracy of the FHNC/SOC approximation has been set to $\sim 1\,\mathrm{MeV/A}$ for nuclear matter at saturation density [105]. The FHNC/SOC has been applied to study the equation of state of nuclear and neutron matter [15], including three body terms in the hamiltonian. It is very difficult to apply the variational formalism with state dependent correlations to study asymmetric nuclear matter with an arbitrary asymmetry $x = \rho_p/\rho$ and all the calculations, which are then later on used to study $\beta-$stable matter, are based in quadratic parameterizations of the correlation energy

$$E(\rho, x) = T_F(\rho, x) + V_0(\rho) + (1 - 2x)^2 V_2(\rho) \tag{124}$$

where

$$T_F(\rho, x) = \frac{3}{5}\frac{\hbar^2}{2m}(3\pi^2\rho)^{2/3}\left[x^{5/3} + (1 - x)^{5/3}\right] \tag{125}$$

is the kinetic energy of the asymmetric Fermi sea and V_0 and V_2 are related to the correlation energy of neutron and nuclear matter. In this parameterization, the symmetry energy of nuclear matter is

$$E_s(\rho) = \frac{1}{8}\frac{\partial^2 E(\rho, x)}{\partial x}\Big|_{x=1/2} = \frac{5}{9}T_F(\rho, 1/2) + V_2(\rho). \tag{126}$$

The extension of the FHNC/SOC to finite nuclei is an important issue in order to have a systematic study with the same basic tools for nuclei and nuclear matter. After the first efforts based on low order cluster expansions [106, 107], the FHNC formalism was extended to doubly closed shell nuclei, both in ls and jj coupling schemes, using Jastrow correlated wave functions [108, 109, 110] and semi-realistic interactions [111]. Very recently, the FHNC/SOC has been generalized to deal with realistic potentials and state dependent correlations, with non-central components for double closed shell nuclei as ^{16}O and ^{40}Ca [112, 113]. The most complete calculations [113] deal with the Argonne V_{14},[4] supplemented with the Urbana VII model of the three-body interaction[88]. The two-body correlation function includes operators up to tensor components in Eq. (98) and the single particle wave functions were taken from a Woods-Saxon mean field potential. The results are rather promising and one can conclude that now a days the calculations in finite nuclei with realistic interactions have achieved the same degree of accuracy than in nuclear matter.

As we have already mentioned, a full minimization of the variational energy respect to arbitrary variations of $f^{(p)}(r)$ is impossible. The correlations, in the most sophisticated calculations, both in nuclear matter and finite nuclei, are generated by solving a set of coupled Euler-Lagrange equations obtained by minimizing the second order cluster expansion of the energy. The differential equations are solved with the boundary conditions:

$$f^{(p=1)}(r \geq d^{(p=1)}) = 1, \tag{127}$$

and

$$f^{(p>1)}(r \geq d^{(p>1)}) = 0, \tag{128}$$

where $d^{(p)}$ are the healing distances in each correlation channel. To ensure the continuity of the first derivative of the correlations

$$\frac{\partial f^{(p)}}{\partial r}\Big|_{r=d^{(p)}} = 0 \tag{129}$$

one introduces Lagrange multipliers $\lambda^{(p)}$ which are varied to satisfy the condition of the above equation.

Some additional variational parameters are introduced because the second order minimization is actually performed by using a "quenched" potential

$$\bar{v}_{ij} = \sum \alpha^{(p)} v^{(p)}(r_{ij}) \hat{O}^{(p)}. \tag{130}$$

These quenching parameters $\alpha^{(p)}$ are interpreted as representing medium effects. In this way the two body correlations contain several variational parameters

$$F_{ij} = \sum_{p=1,8} f^{(p)}(r_{ij}; d^{(p)}, \alpha^{(p)}) O_{ij}^{(p)} \tag{131}$$

which will be determined by energy minimization. The number of parameters is reduced in a drastic way by taking all the healing distances equal $d^{(p)} = d_c$, except those associated to the tensor channels d_t. The quenching factors are typically assumed to be 1 for the scalar channels and those containing L^2, while all other channels are quenched by the same amount $\alpha^{(p)} = \alpha$ [15, 114].

A main drawback of a variational calculation is that even if the expectation value of the hamiltonian is evaluated exactly for a given trial wave function, one has only un upper-bound on the exact energy and an approximation to the exact many body wave function. The way to proceed further is provided by the Correlated Basis Function (CBF) Method, which was introduced nearly forty years ago by Feenberg and his collaborators [91, 115]. Several people have contributed later on to make the method efficient and competitive, pushing its applications to very different physical systems [17, 116]. The CBF method provides the general frame to systematically improve on a trial wave function by introducing a complete set of correlated basis functions. The idea is to perform a perturbation theory built on such correlated basis, with the hope that the correlated basis states are close enough to the eigenstates of the hamiltonian that a lower order in the perturbation theory will be sufficient to take care of these small differences.

The set of correlated basis states Ψ_n, is built by applying the many-body correlation operator, $F(1, 2, ..., A)$, usually determined in the variational calculation, to model basis functions, ϕ_n,

$$\Psi_n(1, 2, ..., A) = F(1, 2, ..., A) \phi_n(1, 2, ..., A). \tag{132}$$

The zero order of the CBF theory, i.e. taking only one basis function, reduces to the variational procedure. Therefore it is crucial to have a good variational description of the ground state in order to have a fast convergence of the perturbative series. The model function ϕ_0 is also used to define the Fermi level and as before particle states above and hole states below this Fermi level. The model states ϕ_n refer then to some particle-hole configuration with respect to ϕ_0.

In order to perform perturbation theory we need to decompose the hamiltonian in an unperturbed hamiltonian H_0 and a perturbation H_I,

$$H = H_0 + H_I. \tag{133}$$

Here they are defined in terms of matrix elements of H in the correlated basis $| i \rangle$. The diagonal matrix elements

$$E_i^v = \frac{\langle i | H | i \rangle}{\langle i | i \rangle} \tag{134}$$

define the unperturbed hamiltonian:

$$\langle i | H_0 | j \rangle = \delta_{i,j} E_i^v \tag{135}$$

while H_I is given by

$$\langle i \mid H_I \mid j \rangle = (1 - \delta_{i,j}) \frac{\langle i \mid H \mid j \rangle}{\langle i \mid j \rangle}. \tag{136}$$

By construction the diagonal matrix elements of H_I are zero and therefore there are no first order terms in the perturbation expansion.

A main characteristic of the CBF theory is the non-orthogonality of the basis,

$$N_{ij} = \frac{\langle i \mid j \rangle}{(\langle i \mid i \rangle \langle j \mid j \rangle)^{1/2}} \neq \delta_{i,j}. \tag{137}$$

Therefore, it is necessary to use non-orthogonal perturbation theory [117]. The perturbative correction to E_0^v, in a non-orthogonal basis is given by [117]

$$\begin{aligned}
\Delta E_0 = E_0 - E_0^v &= \sum_{p \neq 0} \frac{W_{0p}(0) W_{p0}(0)}{E_0 - E_p^v} \\
&+ \sum_{q \neq p \neq 0} \frac{W_{0p}(0) W_{pq}(0) W_{q0}(0)}{(E_0 - E_p^v)(E_0 - E_q^v)} + \dots
\end{aligned} \tag{138}$$

Due to the non-orthogonality of the basis, the interaction $W_{ij}(0)$ contains the overlap matrix element N_{ij},

$$W_{ij}(0) = H_{ij} - E_0 N_{ij} \tag{139}$$

and carries an additional energy dependence, besides the one coming from the denominators.

To eliminate the unknown E_0 from the perturbative series, one expands Eq. (138) around $E_0 = E_0^v$. In this way,

$$W_{ij}(0) = (H_{ij} - E_0^v N_{ij}) - \Delta E_0 N_{ij} \equiv W_{ij}^v(0) - \Delta E_0 N_{ij}. \tag{140}$$

Notice that, $W_{ij}^v(0)$ depends on the variational energy E_0^v. The expansion for the energy denominators gives

$$\frac{1}{E_0 - E_p^v} = \frac{1}{E_0^v - E_p^v + \Delta E_0} = \frac{1}{E_0^v - E_p^v} \sum_{i=0}^{\infty} \left(-\frac{\Delta E_0}{E_0^v - E_p^v} \right)^i. \tag{141}$$

Actually, the analysis of the series is easier by expressing,

$$W_{ij}^v(0) = W_{ij}^v(i) + (E_i^v - E_0^v) N_{ij}, \tag{142}$$

with $W_{ij}^v(i) = H_{ij} - E_i^v N_{ij}$. The series can then be written in terms of $W_{ij}^v(i)$

$$\begin{aligned}
\Delta E_0 &= \sum_{p \neq 0} (W_{0p}^v(0) - \Delta E_0 N_{0p}) \left(\frac{W_{p0}^v(p)}{E_0 - E_p^v} - N_{p0} \right) \\
&+ \sum_{q \neq p \neq 0} (W_{0p}^v(0) - \Delta E_0 N_{0p}) \left(\frac{W_{pq}^v(p)}{E_0 - E_p^v} - N_{pq} \right) \left(\frac{W_{q0}^v(q)}{E_0 - E_q^v} - N_{q0} \right) + \dots \tag{143}
\end{aligned}$$

Due to the correlations introduced in the wave functions, the calculation of matrix elements is much more involved than in normal perturbation theory. The CB matrix elements are constructed from the matrix elements of $F^+ F$ and $F^+ H F$ on Fermi gas states, characterized by the number of particles and holes. The matrix elements are calculated by cluster expansions. After expanding the energy denominators of the series (Eq. (143)), a careful analysis of the cluster expansion of the matrix elements and of the energy dependence of the different terms

leads to the conclusion that ΔE_0 is given by the sum of all linked Goldstone type diagrams (see section 2.1) built up with $W_{ij}^v(i)$ and N_{ij} interaction boxes. The interaction boxes (or equivalently the matrix elements) are the sums of only linked cluster diagrams. Therefore, the CBF perturbation series is well behaved in the thermodynamic limit [118].

In dealing with CBF perturbation theory we are confronted with two types of diagrams, the Goldstone type diagrams representing the terms of the series and the diagrams corresponding to the cluster expansion of the matrix elements, which are summed up by means of FHNC techniques.

Perturbative CBF calculations for the binding energy of nuclear matter have been performed up to second order. In this case, the perturbative correction to the ground state energy is expressed as:

$$
\begin{aligned}
\Delta E_0 &= \sum_{p \neq 0} W_{0p}^v(0) \left(\frac{W_{p0}^v(p)}{E_0^v - E_p^v} - N_{p0} \right) \\
&= \sum_{p \neq 0} \frac{W_{0p}^v(0) W_{p0}^v(0)}{E_0^v - E_p^v} = \sum_{p \neq 0} \frac{\mid H_{0p} - E_0^v N_{p0} \mid^2}{E_0^v - E_p^v},
\end{aligned} \tag{144}
$$

and has been calculated within the set of $2p-2h$ correlated basis states. In the thermodynamical limit, the energy denominators can be expressed in terms of the variational estimate of the single particle energies, $e^v(p)$,

$$
E_0^v - E^v(\mathbf{p}_1, \mathbf{p}_2, \mathbf{h}_1, \mathbf{h}_2) = e^v(h_1) + e^v(h_2) - e^v(p_1) - e^v(p_2). \tag{145}
$$

As expected, the second order correction to the ground state energy, increases the binding. In the first calculations, the correlation operator was taken of Jastrow type and in this case the perturbative second order correction was large [119]. On the other hand, the corrections are much smaller, when the correlation with the full operatorial structure is used. Therefore, a significant improvement in the convergence of the series is expected. Typical values of second order corrections to the binding energy at saturation density of nuclear matter range from ~ -1 to ~ -3 MeV. A very recent estimation for the Argonne V_{18} and the Urbana IX model for the three-body force, is -1.89 MeV at saturation density [16].

The CBF perturbation theory has also been implemented to study other observables, besides the hamiltonian, like the self-energy, the momentum distribution, the single particle spectral function, the different nuclear response functions, etc. In the previous section 2.3 we have considered the self-energy of a nucleon as the key quantity to calculate the single-particle Green's function. Here one can calculate the imaginary part and split it similar to (79) and (80) into two pieces, the correlation term, i.e. coupling to $2h1p$ correlated configurations and the polarization term corresponding to the coupling to $2p1h$ configurations. The imaginary part of $\Sigma^{2h1p}(k, \omega)$ for a particle state, in second order perturbation theory is defined as

$$
Im\Sigma^{2h1p}(k, \omega < e^v(k_F)) = \frac{\pi}{2} \sum \mid \langle \mathbf{k} \mid H - E_0^v \mid \mathbf{p}_1; \mathbf{h}_1, \mathbf{h}_2 \rangle \mid^2 \delta(\omega + e^v(p_1) - e^v(h_1) - e^v(h_2)) \tag{146}
$$

while

$$
Im\Sigma^{2p1h}(k, \omega > e^v(k_F)) = \frac{\pi}{2} \sum \mid \langle \mathbf{k} \mid H - E_0^v \mid \mathbf{p}_1, \mathbf{p}_2; \mathbf{h}_2 \rangle \mid^2 \delta(\omega + e^v(h_2) - e^v(p_1) - e^v(p_2)), \tag{147}
$$

Similar expressions hold for the hole states. Using dispersion relations one can calculate the corrections to the variational estimate of the single particle potential

$$
\Delta e(k) = e(k) - e^v(k) = \frac{P}{\pi} \int_{-\infty}^{\infty} \frac{Im\Sigma(k, \omega)}{e^v(k) - \omega} d\omega. \tag{148}
$$

In the case of the single particle momentum distributions, the second order perturbative correction to $n^v(k)$ has been obtained by calculating the expectation value of the occupation number operator $a_{\mathbf{k}}^{\dagger} a_{\mathbf{k}}$ on the perturbed ground state $\mid 0_{per} \rangle$ containing two particle two-hole correlated states:

$$\mid 0_{per} \rangle = \mid 0_v \rangle + \frac{1}{4} \sum \alpha(\mathbf{p}_1, \mathbf{p}_2; \mathbf{h}_1, \mathbf{h}_2) \mid \mathbf{p}_1 \mathbf{p}_2; \mathbf{h}_1 \mathbf{h}_2 \rangle, \tag{149}$$

where

$$\alpha(\mathbf{p}_1, \mathbf{p}_2; \mathbf{h}_1, \mathbf{h}_2) = \frac{\langle 0_v \mid H - E_0^v \mid \mathbf{p}_1, \mathbf{p}_2; \mathbf{h}_1, \mathbf{h}_2 \rangle}{(e^v(h_1) + e^v(h_2) - e^v(p_1) - e^v(p_2))}, \tag{150}$$

and keeping the terms of order α^2 [120].

However, there are still some problems with orthogonality corrections when the series is truncated at a given order. Moreover, it is not straightforward to extract the orthogonalized eigenvectors in a non-orthogonal CBF theory. Therefore, even if the applications of the non-orthogonal perturbation theory are rather successful, it is desirable to have also a method available in a orthogonal scheme. In this way, the N_{ij} boxes would be eliminated from the diagrams and the parallelism with normal perturbation theory becomes more transparent. To this end, one can try a Schmidt orthogonalization process, however it happens that the variational estimates of the hamiltonian on the Schmid orthogonalized states are worse than the ones calculated with the non-orthogonal basis. Very recently, a new orthogonalization procedure has been devised [121], in which the diagonal matrix elements of the hamiltonian and of the identity operator are preserved. It is a two step process which combines the Schmid orthogonalization with the Löwdin transformation [122]. Standard perturbation theory may be used in this new set of states. Although both schemes should be equivalent, in practice orthogonal CBF theory is more efficient particularly in calculating the spectral functions [123, 124] or the nuclear response functions [125, 126, 127].

The one-body Green's function has also been studied in the framework of CBF. Instead of computing the Green's function from a Dyson equation, as in the perturbative scheme discussed in the previous section, one directly calculates the single particle spectral functions. The starting point is the variational estimate, which is equivalent to approximate the true ground state by the variational ground state wave function and take 1 particle and 2 particle-1 hole basis correlated states for A+1 particles in the case of $S_p(k, \omega)$ and the 1 hole and 2 hole -1 particle correlated states for A-1 particles for $S_h(k, \omega)$. The projection into 1 hole (1 particle) state is the dominant one and is given by

$$S_{1h(1p)}^{(v)}(k, \omega) = \mid \varphi_{\mathbf{k}}^{h(p)} \mid^2 \delta(\omega - e^v(k)) \Theta \left[\pm(k_F - k) \right], \tag{151}$$

where the upper (lower) sign in the argument of the Θ-function applies to the hole (particle) spectral function, $e^v(k)$ is the variational single particle energy and the overlap matrix element $\varphi_{\mathbf{k}}^{h(p)}$ is defined by

$$\varphi_{\mathbf{k}}^h = \langle 0_v \mid a_{\mathbf{k}}^{\dagger} \mid h \rangle. \tag{152}$$

Where $\mid h \rangle$ is the basis correlated state of A-1 particle build on a Slater determinant where the state with momentum k is missing. In a similar way,

$$\varphi_{\mathbf{k}}^p = \langle 0_v \mid a_{\mathbf{k}} \mid p \rangle. \tag{153}$$

where in this case the state $\mid p \rangle$ represents the correlated state of A+1 particles build on a Slater determinant that besides having all the states occupied up to the Fermi level it has an additional particle on the state $\mathbf{k}$ above the Fermi level. Actually these type of intermediate

states are the only non-vanishing contributions in any uncorrelated ground-state. In such a case, the spectral functions $S_{unc,h(p)}(k,\omega)$ are just δ-functions with strength unity:

$$S_{unc,h(p)} = \delta(\omega - \frac{\hbar k^2}{2m})\Theta\left[\pm(k_F - k)\right].\tag{154}$$

As correlations are present in the CBF states also other intermediate states contribute to the zero order approximation to the spectral function. The contribution from 2h-1p (2p-1h) correlated states is spread out in energy and can be interpreted as a background contribution to be added to the quasi-particle part (δ-function) of the spectral function. This spreading produces a considerable quench of the quasi-particle peak. On top of this variational estimate one can build perturbation corrections, which take into account the admixture of more complicated configurations in the states considered in the definition of the spectral function. For instance, the 2p-2h admixture in the ground state, and the 2h-1p (2p-1h) in the one-hole (particle) have been studied [123, 124]. As a consequence of these corrections, the δ-peak of the quasiparticle, acquires a width (except for $k = k_F$), which is related to the imaginary part of the self-energy at the quasiparticle-energy. For $k = k_F$, the on-shell imaginary part of the self-energy is zero and the quasiparticle peak is a δ-function which strength (Z_{k_F}) which defines the discontinuity of the momentum distribution at $k = k_F$.

We can conclude that CBF has reach its maturity and systematic studies of different observables, for both nuclear matter and nuclei are available. The starting wave function is realistic enough that the perturbative corrections to the different quantities can be safely calculated up to second order. The formal properties of the perturbative series have been established and the efforts now can be addressed to improve the evaluation of the matrix elements or to study also higher orders in the perturbative expansion.

2.5   *Variational and Quantum Monte Carlo Techniques*

There are various possibilities to apply the techniques of Monte Carlo (MC) sampling in calculations of quantum many-body systems. For example one can use MC based algorithms to sample the multidimensional integral occurring in the evaluation of the expectation value of the hamiltonian, or any other operator, on a given trial function (Eq. (92)). In fact for simple interactions and central correlations the procedure is well established and it has been applied both for bosons and fermions, for systems with finite and infinite particle numbers. This type of calculations are known as Variational Monte Carlo (VMC) methods. However, there are also methods based on stochastic algorithms, which aim at an exact integration of the many-body Schrödinger equation. Those are generically known as Quantum Monte Carlo (QMC) methods. VMC and QMC calculations in systems of liquid helium, both ^{4}He and ^{3}He, which follow Bose and Fermi statistics respectively, have motivated an enormous progress in Monte Carlo Methods. However, the nuclear many-body hamiltonian is much more complicated and requires to introduce strong state dependence correlations in the nuclear wave function. Therefore the progress in accurate nuclear ground state calculations based on MC techniques has been rather slow. It is only recently, that the drastic improvement of the computational resources, i.e. parallel computers, allows to increase the number of nucleons involved in the calculations.

Once the trial wave function is chosen, the variational Monte Carlo method provides an exact - at least in the statistical sense - evaluation of the expectation value, which is free of the approximations involved in the integral equation methods discussed in the previous section. However, we should not consider these methods as competing ones but rather as a complementary ones. For instance, it is clear that Monte Carlo methods have difficulties in considering the long-range behavior of the distribution function of an infinite homogeneous

system because of the finite size of the simulating box (see below). On the other hand one can very well determine this long-range behavior in the context of HNC methods. In the case of finite nuclei, Monte Carlo methods have enormous problems in increasing the number of nucleons of the nucleus under consideration. On the other hand recent calculations with FHNC techniques can easily be applied to nuclei with A=40. For the systems, where both methods can be applied, they can help each other in looking for the appropriate correlation, in understanding the physical requirements of the wave function and in evaluating the accuracy of the approximations involved in the FHNC method.

Recent reviews on Quantum Monte Carlo methods can be found in Refs.[18, 128, 129]. Another review-like book with presentation of the methodology and physical applications is [130]. Two introductions into this field and rather comprehensive reviews by R. Guardiola on both the Variational and the Quantum Monte Carlo method have been published in Refs.[131, 132]. More oriented to nuclear physics is the paper of Carlson and Wiringa on variational Monte Carlo in finite nuclei [133]. A recent overview including also Green Function Monte Carlo for nuclear systems is due to S. Pieper [134]. Finally, the generalization to finite temperature, focusing mainly to applications in condensed matter physics has recently been reviewed by D. Ceperley [19].

Here we will mainly discuss VMC calculations. In order to explain the main ideas we will, as in the previous sub-section, use a simple system of bosons, obeying the hamiltonian of Eq. (93) with the scalar interaction of Eq. (104). First we consider a droplet of A ^{4}He atoms. A trial function satisfying the symmetry requirements is given by,

$$\Psi(\mathbf{r}_1, \mathbf{r}_2, ..., \mathbf{r}_A) = \prod_{i<j}^{A} f(r_{ij}) \prod_{i=1}^{A} \phi(r_i) \tag{155}$$

i.e., the product of a Jastrow factor times a model wave function that assigns the same single particle wave function to all the atoms. In this case, for spinless particles and local interactions, the expectation value of the hamiltonian can easily be written in a form appropriate for Monte Carlo calculations. Let $\mathbf{R}$ represent the set of the $3A$ spacial coordinates of the atoms in the droplet. We define a local energy $E_L(\mathbf{R})$ by

$$E_L(\mathbf{R}) = \frac{1}{\Psi(\mathbf{R})} H \Psi(\mathbf{R}) \tag{156}$$

and introduce a probability distribution function

$$p(\mathbf{R}) = \frac{\mid \Psi(\mathbf{R}) \mid^2}{\int d\mathbf{R}' \mid \Psi(\mathbf{R}') \mid^2}, \tag{157}$$

which by definition is normalized to 1. Notice also that for local potentials, the contribution of the potential to the local energy is just the value of the potential for the given configuration $\mathbf{R}$. The energy is given by

$$E_v = \frac{\langle \Psi \mid H \mid \Psi \rangle}{\langle \Psi \mid \Psi \rangle} = \frac{\int d\mathbf{R} \frac{|\Psi(\mathbf{R})|^2 H \Psi(R)}{\Psi(R)}}{\int d\mathbf{R}' \mid \Psi(\mathbf{R}') \mid^2} = \int d\mathbf{R} \, p(\mathbf{R}) \, E_L(\mathbf{R}). \tag{158}$$

The Monte Carlo way of evaluating this integral is to consider $p(\mathbf{R})$ as the importance sampling distribution and $E_L(\mathbf{R})$ as the function to be sampled. The essence of the Monte Carlo method is to generate a set of statistically independent configurations $(\mathbf{R}_i)$ which are distributed according to the probability distribution $p(\mathbf{R})$. Once this set of points $(\mathbf{R}_i)$ is obtained, the expectation value may be calculated through

$$E_v = \lim_{N \to \infty} \frac{1}{N} \sum_{i=1}^{N} E_L(\mathbf{R}_i). \tag{159}$$

Actually, this way to organize the integral of Eq. (158) is a special example of the more general expression

$$E_v = \frac{\int d\mathbf{R} \frac{\Psi^\dagger(\mathbf{R}) H \Psi(\mathbf{R})}{W(\mathbf{R})} W(\mathbf{R})}{\int d\mathbf{R}' \frac{\Psi^\dagger(\mathbf{R}') \Psi(\mathbf{R}')}{W(\mathbf{R}')} W(\mathbf{R}')}, \tag{160}$$

where $W(\mathbf{R})$ is a probability distribution function. When $W(\mathbf{R}) = \Psi^\dagger(\mathbf{R})\Psi(\mathbf{R})$ we recover Eq. (158). Once we have a set of configurations in the $3A$ dimensional space proportional to $W(\mathbf{R})$ then the calculation of E_v or the expectation value of any other operator $\hat{O}$

$$O_v = \frac{\langle \Psi \mid \hat{O} \mid \Psi \rangle}{\langle \Psi \mid \Psi \rangle} \tag{161}$$

is straightforward

$$O_v = \frac{\sum \frac{\Psi^\dagger(\mathbf{R}) \hat{O} \Psi(\mathbf{R})}{W(\mathbf{R})}}{\sum \frac{\Psi^\dagger(\mathbf{R}) \Psi(\mathbf{R})}{W(\mathbf{R})}}, \tag{162}$$

where the sum runs over all the configurations $(\mathbf{R}_i)$.

In order to get an estimate for the accuracy of the MC evaluation of the integrals, the samplings are grouped in blocks, each block with a sufficiently large number of points $(\mathbf{R}_j \ j = 1, \text{nmov})$, nmov being the number of configurations in each block. The central limit theorem guarantees that the average values of the energy obtained in each block i,

$$E_v^i = \frac{1}{\text{nmov}} \sum_{j=1}^{\text{nmov}} E_L(\mathbf{R}_j) \tag{163}$$

are distributed as a Gaussian centered around the true average value E_v

$$E_v = \frac{1}{\text{nblock}} \sum_{i=1}^{\text{nblock}} E_v^i \tag{164}$$

where nblock is the number of blocks and the statistical error is given by

$$\sigma = \frac{1}{\sqrt{\text{nblock} - 1}} \left(\frac{1}{\text{nblock}} \sum_{i=1}^{\text{nblock}} (E_v^i)^2 - E_v^2 \right)^{1/2}. \tag{165}$$

The configurations $(\mathbf{R}_i)$ following the importance sampling function can be generated through the so-called Metropolis algorithm[135], which yields a sequence of random numbers, a Markov chain, distributed according to the required distribution probability. The way to generate a sequence of configurations $(\mathbf{R}_i)$ by means of the Metropolis algorithm is rather simple and may be described as follows: Assume that we are at a given configuration $\mathbf{R}_{old}$, and the value of the wave function for this configuration is $w_{old} = \Psi(\mathbf{R}_{old})$ then one tries to generate a new configuration by defining $3A$ new coordinates

$$\mathbf{R}_{new} = \mathbf{R}_{old} + (\text{RAND}() - 0.5) * step. \tag{166}$$

where RAND() produces random numbers uniformly distributed in $[0, 1]$ and *step* defines the scale of the Monte Carlo moves. The value of the wave function at $\mathbf{R}_{new}$ is w_{new}.

Now we perform the Metropolis question to see if we are going to accept this new configuration $\mathbf{R}_{new}$ in our Markov-chain: If the probability of the new configuration $p(\mathbf{R}_{new})$ is larger

than the older, i.e. if $w_{new}^2 > w_{old}^2$, then $\mathbf{R}_{new}$ is accepted. If the probability is smaller, then $\mathbf{R}_{new}$ is accepted with probability w_{new}^2/w_{old}^2. Both cases are included in the following condition:

$$\text{if}(w_{new}^2/w_{old}^2 < RAND()) \tag{167}$$

then $\mathbf{R}_{new}$ is accepted and is the starting configuration for the next move. If the condition (167) is not fulfilled, the move is rejected and we try to generate another configuration from $\mathbf{R}_{old}$. One keeps track of the number of acceptances, and a efficient calculation should keep the percentage of acceptances between 40% and 60%. Also one can allow for several moves between the different blocks in order to reduce the correlations between the different calculations of the energy. It is also convenient to perform several moves at the beginning of the process, in order to reach the region where the Metropolis algorithm works properly. In the Monte Carlo language this is known as thermalization.

In the case of infinite homogenous systems one can of course not perform a simulation with an infinite number of particles. The usual way of dealing with these systems consists in representing the system in a simulation cell with periodic boundary conditions. If the size of the cells is L^3, the density of the system determines the number of particles A that we should consider for each cell, $\rho = A/L^3$. Metropolis moves are always recast into the main simulation cell, but in implementing the algorithm one must consider the particles in the periodic images as well. At a given density, the number of particles which can be treated in a calculation defines a clear limitation to the size of the simulation cell. Typical number of particles in the simulation box range between 50 and 100.

There are no essential differences in the case of fermion systems with respect to what we have discussed for boson systems so far. There are, however, some technical problems, associated with the calculation of determinants (the model wave function should be antisymmetric) and the manipulation of spin and isospin degrees of freedom. When the interaction and the correlations do not depend on the discrete (spin and isospin) degrees of freedom, the trial wave function can be considered as the product of a Jastrow factor and as many Slater determinants as fermion species, i.e. one corresponding to spin up and the other to spin down. Once a configuration is defined, each determinant is a number and the acceptance criterium for a Metropolis move contains the squared quotient of two determinants times the contributions of the correlation factors. The number of operations involved in the computation of a determinant is proportional to A^2 as a consequence, moving A particles involves A^3 operations. There is an algorithm, based on the calculation of a determinant by using the matrix of cofactors which reduces the number of operations to A^2, which is of course important for calculation with larger number of fermions[136].

In the variational method one aims to a minimization of the energy. This implies that one should perform VMC calculations for several variational parameters. This usually requires huge amounts of computing time. Besides, the statistical fluctuations of the results may give an incorrect localization of the minimum. To avoid this problem, a method called reweighting of configurations has been introduced. This method tries to use configurations corresponding to the same importance sampling function to calculate the energy for wave functions which have small changes in their variational parameters [136].

In the nuclear case, the strong state dependence of the interaction and the correlation, produce several complications that limit the application of the method to a small number of nucleons. Actually all the applications with realistic potentials refer to light nuclei and only very recently attempts have been made to study homogeneous systems [137].

For a finite number of nucleons, the trial wave function is a symmetrized product of non-commuting two-body operatorial correlations $F_2(i,j)$ (Eq. (98)) times a Slater determinant of single particle functions (Eq. (91)). The trial wave function must be translationally invariant,

and the correlation function fulfils this condition automatically . Also the implementation of the translational invariant to the model wave function is rather straightforward in the Monte Carlo method. For instance, if the model function has some dependence on the single particle coordinates $\mathbf{r}_i$, one just substitutes that set of coordinates by $\tilde{\mathbf{r}}_i$ with $\tilde{\mathbf{r}}_i = \mathbf{r}_i - \mathbf{R_{cm}}$ and $\mathbf{R}_{cm} = 1/A \sum \mathbf{r}_i$. The fact that the trial wave function describes a localized bound state, is either reflected in the correlation operator

$$ F_{ij}(r_{ij}) \to 0 \qquad , r_{ij} \to \infty \tag{168} $$

or in the model wave function, by requiring that the model wave function tends to zero when one of the particles is moved far away.

For very light nuclei one can take the model function (ϕ) as a pure spin-isospin function with no spatial dependence, for instance for triton and the ^{4}He nucleus the following functions have been used [133, 138]

$$ | \phi(^3H)\rangle = \mathcal{A} \, |\downarrow n \uparrow n \downarrow p\rangle \tag{169} $$

and

$$ | \Phi(^4He)\rangle = \mathcal{A} \, |\downarrow n \uparrow n \downarrow p \uparrow n\rangle \tag{170} $$

where $\mathcal{A}$ is the antisymmetrizer and the up- and down-arrows indicate the spin of the different nucleons. In this case the localization is impose on the correlation functions. One of the problems is that the size of the spin-isospin space of A nucleons increases very rapidly. There are $N_s = 2^A$ possible spin states ranging from all particles having their spins pointing down to all having their spins pointing up. If one fixes the charge of the system, i.e. the number of protons, then there are

$$ N_{char} = \frac{A!}{Z!(A-Z)!} \tag{171} $$

states in the isospin space with the same total charge. The total dimension is therefore $N_{dim} = N_s \times N_{char}$ For instance in the case of the ^{4}He, $N_s = 12$ and $N_{char} = 6$ with $N_{dim} = 96$. While for the ^{3}H, $N_s = 8$ and $N_{char} = 3$ while $N_{dim} = 24$. However for the ^{16}O, $N_s = 65536$ and $N_{char} = 12870$ while $N_{dim} = 843448320$. Each correlation operator F_{ij} is a very sparse matrix in the spin-isospin space. In evaluating the expectation value, this matrix acts on a vector in spin-isospin space to produce another vector. For instance the spin-isospin vector corresponding to the model wave function of ^{4}He (Eq. (170)) has 24 non zero components, as a result of the antisymmetrization. When the correlations act on those initial vectors other states are generated. One can try a straightforward generalization of the VMC methods discussed above by writing

$$ \Psi = \sum_{p=1}^{M} \Psi_p \tag{172} $$

where Ψ_p corresponds to the term in Ψ in which the A(A-1)/2 correlation operators F_{ij} operate in a specific order labeled by the index p. The energy expectation value is given by

$$ E_v = \frac{\sum_{p,q=1}^{M} \int \Psi_p^\dagger H \Psi_q d\mathbf{R}}{\sum_{p,q=1,M} \int \Psi_p^\dagger \Psi_q d\mathbf{R}} \tag{173} $$

where the spin isospin degrees of freedom are treated explicitly. However, to sample the coordinates using the Metropolis algorithm would still be not practical, because it would be necessary to take into account all the $(A(A-1)/2)^2$ possible terms, related to the ordering of the correlation operators in each side of the expectation value. Instead, one can sample randomly the coordinates $\mathbf{R}$ and the order labels p and q using for the importance sampling function

$$ W_{pq}(\mathbf{R}) =| \, Re[\Psi_p^\dagger(\mathbf{R})\Psi_q(\mathbf{R}) \, | \tag{174} $$

where the absolute magnitude is required in order to be sure that the weight function is never less than zero. The statistical error per sample in configuration space is increased by sampling the order of the operators. However, the time saved by evaluating each time only one term in the sum (Eq. (173)) increases the efficiency of the calculation. The way to proceed is the following: From an initial configuration $X = (\mathbf{R}, p\&q)$ a trial configuration $X' = (\mathbf{R}', p'\&q')$ is generated. The Metropolis condition (167) is now applied to the sampling functions $W_{pq}(\mathbf{R})$ and $W_{p'q'}(\mathbf{R}')$ to see if X' is accepted or rejected.

Special codifications of the action of the operators on the spin-isospin vectors, based on binary representations of those vectors are useful. However, calculations performing the full spin-isospin summations, as the ones just described, are feasible with present computers only up to A=8.

To study heavier nuclei one needs to sample also the spin-isospin states in a random walk which takes place in a combined spin, isospin, and coordinate space [139]. The main problem in sampling over spin-isospin states is the increase in the statistical error if the sampling is done blindly. In order to reduce the variance, the spin-isospin states must be treated in a manner similar to that commonly used for the spatial coordinates. In order to devise the proper strategy, we write the expectation value of the hamiltonian as

$$E_v = \frac{\int d\mathbf{R} \sum_{a,b} \Psi_a^\dagger(\mathbf{R}) H_{ab} \Psi_b(\mathbf{R})}{\int d\mathbf{R} \sum_a \Psi_a^\dagger(\mathbf{R}) \Psi_a(\mathbf{R})}, \tag{175}$$

in this case a and b represent spin-isospin states. The basis of spin-isospin states is just the one discussed above, i.e. the states where each nucleon has a definite third component of spin and isospin. The Monte Carlo strategy consists in sampling values of $\mathbf{R}$ and a, while explicitly summing over all spin-isospin states b, for each choice of $\mathbf{R}$ and a. The full summation over b, although it is a lengthy calculation, reduces the statistical error of the calculation significantly, since for the exact wave function

$$\sum_b H_{ab} \Psi_b = E \Psi_a \tag{176}$$

for each configuration $(\mathbf{R}, a)$.

The generalization of the standard Metropolis algorithm in order to sample $\mathbf{R}$ and a in the combined coordinate-spin-isospin space, must allow not only to move the particles in coordinate space but also for changes in the orientation of the spins and isospins of the nucleons. The way to do that is by flipping the third component of the spin and/or by exchanging the spin-isospin of two nucleons, chosen in a random way. Of course these are not the only possibilities but these movements are easy to implement and enough to sample the full spin-isospin space. As before, the proposed move is accepted or rejected according to the ratio of the squares of the wave function evaluated at $(\mathbf{R}, a)$ and $(\mathbf{R}', a')$, as in standard variational Monte Carlo. In this way the Monte Carlo method has been applied to ^{16}O, to calculate the energy, form factor and charge distribution, using the Reid V6 interaction, i.e. including up to the tensor channels in the general expression of the force (Eqs. (94,95)).

Another alternative is to perform a cluster expansion for the non-central correlations while the central correlations and the antisymmetry are treated to all orders. The different terms are exactly evaluated with Monte Carlo techniques. This procedure has allowed to study ^{16}O with the full Argonne V_{14} two-nucleon interaction, supplemented with the Urbana VII three-nucleon potentials, using a trial wave function which contains pair- and triplet-correlation operators. Not only the binding energy but also other quantities like density distribution, momentum distributions, charge form factors and response functions have been studied [140, 141].

To go beyond VMC one needs to invent an algorithm to generate the exact ground state wave function. These new algorithms are generally called as Quantum Monte Carlo and they

try to integrate the many-body Schrödinger equation by means of stochastic procedures. The simplest of these methods is the so called Diffusion Monte Carlo (DMC) which approximates the many-body time dependent Green's function by calculating the time evolution operator in small time steps. The starting point is to consider the many-body Schrödinger equation in imaginary time,

$$-\frac{\partial \Psi(\mathbf{R},t)}{\partial t} = (H - E)\Psi(\mathbf{R},t) \tag{177}$$

The formal solution of Eq. (177) is

$$\Psi(\mathbf{R},t) = \exp\left(-\left[H - E\right]t\right)\Psi(\mathbf{R},0) \tag{178}$$

where the propagator $\exp\left[-(H - E)t\right]$ is called Green's function, and E is a convenient energy shift. The imaginary time evolution of an arbitrary starting state $\Psi(\mathbf{R},0)$, once expanded in the basis of stationary states $(\phi_i(\mathbf{R}))$ of the hamiltonian, is given by

$$\Psi(\mathbf{R},t) = \sum_i \exp\left(-\left[E_i - E\right]t\right)c_i\phi_i(\mathbf{R}). \tag{179}$$

The amplitudes of the different states change with time, increasing or decreasing depending on the sign of $(E_i - E)$. Independently of the value of the energy shift E, the most important amplitude after a long time will be the one corresponding to the state with the lowest energy E_0. In other words the DMC method projects out the ground state wave function from the trial wave function using

$$\Psi_0 = \lim_{t \to \infty} \quad \exp\left[-(H - E_0)t\right]\Psi_T , \tag{180}$$

provided that the overlap between the starting trial function and the true ground state is different than zero ($c_0 \neq 0$). The eigenvalue E_0 is exactly calculated during the process. The starting trial wave function is represented by a set of random vectors or walkers $(\mathbf{R}_1, \mathbf{R}_2, ...\mathbf{R}_{Nw})$ distributed with probability proportional to the trial wave function, in such a form that the time evolution of the wave function is represented by the evolution of the set of walkers. Notice that the quantity interpreted as a probability distribution function is the wave function of the system, and not its squared as in VMC. Along the iteration process, going from a wave function to another wave function, means to change the random numbers representing the wave function. Each walker generates a number of descendants (none, one or more than one) which will finally accommodate to the exact wave function. The method is iterative and the ground state is asymptotically approached. In its simplest form, the DMC is only appropriate to describe the ground state of boson systems. In this case the wave function is positive and can be used as a probability distribution function. In the case of fermions, the ground state wave function is not positive definite, and one should be careful to interpret the wave function as a probability distribution function, giving rise to the so called "sign problem". Importance sampling combined with the so called fixed node approximation allows to build a method also in this case.

The actual computation of the time evolution is done in small time steps τ, by writing the Green's function as a product over short time intervals

$$\exp\left(-\left[H - E\right]t\right) = \prod_{i=1}^{n} \exp\left(-\left[H - E\right]\tau\right), \tag{181}$$

where $\tau = t/n$. These short time propagators are then approximated as the product of free particle propagators and a propagator involving the potential,

$$\exp\left(-H\tau\right) \approx \exp\left(-V\tau\right)\exp\left(-K\tau\right) \tag{182}$$

where V is the interaction and K the kinetic energy operator. Their coordinate representation is rather simple,

$$G_K(\mathbf{R}', \mathbf{R}, t) = \langle \mathbf{R}' \mid \exp{-Kt} \mid \mathbf{R} \rangle = \frac{1}{(4\pi Dt)^{3A/2}} \exp\left(-(\mathbf{R}' - \mathbf{R})^2/4Dt\right). \qquad (183)$$

Where $D = \hbar^2/2m$ is called the diffusion constant. If the potential is local the Green's function related to the potential is,

$$G_V(\mathbf{R}', \mathbf{R}, t) = \langle \mathbf{R}' \mid \exp{(-Vt)} \mid \mathbf{R} \rangle = \exp{(-V(\mathbf{R})t)}\delta(\mathbf{R} - \mathbf{R}'). \qquad (184)$$

The coordinate representation of the total Green function for short times including the energy shift is given by

$$G(\mathbf{R}', \mathbf{R}, \tau) = G_K(\mathbf{R}', \mathbf{R}, \tau)exp[E - V(\mathbf{R})] + O(\tau^2). \qquad (185)$$

Using the above expressions, the propagation in coordinate space reads

$$\langle \mathbf{R} \mid \Psi(\tau + \delta\tau) \rangle = \int d\mathbf{R}' \langle \mathbf{R} \mid G(\delta\tau) \mid \mathbf{R}' \rangle \langle \mathbf{R}' \mid \Psi(\tau) \rangle. \qquad (186)$$

This integral equation is solved by using Monte Carlo methods to sample the free particle propagator and including branching to take the potential into account, thus allowing for the process of replication of the walkers. The equation is iterated until convergence. In conclusion the scheme is well defined once one has found an appropriate approximation for the short time Green's function, and a collection of walkers describing the starting state has been chosen. These walkers are evolved in time, obtaining a new collection of walkers. If the number of time steps is large enough the final walkers will represent the ground state wave function. An important improvement is obtained by introducing an importance sampling function to increase the statistical accuracy of the method.

The method is well established for systems of bosons interacting through central scalar interactions. For fermions one must deal with the so called sign problem, on which a lot of progress has been achieved in the last years, see [144, 143]. Realistic applications are in the context of quantum liquids to study ^{4}He and ^{3}He. In the nuclear case, using realistic interactions there are only applications for a few number of nucleons. Recent calculations are able to arrive up to 7 nucleons, calculating the ground state and low-lying excited states [142]. Also new algorithms are being designed to treat the nuclear or neutron matter case with realistic interactions [137, 145].

3 Effects of Correlations derived from Realistic Interactions

3.1 *Models for the NN Interaction*

In our days there is a general agreement between physicists working on this field, that quantum chromo dynamics (QCD) provides the basic theory of the strong interaction. Therefore also the roots of the strong interaction between two nucleons must be hidden in QCD. For nuclear structure calculations, however, one needs to determine the NN interaction at low energies and momenta, a region in which one cannot treat QCD by means of perturbation theory. On the other hand, the system of two interacting nucleons is by far too complicate to be treated by
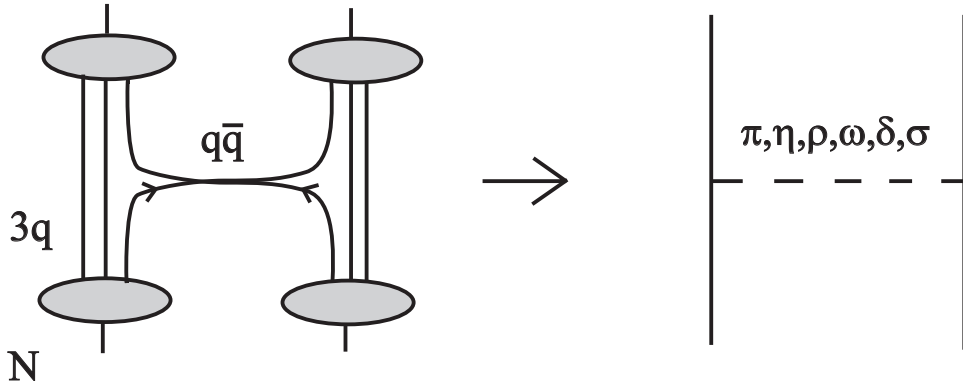
Figure 15: Nucleon-Nucleon interaction in the quark- and meson-exchange picture. The lines in the left part of the figure refer to propagating quarks, whereas those in the right part refer to nucleons and mesons.

means of lattice QCD calculations. Therefore one has to consider phenomenological models for the NN interaction.

Attempts have been made to develop models for the NN interaction, which consider the QCD degrees of freedom, quarks and gluons explicitly. As an example we mention the non-relativistic constituent quark models, which are very successful in describing the properties of baryons[146]. Based on such constituent quark models, so-called quark cluster models have been developed for the NN interaction[1, 147, 148]. These models include the effects of one-gluon-exchange terms and account for the exchange of mesons between the quarks. This exchange of mesons within the quark model is schematically displayed in the left part of Fig. 15. The exchange of a quark-antiquark pair is substituted by the exchange of mesons of various kinds. This interpretation is in line with the arguments of t'Hooft and Witten[149, 150]. They demonstrated that in the low-energy regime, the relevant degrees of freedom of QCD should be well described in terms of a meson theory. This means that also the quark-antiquark exchange processes displayed in that figure should be dominated by the exchange of the collective quark-antiquark modes, i.e. the exchange of mesons. Such constituent quark cluster models are very successful in describing the main features of the baryon-baryon interaction, however, the accuracy of the fits of these interactions to the empirical NN scattering phase shifts is not sufficient to use such interactions based on a quark model for nuclear structure calculations.

If one considers the meson degrees of freedom as the most important degrees of freedom for QCD at low energies, it is quite natural to describe the NN interaction in terms of mesons, which are exchanged between nucleons. The internal structure of the nucleons can then be parameterized in terms of meson-nucleon form-factors. Detailed discussions of these meson exchange models have been presented, e.g. in [2, 151, 152, 153]. The basic idea of this meson exchange model dates back to 1935, when Yukawa suggested that a new particle with "intermediate" mass, eventually called a meson, should be responsible for the strong interaction between nucleons[154].

In modern one-meson or one-boson-exchange (OBE) model of the interaction one assumes that the basic NN interaction is described by the exchange of all mesons displayed in the right-hand part of Fig. 15. The diagram of that figure can be interpreted as a Feynman diagram representing the simplest non-trivial contribution to the two-nucleon Green's function. Such contributions can be evaluated by using essentially the same rules as discussed in subsection 2.3. The basic building blocks for evaluating these contributions are the operators for the

meson-nucleon vertices, which are given by

$$
\begin{aligned}
\Gamma_{\rm s} &= \sqrt{4\pi}g_{\rm s} & \text{for a scalar meson,} \\
\Gamma_{\rm ps} &= i\sqrt{4\pi}g_{\rm ps}\gamma^5 & \text{for a pseudoscalar meson,} \\
\Gamma_{\rm v} &= \sqrt{4\pi}\left[g_{\rm v}\gamma^\mu + \frac{f_{\rm v}}{2m}i\sigma^{\mu\nu}k_\nu\right] & \text{for a vector meson.}
\end{aligned}
\tag{187}
$$

The γ^μ are the usual matrices using the conventions of Bjorken and Drell[155], the tensor operator is defined by the commutator $\sigma^{\mu\nu} = i[\gamma^\mu, \gamma^\nu]$ and k_μ refers to the 4-momentum of the exchanged meson. Matrix elements of these operators have to be calculated between Dirac spinors for plane waves. In the helicity representation these Dirac spinors are given as

$$
u(\vec{q}, \lambda) = \sqrt{\frac{E_q + m}{2m}} \left(\begin{array}{c} 1 \\ \frac{2\lambda q}{E_q + m} \end{array} \right) |\lambda >
\tag{188}
$$

where λ refers to the helicity, i.e. the projection of the nucleon spin on the direction of the momentum $\vec{q}$ and

$$
E_q = \sqrt{\vec{q}^2 + m^2}
\tag{189}
$$

is the relativistic energy of the free nucleon. Note that the Dirac spinors of Eq. (188) are normalized due to

$$
\bar{u}(\vec{q}, \lambda)u(\vec{q}, \lambda) = u^\dagger(\vec{q}, \lambda)\gamma^0 u(\vec{q}, \lambda) = 1 \,.
\tag{190}
$$

Instead of using the pseudoscalar coupling $\Gamma_{\rm ps}$ in (187) one also often employs the pseudovector coupling

$$
\Gamma_{\rm pv} = i\sqrt{4\pi}\frac{f_{\rm pv}}{m_{\rm mes}}\gamma^\mu\gamma^5 k_\mu \,.
\tag{191}
$$

Both couplings yield equivalent results for on-shell nucleons, if one identifies $m_{\rm mes}g_{\rm ps} = 2mf_{\rm pv}$. For nucleons described by Dirac spinors different from those of a free particle like in (188), however, the pseudovector coupling suppresses the enhancements due to the antiparticle admixture as compared to pseudoscalar coupling.

If now one considers the interaction of two nucleons in the center-of-mass frame with momenta $\vec{q}$ and $-\vec{q}$ before and the momenta $\vec{q'}$ and $-\vec{q'}$ after the interaction, the matrix element for the exchange of a meson of the kind α is given by

$$
\mathcal{V}_\alpha(\vec{q'}, \vec{q}) = (\bar{u}(-q')\Gamma_\alpha u(-q)) \, P_\alpha(k) \, (\bar{u}(q')\Gamma_\alpha u(q)) \,,
\tag{192}
$$

with the Dirac spinors u as defined in (188). Momentum conservation requires that the 4-momentum of the exchanged meson is $k = q - q'$ and the meson propagators are given by

$$
\begin{aligned}
P_{\rm s} &= \frac{1}{k^2 - m_{\rm s}^2} & \text{for scalar and pseudoscalar mesons,} \\
P_{\rm v} &= \frac{-g_{\mu\nu} + k_\mu k_\nu/m_{\rm v}^2}{k^2 - m_{\rm v}^2} & \text{for vector mesons.}
\end{aligned}
\tag{193}
$$

A very efficient way for the evaluation of the OBE matrix elements in (192) using the helicity representation for the Dirac spinors has been presented in [151]. The two-particle states can be expanded in terms of eigenstates with respect to the total angular momentum J. Since the OBE amplitudes are invariant under rotation the angular momentum is a good quantum number and one obtains matrix elements

$$
\langle \lambda_1' \lambda_2' q' | \mathcal{V} | \lambda_1 \lambda_2 q \rangle_J = 2\pi \int_0^\pi d\theta \, \sin\theta \, d_{\lambda\lambda'}^J(\theta) \, \langle \lambda_1' \lambda_2' \mathbf{q'} | \mathcal{V} | \lambda_1 \lambda_2 \mathbf{q} \rangle \,,
\tag{194}
$$

where λ_i denotes the helicity of nucleon i, θ is the angle between the momenta $\vec{q}$ and $\vec{q'}$, and the $d^J_{\lambda\lambda'}$ are the reduced rotation matrices with $\lambda = \lambda_1 - \lambda_2$ and $\lambda' = \lambda'_1 - \lambda'_2$. Inspection of the symmetries for the matrix elements in (194) shows that there are six independent matrix elements between the various helicity states for each J. These matrix elements in the helicity representation can easily be transformed into the conventional basis of partial waves for two nucleons

$$|\lambda_1\lambda_2 q\rangle_J \implies |^{2S+1}L_J q\rangle\,, \tag{195}$$

where S identifies the total spin of the nucleons, L is the orbital angular momentum of the relative motion, which is usually labeled by the letter S, P, $D\ldots$ for $L = 0, 1, 2\ldots$, and $J = L + S$ is the total angular momentum. The Pauli principle for the interacting nucleons requires that the total isospin T_{iso} is related to these quantum numbers by the requirement that the sum $L + S + T_{\mathrm{iso}}$ is an odd number.

As discussed before, one can account for the composite structure of the mesons and baryons by introducing form factors. This means that one may consider the coupling constants in (187) not as universal constants but as depending on the 4-momenta of the interacting hadrons. A simple choice for such a form factor, which is commonly used, is to assume that it depends only on the momentum transfer k, the momentum of the meson, and takes the form

$$g_\alpha(k) = g_\alpha \left(\frac{\Lambda_\alpha^2 - m_\alpha^2}{\Lambda_\alpha^2 - k^2} \right)^\nu\,, \tag{196}$$

with a cut-off parameter Λ and an exponent ν, which is 1 for the so-called monopole form factor.

The operators defining the meson nucleon vertices in (187) as well as the meson propagators in (193) refer to a relativistic description. This means that the two-body amplitudes which we have defined so far should be considered as an irreducible interaction kernel $\mathcal{V}$ to be used in a relativistic equation like Bethe-Salpeter equation, which can schematically be written

$$\mathcal{T}_{\mathrm{BS}}(q', q; P) = \mathcal{V}(q', q; P) + \int d^4k \frac{i}{(2\pi)^4} \mathcal{V}(q', k; P)\mathcal{G}_{\mathrm{BS}}(k; P)\mathcal{T}_{\mathrm{BS}}(k, q; P)\,. \tag{197}$$

Note that this is an integral equation in the 4-dimensional space of momentum vectors. The momenta of the interacting nucleons are defined in terms of the center-of-mass momentum P, which is conserved, and the relative momenta q, q', and k in such a way that the momenta of the particles are, e.g., $p_i = 1/2P \pm k$. In the center of mass frame the total momentum P has a time like component, which is identical to the total energy $\sqrt{s}$, with s referring to the corresponding Mandelstam variable (see e.g. [156]), whereas the space component of P is equal to zero. The uncorrelated two-particle Green's function $\mathcal{G}_{\mathrm{BS}}$ occurring in (197) can be written as a product of relativistic single-particle Green's functions

$$\mathcal{G}_{\mathrm{BS}}(k; P) = \left(\frac{1}{\frac{1}{2}\not{P} + \not{k} - m + i\eta} \right)^{(1)} \left(\frac{1}{\frac{1}{2}\not{P} - \not{k} - m + i\eta} \right)^{(2)}\,, \tag{198}$$

where the superscript (1) or (2) refers to the corresponding nucleon. It is common practice to ignore the propagation of the solutions of negative energy and furthermore reduce the 4-dimensional Bethe–Salpeter equation (197) to an integral equation in three dimensions by fixing the time component of k in a covariant way. One of the possible choices is the approach suggested by [157]:

$$\mathcal{G}_{\mathrm{BBS}}(k; P) = \delta(k_0) \frac{i}{2\pi} \frac{m^2}{E_k} \frac{\Lambda^{+(1)}(k)\Lambda^{+(2)}(-k)}{\frac{1}{4}s - E_k^2 + i\eta}\,, \tag{199}$$

with $\Lambda^{+(i)}$ referring to the projector on Dirac states with positive energy for particle i

$$
\begin{aligned}
\Lambda^{+(i)}(k) &= \left(\frac{\gamma^0 E_k - \vec{\gamma} \cdot \vec{k} + m}{2m} \right)^{(i)} \\
&= \sum_{\lambda_i} |u(\vec{k}, \lambda_i) >< \bar{u}(\vec{k}, \lambda_i)|
\end{aligned}
\tag{200}
$$

with u the Dirac spinors of (188). The assumption of the Blankenbecler–Sugar propagator, that the time-like component k_0 vanishes, means that for the propagation of the intermediate states both nucleons are considered to be off-shell by the same amount and the irreducible interaction terms do not transfer energy between the interacting nucleons. This implies that no energy transfer should be assumed for the meson propagators if one considers the contributions of OBE in the Blankenbecler–Sugar approximation. Replacing the Bethe–Salpeter propagator $\mathcal{G}_{\text{BS}}$ in (197) by the Blankenbecler–Sugar approximation one obtains

$$
\mathcal{T}(q', q) = \mathcal{V}(q', q) + \int \frac{d^3 k}{(2\pi)^3} \mathcal{V}(q', k) \frac{m^2}{E_k} \frac{\Lambda^{+(1)}(k)\Lambda^{+(2)}(-k)}{q^2 - k^2 + i\eta} \mathcal{T}(k, q) ,
\tag{201}
$$

where we have replaced s by $4E_q^2$, using $E_q = \sqrt{q^2 + m^2}$. Assuming that the matrix elements of $\mathcal{V}$ are calculated between spinors, which correspond to the solution of the Dirac equation with positive energy (to account for the projectors Λ^+), we may define

$$
\begin{aligned}
V(\mathbf{q}', \mathbf{q}) &= \sqrt{\frac{m}{E_{q'}}} \mathcal{V}(q', q; P) \sqrt{\frac{m}{E_q}} , \\
T_{\text{scat}}(\mathbf{q}', \mathbf{q}) &= \sqrt{\frac{m}{E_{q'}}} \mathcal{T}(q', q; P) \sqrt{\frac{m}{E_q}} .
\end{aligned}
\tag{202}
$$

This allows us to rewrite the Blankenbecler–Sugar equation (201) as

$$
T_{\text{scat}}(\vec{q}', \vec{q}) = V(\vec{q}', \vec{q}) + \int \frac{d^3 k}{(2\pi)^3} V(\vec{q}', \vec{k}) \frac{m}{q^2 - k^2 + i\eta} T_{\text{scat}}(\vec{k}, \vec{q}) ,
\tag{203}
$$

which has the form of the non-relativistic Lippmann–Schwinger equation (2) for the scattering T_{scat} matrix. This means that if we evaluate the relativistic matrix elements of $\mathcal{V}$ and apply the so-called "minimal relativity" factors of (202), the (relativistic) Blankenbecler–Sugar equation (201) becomes identical to the non-relativistic scattering equation. The states of this scattering equation can be rewritten in the usual partial-wave basis and the integral (203) can be solved with the techniques as described by [62].

Alternatives to the Blankenbecler–Sugar approach to reduce the Bethe–Salpeter equation to a three-dimensional integral equation have been developed. As examples we mention the approaches introduced by Kadychevsky[158], Gross[159], Thompson[160], Schierholz[161], and Erkelenz[151]. A detailed discussion of the various approaches has been presented by Brown and Jackson[153].

With the OBE ansatz one can now solve the Blankenbecler–Sugar or a corresponding scattering equation and adjust the parameter of the OBE model to reproduce the empirical NN scattering phase shifts as well as binding energy and other observables for the deuteron. Typical sets of parameters resulting from such fits are listed in table 1.

Some of the OBE parameters, such as the masses of the π, η, ρ, ω, and δ mesons, are not free parameters but are taken from the mass table [162]. Other parameters, such as the cut-off

Table 1: Parameters of the realistic OBE potentials Bonn A, B and C (see table A.1 of [2]). The second column displays the type of meson: pseudoscalar (ps), vector (v) and scalar (s) and the third its isospin T_{iso}.

Meson		T_{iso}	m_α [MeV]	Bonn A		Bonn B		Bonn C	
				$g_\alpha^2/4\pi$	Λ_α [MeV]	$g_\alpha^2/4\pi$ [MeV]	Λ_α [MeV]	$g_\alpha^2/4\pi$	Λ_α
π	ps	1	138.03	14.7	1300	14.4	1700	14.2	3000
η	ps	0	548.8	4	1500	3	1500	0	-
ρ	v	1	769	0.86[a]	1950	0.9[a]	1850	1.0[a]	1700
ω	v	0	782.6	25[a]	1350	24.5[a]	1850	24[a]	1400
δ	s	1	983	1.3	2000	2.488	2000	4.722	2000
σ[b]	s	0	550[b]	8.8	2200	8.9437	1900	8.6289	1700
			(710-720)[b]	17.194	2000	18.3773	2000	17.5667	2000

[a] The tensor coupling constants are f_ρ=6.1 g_ρ and $f_\omega = 0$.
[b] The σ parameters in the first line apply for NN channels with isospin 1, while those in the second line refer to isospin 0 channels. In this case the masses for the σ meson of 710 (Bonn A) and 720 MeV (Bonn B and C) were considered.

parameters Λ and the contributions from η and δ exchange, do not effect the fit very much but are used as a fine tuning. The coupling constant for the π is very well constrained by the πN scattering data.

Also the coupling constants for the ρ meson, in particular the large tensor coupling f_ρ are deduced from a dispersion analysis of πN data in [163]. As we will see below, this strong coupling for the ρ is of some significance for the nuclear structure calculation. A non-relativistic reduction for the ρ exchange, similar to the one performed for the π in the preceding subsection, yields a tensor component for the NN interaction with a sign opposite to the one deduced from one-pion-exchange in (207). Therefore a strong ρ exchange reduces the tensor force originating from the π exchange significantly.

The ω coupling constant used in the OBE potential displayed here but also in other realistic OBE models is rather large. A simple quark model with SU(3) flavor predicts the ω coupling to be nine times as large as that for the corresponding isovector vector meson, the ρ. The strong ω exchange contribution, however, is required to obtain sufficient repulsion for the NN interaction at short distances. A possible reason for this discrepancy may be that the ω exchange in the OBE model contains an effective parameterization of short-range repulsion originating from quark effects[1]. Another explanation would be that this strong ω exchange simulates also repulsive $\pi - \rho$ exchange terms with intermediate isobar excitations[164] (see also discussion below).

The only part of the OBE model, that has a purely phenomenological origin is the σ exchange, which describes the medium-range attraction of the NN interaction. This exchange of the scalar σ meson is used to describe various two-π exchange processes, which are irreducible with respect to intermediate NN states and therefore not accounted for by summing ladder diagrams of one-pion-exchange in the Lippmann-Schwinger equation. Such two-π exchange
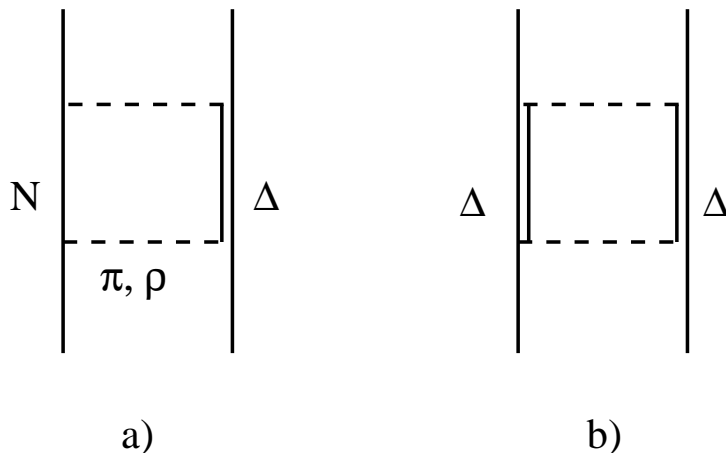
Figure 16: Contributions to the NN interaction beyond the OBE approach due to interme-
diate $N\Delta$ (a) and $\Delta\Delta$ excitations (b)

processes can be studied in a systematic way by means of dispersion relations using experi-
mental information from πN scattering processes. Such studies of the medium-range attraction
employing dispersion relations have been performed e.g. by Vinh Mau and collaborators[27]
and the group in Stony Brook[28]. They are the basis of the medium range attraction, which
is used in the so-called Paris potential[165].

Another way to determine the effects of these irreducible two-π exchange processes is to
evaluate such contributions explicitly. A rather important contribution of this kind are the
processes displayed in Fig. 16, in which the interacting nucleons are excited to intermediate
$N\Delta$ or $\Delta\Delta$ excitations (with Δ representing the isobar excitation of the nucleon at 1232 MeV
with spin and isospin 3/2). Since the $N \to \Delta$ excitation requires a change of the spin and isospin
of the baryon, such excitations could only be formed by the exchange of non-scalar, isovector
mesons like the π and ρ meson. The dominant contribution will be the iterated two-π exchange
which yields attraction. In a simple OBE model this attraction would be described in terms of
σ meson exchange. Note that in NN channels with isospin $T = 0$ only $\Delta\Delta$ intermediate states
can be reached because of isospin conservation. In $T = 1$ channels one obtains contributions
from intermediate $N\Delta$ and $\Delta\Delta$ states. This is a plausible explanation for the feature that the
masses of the σ mesons listed in table 1 are larger for $T = 0$ than for $T = 1$.

Corresponding terms with π and ρ exchange are repulsive and of shorter range[164]. They
might be simulated by a strong ω exchange as discussed above[40].

During the past few years, considerable progress has been made in constructing realistic
models for the NN interaction. In 1993, the Nijmegen group published a new phase-shift analysis
including selected proton-proton and proton-neutron scattering data below a laboratory energy
of 350 MeV with a χ^2 per datum of 0.99 for 4301 data[166]. Based on these data charge-
dependent NN potentials have been constructed by the Nijmegen group[167], the Argonne
group[89] (Argonne V_{18}) and Machleidt et al.[168] (CD-Bonn) which reproduce the NN data
with a χ^2 of 1.03, 1.09 and 1.03, respectively. In order to achieve fits with such a high accuracy
one has to go beyond the OBE ansatz discussed so far. Machleidt et al.[168] obtain such an
accurate fit in the so called CD-Bonn potential by adjusting the parameters of the σ meson
exchange in each partial wave, separately.

One may say that these charge-dependent NN interactions are essentially phase-shift equiv-
alent, the on-shell matrix elements of the NN transition matrix T are almost identical. This

does, however, not imply that the models for the NN interaction underlying these descriptions are identical. Moreover, the off-shell properties of each potential may be rather different. All models for the NN interaction V include a one-pion exchange (OPE) term, using essentially the same πNN coupling constant. However, even this long range part of the NN interaction, which is believed to be well understood, is treated quite differently in these models.

The CD-Bonn potential is based on the relativistic meson field theory, which has been outlined above. Including the "minimal relativity" factors of (202) one obtains an expression for the One-Pion-Exchange contribution to the NN interaction of two nucleons in the $^3S_1$ channel, in plane wave states with momenta k and k' for the initial and final state, respectively, which is of the form

$$< k'|V_{SS}^{\pi}|k> = -\frac{g_{\pi}^2}{4\pi}\frac{1}{2\pi m^2}\sqrt{\frac{m^2}{E_k E_{k'}}}\int_{-1}^{1} d\cos\theta \left(\frac{\Lambda^2 - m_{\pi}^2}{\Lambda^2 + q^2}\right)^2 \frac{k'k\cos\theta - (E_k E_{k'} - m^2)}{q^2 + m_{\pi}^2}, \quad (204)$$

where q^2 denotes the momentum transfer,

$$q^2 = (\vec{k} - \vec{k'})^2 = k^2 + k'^2 - 2kk'\cos\theta. \quad (205)$$

Note that the expression (204) contains a dependence on the momenta k and k', which cannot be reduced to a dependence on the momentum transfer. This demonstrates that this expression for the One-Pion-Exchange yields a non-local interaction. Results for such matrix elements as a function of k, keeping $k' = 95$ MeV/c fixed, are displayed in Fig. 17[169].

If now we introduce in (204) the nonrelativistic approximation for

$$E_k E_k' - m^2 \approx \frac{1}{2}k^2 + \frac{1}{2}k'^2, \quad (206)$$

ignore the form-factor $(\Lambda^2 - m_{\pi}^2)/(\Lambda^2 + q^2)$ and the "minimal relativity" factors, we obtain

$$\langle k'|V_{SS}^{\pi}|k\rangle_{\text{local}} = -\frac{g_{\pi}^2}{4\pi}\frac{1}{2\pi M^2}\int_{-1}^{1} d\cos\theta \left(\frac{m_{\pi}^2}{2(q^2 + m_{\pi}^2)} - \frac{1}{2}\right). \quad (207)$$

This can be viewed as the local approximation to the OPE since the matrix element depends on the momentum transfer q^2, only. It can easily be transformed into the configuration-space representation, resulting in a Yukawa term plus a δ function, which originates from the Fourier transform of the constant $1/2$ in Eq. (207). The various steps leading to this result are shown in Fig. 17. It is obvious from this figure that all of the steps leading to the local expression (207) are not really justified for momenta k around and above 200 MeV, a region of relative momenta which is of importance in the deuteron wave function. This is true for the matrix elements V_{SS} as well as V_{SD}.

Potentials like the Argonne but also the Nijmegen potentials contain the OPE contribution in the local approximation regularizing the limit of small r. In the case of the Argonne potentials the regularization is made in terms of a Gaussian function[89]. It is remarkable that this regularization leads to matrix elements in the SD-channel which are close to those derived from the relativistic expression of the Bonn potential. This is not the case in the SS channel, where the removal of the δ function term is very significant. This comparison of the various approximations to the OPE part of the NN interaction demonstrates that even this long range part of the NN interaction is by no means settled. The local approximation and the regularization by form factors have a significant effect.

The description of the short-range part is also different in these models. The NN potential Nijm-II [167] is a purely local potential in the sense that it uses the local form of the OPE
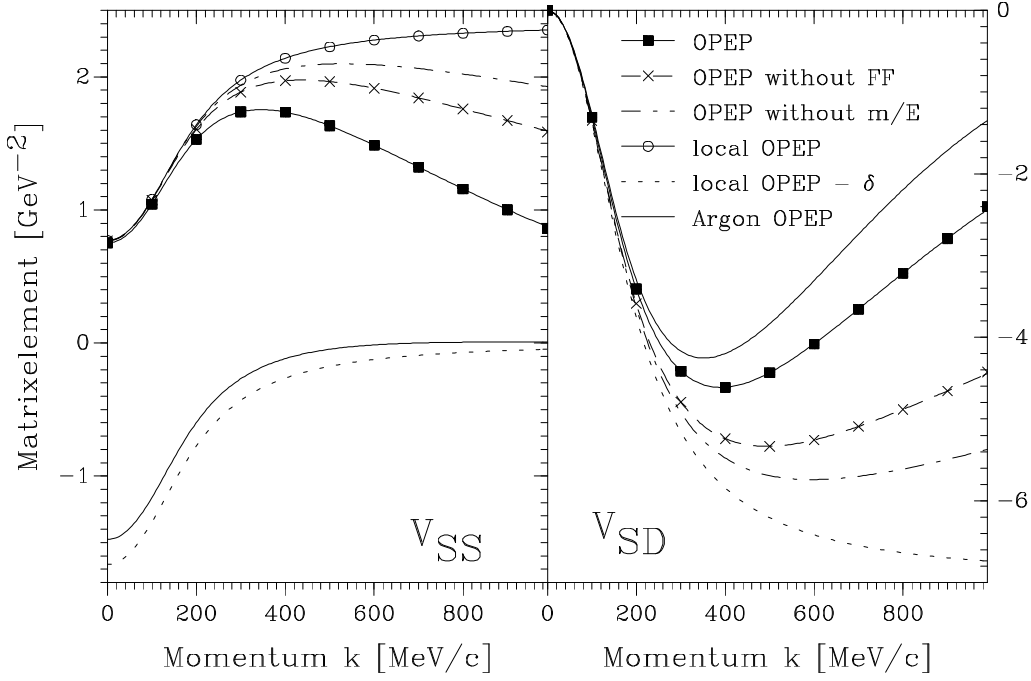
Figure 17: Plane-wave matrix elements of the one-pion-exchange potential (OPEP) using various approximations. As an example, the matrix elements in momentum space $\langle k'|V|k\rangle$ are shown as functions of k for a fixed value of $k' = 95$ MeV/c. The left part of the figure exhibits matrix elements for the partial waves ${}^3S_1$–${}^3S_1$, while the right part shows the tensor component in the ${}^3S_1$–${}^3D_1$ channel with k referring to the momentum in the ${}^3D_1$ partial wave.

potential for the long-range part and parameterizes the contributions of medium and short-range in terms of local functions (depending only on the relative displacement between the two interacting nucleons) multiplied by a set of spin-isospin operators. The same is true for the Argonne V_{18} potential [89]. The NN potential denoted by Nijm-I [167] uses also the local form of OPE but includes a $\mathbf{p^2}$ term in the medium- and short-range central-force (see Eq. (13) of Ref. [167]) which may be interpreted as a non-local contribution to the central force. The CD-Bonn potential is based consistently upon relativistic meson field theory [2]. Meson-exchange Feynman diagrams are typically nonlocal expressions that are represented in momentum-space in analytic form. It has been shown [168] that ignoring the non-localities in the OPE part leads to a larger tensor component in the bare potential.

By construction, all realistic NN potentials reproduce the experimental value for the energy of the deuteron of –2.224 MeV. However, the various contributions to the total deuteron energy originating from kinetic energy and potential energy in the ${}^3S_1$ and ${}^3D_1$ partial waves of relative motion,

$$
\begin{aligned}
E &= \langle \Psi_S|T|\Psi_S\rangle + \langle \Psi_D|T|\Psi_D\rangle + \langle \Psi_S|V|\Psi_S\rangle + \langle \Psi_D|V|\Psi_D\rangle + 2\langle \Psi_S|V|\Psi_D\rangle \\
&= T_S + T_D + V_{SS} + V_{DD} + V_{SD},
\end{aligned}
\tag{208}
$$

exhibit quite different results. This can be seen from the numbers listed in Table 2. In this table, we display the various contributions to the deuteron binding energy employing the four potentials introduced above.

Pot.	T_S [MeV]	T_D [MeV]	V_{SS} [MeV]	V_{DD} [MeV]	V_{SD} [MeV]	P_D [%]
CD-Bonn	9.79	5.69	-4.77	1.34	-14.27	4.83
Argon V_{18}	11.31	8.57	-3.96	0.77	-18.94	5.78
Nijm I	9.66	7.91	-1.35	2.37	-20.82	5.66
Nijm II	12.11	8.10	-5.40	0.59	-17.63	5.64

Table 2: Contributions to the kinetic and potential energy of the deuteron originating from the $^3S_1$ and $^3D_1$ parts of the wave function as defined in Eq. 208. Results are listed for the charge-dependent Bonn potential (CD-Bonn [168]), the Argonne V_{18} [89], the Nijmegen potentials Nijm I and Nijm II [167]. The last column of this Table shows the calculated D-state probabilities of the deuteron.

The kinetic energies are significantly larger for the local potentials V_{18} and Nijm II than for the two interaction models CD-Bonn and Nijm I which contain non-local terms. The corresponding differences in the S-wave functions can be seen in Fig. 18. The local potentials yield a stronger suppression of the $^3S_1$ wave function for small relative distances. This reflects stronger repulsive short-range components of the local interactions. These stronger short-range components are accompanied by larger high momentum components in the momentum distribution, which yields larger kinetic energies.

Comparing the contributions to the potential energy, displayed in Table 2, one finds large differences particularly for the tensor contribution V_{SD}. The dominant part of this tensor contribution should originate from the tensor component of the one-pion-exchange potential which we discussed above.

Although the modern NN potentials yield essentially the same NN scattering phase shifts and the same binding energy for the deuteron, there are significant differences in the contributions to both the kinetic and potential energy of the deuteron in the various partial waves. Speaking in general terms, these differences can be traced back to off-shell differences between the potentials. In particular it is the inclusion of non-local contributions in the long-range (π exchange) as well as short-range part of the NN interaction, which is responsible for these differences.

While the definition of a realistic two-body interaction between nucleons is a rather well defined subject with only little differences between the various models, the situation is much less clear for three-body and other many-body forces. As an example let us consider the process displayed in Fig. 19a) with one of the three nucleons being excited to the Δ resonance in the intermediate state. In a many-body theory which does not consider isobar degrees of freedom explicitly, this process should be included as two-meson exchange three-nucleon interaction. If one calculates the expectation value of this three-nucleon force with the uncorrelated ground state of the hole line expansion, the Goldstone diagrams displayed in Fig. 19b) and c) occur. For a nuclear system with total isospin $T = 0$ the contribution in b) vanishes since it represents a Δ - hole (isospin T=1 or 2) admixture to the ground state. The diagram of Fig. 19c) is closely related to the ground state expectation value of the two-body interaction term shown in Fig. 16a). Fig. 19c corresponds to a correction of that two-body diagram which is due to the fact that the intermediate nucleon states below the Fermi level are blocked by the Pauli principle. Such corrections have been included in nuclear structure calculations, which employed NN interactions of the sort shown in Fig. 16[40, 170]. This demonstrates the model dependence of
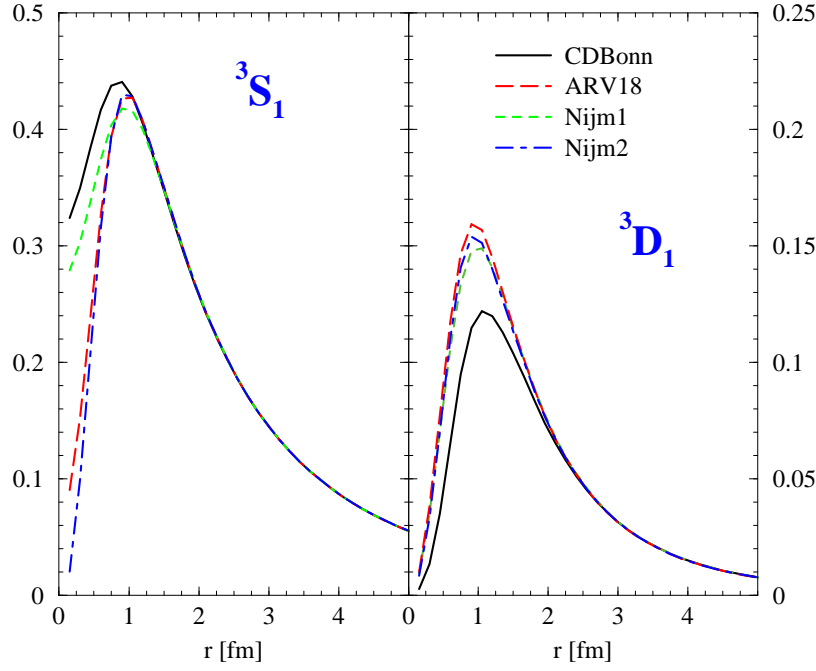
Figure 18: Wave function for the deuteron ($^3S_1$ and $^3D_1$) calculated for different realistic interactions.

such three-nucleon terms.

The models for the three-nucleon interactions which are frequently used in nuclear many-body calculations are based on rather phenomenological grounds. Typically they include a local parameterization of the two-pion exchange terms with intermediate Δ excitations of the form[171]

$$V_{ijk} = A_{2\pi} \sum_{cycl} \left(\{X_{ij}, X_{ik}\} \{\vec{\tau}_i \cdot \vec{\tau}_j, \vec{\tau}_i \cdot \vec{\tau}_k\} + \frac{1}{4} [X_{ij}, X_{ik}] [\vec{\tau}_i \cdot \vec{\tau}_j, \vec{\tau}_i \cdot \vec{\tau}_k] \right) \tag{209}$$

where

$$X_{ij} = \frac{e^{-m_\pi r_{ij}}}{m_\pi r_{ij}} \vec{\sigma}_i \cdot \vec{\sigma}_j + \frac{e^{-m_\pi r_{ij}}}{m_\pi r_{ij}} \left[1 + \frac{3}{m_\pi r_{ij}} + \frac{3}{(m_\pi r_{ij})^2}\right] S_{ij} \tag{210}$$
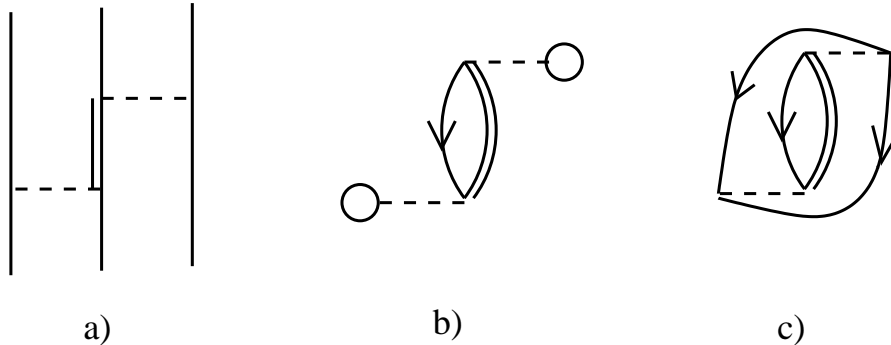
Figure 19: Contributions to the three-body forces as discussed in the text

60

and the symbols [,] and { , } denote commutator and anti-commutator, respectively. Furthermore one introduces a repulsive short range term[87]. The parameters are then adjusted to obtain a good fit to the binding energies of few-body nuclei and nuclear matter. Various three-body forces, labeled e.g. UVII, UIX etc. have been introduced in this way by the Urbana group[88].

3.2 *Ground state Properties of Nuclear Matter and Finite Nuclei*

In the first part of this section we would like to discuss the convergence of the many-body approaches and compare results for nuclear matter as obtained from various calculation schemes presented in section 2. The convergence of the hole-line expansion for nuclear matter has been investigated during the last few years in particular by the group in Catania[60, 61]. Continuing the earlier work of Day[59] they investigated the effects of the three-hole-line contributions for various choices of the auxiliary potential U (see Eq. 11). In particular they considered the standard or conventional choice, which assumes a single-particle potential $U = 0$ for single-particle states above the Fermi level, and the so-called "continuous choice", which has been advocated by the Liege group[11]. This continuous choice supplements the definition of the auxiliary potential of the hole states in Eq. (11) with a corresponding definition (real part of the BHF self-energy) also for the particle states with momenta above the Fermi momentum, $k > k_F$. In this way one does not have any gap in the single-particle spectrum at $k = k_F$.

Fig. 20 shows the results of BHF calculations for the Argonne V_{14}[4] interaction, assuming the standard choice (labeled BHF-s for standard) and the continuous choice (BHF-g) for the auxiliary potential. At $k_F = 1.4$ fm^{-1}, which corresponds to a density close to the empirical saturation density, the standard choice yields an energy of -10.9 MeV per nucleon while the continuous choice leads to -17.1 MeV. At first sight this dependence on the auxiliary potential, a difference of 6 MeV seems very large. One should keep in mind, however, that a Hartree-Fock calculation at the same density for the same interaction yields $+41.8$ MeV per nucleon. This means that the inclusion of two-hole line contributions yields an attractive contribution of 52.7 MeV and 58.9 MeV for the standard and continuous choice, respectively. This means that the uncertainty, how to choose the auxiliary potential, leads to a 10 percent effect in this two-hole line contribution.

Looking at the Bethe-Goldstone equation (7) it is easy to understand that the continuous choice leads to more binding energy. The absolute values for the attractive energy denominators in the Bethe-Goldstone equation, which correspond to the excitation energies of two-particle two-hole excitations are smaller if one accounts for an attractive single-particle potential also in the case of the particle states. This enhances the effects of correlations, leading to more attractive matrix elements for the G-matrix, and provides more binding energy.

The Catania group also evaluated the three-hole line contributions to the energy of nuclear matter for both choices of the auxiliary potential U. Results of such calculations, including the sum of all Bethe-Fadeev ladders, are displayed by symbols in Fig. 20. The contributions of the three-hole line terms are -3.1 MeV and +1.9 MeV per nucleon at $k_F = 1.4$ fm^{-1} for the standard and continuous choice, respectively. This is about a factor 20 smaller than the two-hole line contributions discussed above. This indicates a very good convergence of the hole line expansion for nuclear matter around saturation density. This conclusion is supported by the fact that the results are rather independent on the choice of the auxiliary potential U after the effects of three-hole lines are included. Differences can be observed only for densities, which correspond to k_F around 1.7 fm^{-1} and larger. At those higher densities the effects of four-hole line and higher order terms may get important. Also it is worth noting that the BHF results using the continuous choice are closer to the results with inclusion of three-hole line terms.
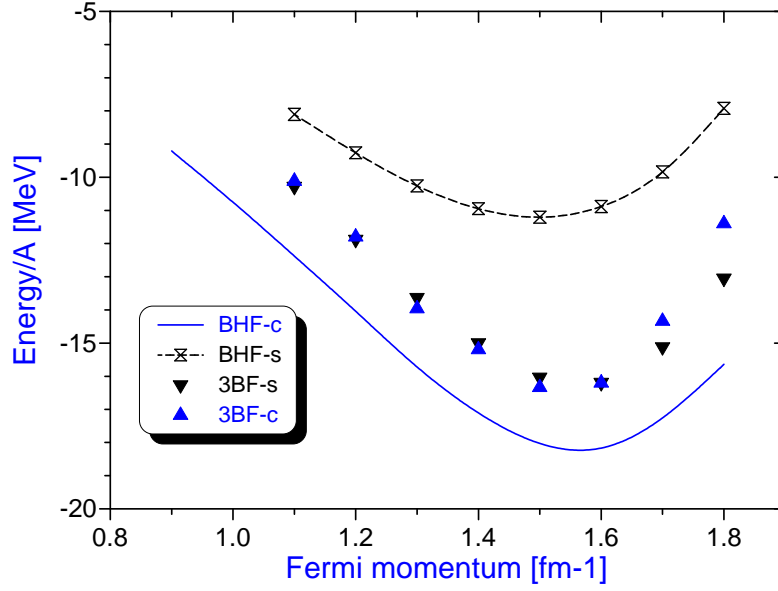
Figure 20: Energy per nucleon calculated for symmetric nuclear matter as a function of the Fermi momentum. Continuous lines represent the results of BHF calculations assuming the standard choice (BHF-s) and the continuous choice (BHF-c) for the auxiliary potential. The symbols (3BF) show results of calculations [61] with inclusion of the three-hole line contributions. The results were obtained using the Argonne V_{14} interaction[4].

How do such results obtained from the hole line expansion compare with those derived from variational calculations? In order to discuss this question we consider as a first step again the results obtained for the Argonne V_{14} interaction at a density of 0.185 fm^{-3}, which corresponds to a Fermi momentum k_F of 1.4 fm^{-1}. As we have seen from the discussion above, the hole-line expansion yields -15. to -15.2 MeV per nucleon if the effects of three-hole line contributions are taken into account. The variational calculation of Wiringa et al.[15] predict an upper bound of -13.4 MeV using the FHNC/SOC approximation at this density. The perturbative corrections within the framework of the CBF theory (see Eq. (143) and subsequent discussion) may provide another -1.5 to -2 MeV[114] so that these very different approaches yield very similar results.

In comparing such numbers one must keep in mind that the results of both approaches should be considered with a kind of "error bar". This error bar should account for conceptual problems: On one side we do not know about the effects of higher order terms in the hole line expansion, on the other side we don't know about the relevance of e.g. elementary diagrams left out in the FHNC/SOC approach. However one should also be aware of uncertainties which are due to technical problems. For example, in performing self-consistent BHF calculations one typically solves the Bethe-Goldstone equation assuming an angle-averaged approximation for the Pauli operator[62, 172]. Recent investigations show that an exact treatment of the Pauli operator may can modify the calculated energy up to around 0.5 MeV per nucleon[173, 174]. Also details of the parameterization of the single-particle energies can lead to differences of this order of magnitude. Uncertainties due to technical reasons must also be considered for the variational calculations. As an example we mention the restriction to a specific variational ansatz for the wave function. As an indication for uncertainties of variational calculations we mention the calculation of the kinetic energy. The kinetic energy can be calculated using different expression. If all many-body clusters are calculated completely these expressions yield
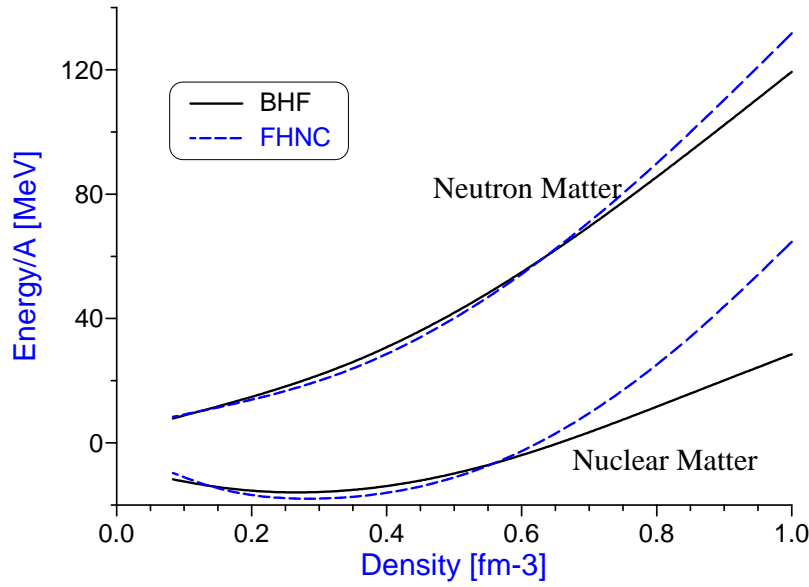
Figure 21: Energy per nucleon calculated for symmetric nuclear matter and pure neutron matter as a function of the Fermi momentum. The results were obtained from BHF[176] and FHNC[114]using the Argonne V_{18} interaction[4].

the same results. So the difference in energies obtained using the so-called Jackson-Feenberg and the Pandharipande-Bethe expression is a measure of the error[175]. This estimates yields error-bars of the order of 1 MeV per nucleon[16] at densities around 0.16 fm^{-1}, the empirical saturation density of nuclear matter.

A comparison between the energies for nuclear matter and neutrons at various densities calculated in the framework of the variational approach[114] and the BHF approximation[176] is displayed in Fig. 21. For both calculations the charge-dependent version of the Argonne potential [89], V_{18} has been used. One finds a rather good agreement between the two approaches at densities up to 0.6 fm^{-3}, which is about 4 times the saturation density of nuclear matter. The predictions of the two approaches deviate from each other at higher densities. This differences at higher densities are to be expected since the convergence of the hole-line expansion should be good at low densities only. Also the variational approach should be less accurate at high densities, genuine n-body correlations should become important. The comparison also shows, however, that quite reliable estimates for the equation of state for symmetric nuclear matter as well as asymmetric nuclear systems can be deduced from such microscopic many-body calculations up to the densities shown in Fig. 21.

While the techniques developed for the variational calculations impose a restriction to the NN interaction to local potentials, more general interactions can be considered in the Brueckner hole-line approximation. Therefore in comparing the features in the predictions derived for various two-body interactions we will restrict ourselves to the discussion of results obtained within the framework of BHF. Results for the saturation points of nuclear matter, i.e. the minima of the energy per nucleon versus density curves, are displayed in Fig. 22. The results presented include predictions from rather old versions of the NN interaction[40] like the Reid soft-core potential[177] (E/A=-10.3 MeV, k_F=1.4 fm^{-1}), but also modern versions like the charge-dependent Bonn potential[168] (E/A=-19.7 MeV, k_F=1.68 fm^{-1}) and Argonne V_{18}[89] (E/A=-16.8 MeV, k_F=1.59 fm^{-1}). All these saturation points form a band, the well known Coester band, an observation which has been made already in 1970[178]: Some interactions,
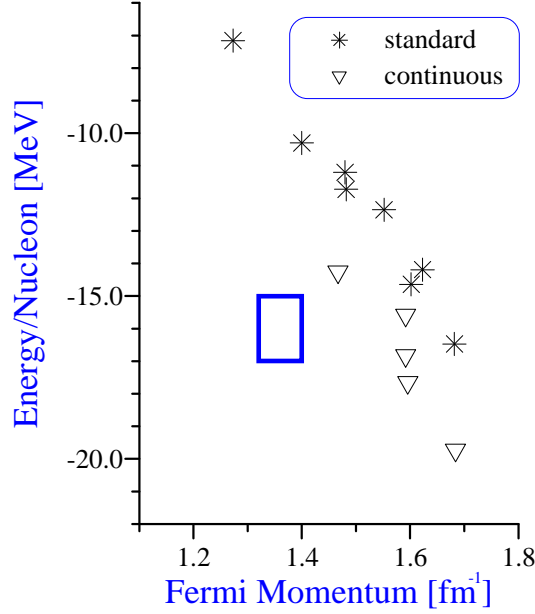
Figure 22: Saturation points of nuclear matter calculated for various realistic NN interactions. Some of those results are taken from [40]. Results were obtained using BHF with standard choice for the auxiliary potential, as well as the continuous choice.

like the Reid soft-core, produce a minimum around the empirical saturation density, $k_F = 1.36$, but predict an energy of only -10 to -11 MeV per nucleon, which is too small as compared to the value -16 MeV taken from the volume term of the empirical mass formula. Other interactions predict an energy, which is close to the empirical value but saturate at a density, which is around 60 percent too high (or even higher).

Traditionally, the saturation properties of the different interactions have been related to the d-state probability in the deuteron predicted by this interaction[40] using the following argument: All interactions produce essentially the same phase-shifts for NN scattering, i.e. they yield the same T-matrix. One may distinguish "soft" interactions, in which the attraction of T originates predominantly from the bare potential V. The attractive terms of higher order, reflecting the importance of correlations are of little importance. Such soft interactions show a small amount of correlations, which is connected to a small d-state probability, a direct indication for weak tensor correlations. The key-quantity of the BHF approximation is the G-matrix, which as we have discussed already in section 2.1, corresponds to the T-matrix except that the terms of higher order in V are quenched because of the Pauli operator and dispersive corrections (the absolute values of the energy denominator are larger in the Bethe-Goldstone equation for the nuclear medium than in the Lippmann-Schwinger equation). For a "soft" interaction this quenching of the attraction in the higher order terms shows only a little effect: the G-matrix is almost as attractive as T therefore one obtains large binding energies at large densities. In contrast, a "stiff" interaction produces more correlations, the attractive contributions of the higher order terms in T are more important, the quenching mechanism is more important and one obtains saturation points for nuclear matter at smaller densities and smaller energies.

In order to explore these saturation features a little bit more in detail, we will focus our attention to those NN interactions which have recently been fitted with high precision to NN

	CDBonn	ArV18	Nijm1	Nijm2	A	B	C	Reid
$< E >$	-17.11	-15.85	-15.82	-13.93	-16.32	-15.32	-14.40	-12.47
$< V >$	-53.34	-62.92	-55.08	-61.94	-52.44	-53.03	-54.95	-61.51
$< T >$	36.23	47.07	39.26	48.01	36.12	37.71	40.55	49.04
$< V_\pi >$	-22.30	-40.35	-28.98	-28.97	-12.48	-26.87	-45.74	-27.37
$< E >_{\text{HF}}$	4.64	30.34	12.08	36.871	7.02	10.07	29.56	176.25
P_D [%]	4.83	5.78	5.66	5.64	4.38	4.99	5.62	6.47

Table 3: Energies calculated for nuclear matter with Fermi momentum $k_F = 1.36$ fm^{-1}. Results are listed for the energy per nucleon calculated in BHF ($< E >$) and Hartree-Fock ($< E >_{HF}$) approximation. Furthermore the expectation value for the NN interaction $< V >$, the kinetic energy $< T_{\text{Kin}} >$ and the one-pion-exchange term $< V_\pi >$ are listed. For completeness we also give the D-state probability calculated for the deuteron P_D. Results are presented for the charge-dependent Bonn (CDBonn) [168], the Argonne V_{18} (ArV18) [89] and two Nijmegen (Nijm1, Nijm2) [167] interactions. For a comparison results are also given for three older versions of the Bonn interaction (A,B,C) [2] and the Reid soft core potential [177], which is supplemented in partial waves in which it is not defined by the OBE C potential. All energies are given in MeV per nucleon.

scattering phase shifts as we already discussed in the preceeding section. In particular we would like to explore the contributions of various components of these interactions to the calculated binding energy. The BHF approach yields the total energy of the system including effects of correlations. Since, however, it does not provide the correlated many-body wave function, one does not obtain any information about e.g. the expectation value for the kinetic energy using this correlated many-body state. To obtain such information one can use the Hellmann-Feynman theorem, which may be formulated as follows: Assume that one splits the total hamiltonian into

$$H = H_0 + \Delta V \tag{211}$$

and defines a hamiltonian depending on a parameter λ by

$$H(\lambda) = H_0 + \lambda \Delta V . \tag{212}$$

If E_λ defines the eigenvalue of

$$H(\lambda)|\Psi_\lambda >= E_\lambda|\Psi_\lambda > \tag{213}$$

the expectation value of ΔV calculated for the eigenstates of the original hamiltonian $H = H(1)$ is given as

$$< \Psi|\Delta V|\Psi >= \left.\frac{\partial E_\lambda}{\partial \lambda}\right|_{\lambda=1} . \tag{214}$$

The BHF approximation can be used to evaluate the energies E_λ, which also leads to the expectation value $< \Psi|\Delta V|\Psi >$ employing this Eq. (214). In the present work we are going to apply the Hellmann-Feynman theorem to determine the expectation value of the kinetic energy and of the one-pion-exchange term $\Delta V = V_\pi$ contained in the different interactions.

First differences in the prediction of nuclear properties[179] obtained from the modern interactions are displayed in table 3 which contains various expectation values calculated for nuclear
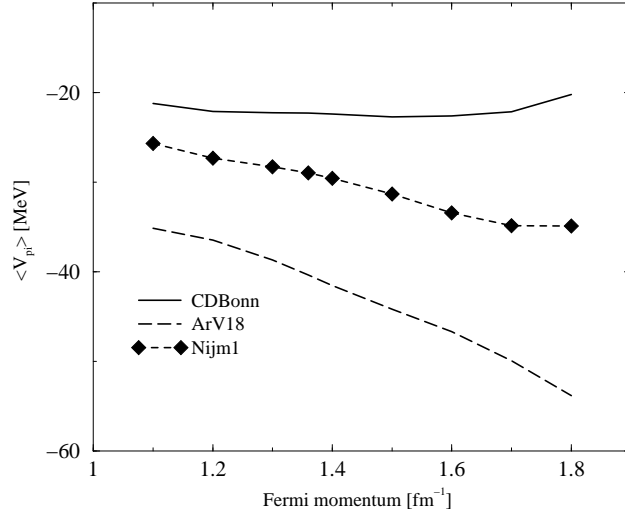
Figure 23: Expectation value of the π-exchange contribution to the energy of nuclear matter as a function of density

matter at the empirical saturation density, which corresponds to a Fermi momentum k_F of 1.36 fm^{-1}. The most striking indication for the importance of nuclear correlations beyond the mean field approximation may be obtained from the comparison of the energy per nucleon calculated in the mean-field or Hartree-Fock (HF) approximation. All energies per nucleon calculated in the (HF) approximation are positive. therefore far away from the empirical value of -16 MeV. Only after inclusion of NN correlations in the BHF approximation results are obtained which are close to the experiment. While the HF energies range from 4.6 MeV in the case of CDBonn to 36.9 MeV for Nijm2, rather similar results are obtained in the BHF approximations. This demonstrates that the effect of correlations is quite different for the different interactions considered. However it is worth noting that all these modern interactions are much "softer" than e.g. the old Reid soft-core potential[177] in the sense that the HF result obtained for the Reid potential (176 MeV) is much more repulsive.

Another measure for the correlations is the enhancement of the kinetic energy calculated for the correlated wave function as compared to the mean field result which is identical to T_{FG}, the energy per particle of the free Fermi gas. At the empirical density this value for T_{FG} is 23 MeV per nucleon. One finds that correlations yield an enhancement for this by a factor which ranges from 1.57 in the case of CDBonn to 2.09 for Nijm1. It is remarkable that the effects of correlations, measured in terms of the enhancement of the kinetic energy or looking at the difference between the HF and BHF energies, are significantly smaller for the interactions CDBonn and Nijm1, which contain non-local terms. The non-local interactions tend to be "softer" in the sense discussed above and therefore lead to more binding energy in nuclear matter.

The table 3 also lists the expectation value for the pion-exchange contribution V_π to the two-body interaction. Here one should note that the expectation value of V_π calculated in the HF approximation is about 15 MeV almost independent of the interaction considered. So it is repulsive and completely due to the Fock exchange term. If, however, the expectation value for V_π is evaluated for the correlated wave function, one obtains rather attractive contributions ranging from -22.30 MeV per nucleon (CDBonn) to -40.35 MeV (ArV18). This expectation value is correlated to the strength of the tensor force or the D-state probability P_D calculated for the deuteron (see table 3 as well). Interactions with larger P_D, like the $ArV18$, yield larger
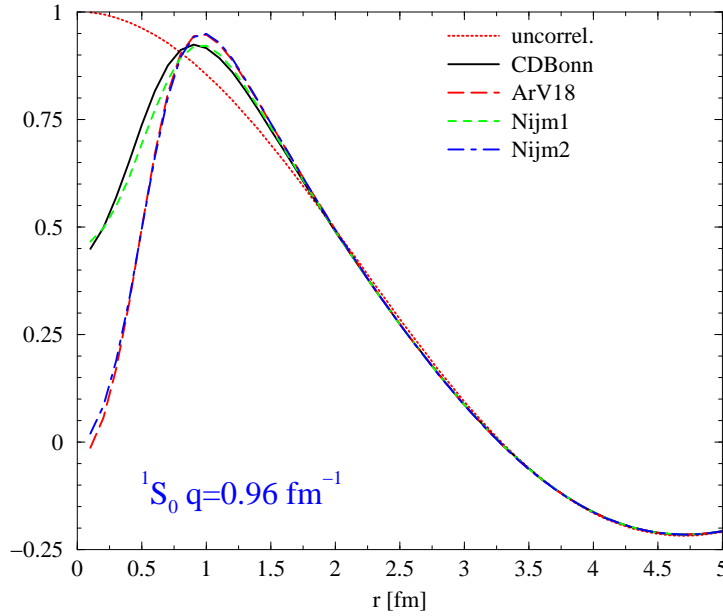
Figure 24: Correlated wave functions $|\psi_{ij}>$ as defined in (10) as a function of the relative distance for the $^1S_0$ partial wave. Results are shown for a pair of nucleons in nuclear matter at empirical saturation density, which heal to an uncorrelated two-nucleon wave function with momentum $q = 0.96$ fm-1 at larger distances. The curves are labeled by the interactions, which were considered.

values for $< V_\pi >$. For a further support of this argument we also give the results for three different version of charge-independent Bonn potentials A, B and C, defined in [2]. All this demonstrates that pionic and tensor correlations are very important to describe the binding properties of nuclei. In fact, the gain in binding energy due to correlations from V_π alone is almost sufficient to explain the difference between the HF and BHF energies.

The importance of pionic correlations has been emphasized by Akmal and Pandharipande[16]. They observe an enhancement of the pionic correlations in FHNC calculations for nuclear matter at high densities and interpret this change in the wavefunction as an indicator for a phase transition to pion condensation[180, 181]. We do not intend to go into a detailed discussion of pion condensation[182], but simply show the expectation values for $< V_\pi >$ as a function of density in Fig. 23. Indeed one finds a smooth enhancement of this expectation value with density if one considers the local representation of the π-exchange as contained in the Argonne V_{18} interaction. It may be questionable if this should be called an indication for a phase transition. Quite a different behavior is obtained if the non-local components are taken into account as they appear e.g. in the CDBonn potential.

Inspecting the expectation values for the kinetic energies we observe a feature very similar to the one observed for the deuteron (see section 3.1): the local interactions, ArV18 and Nijm2, yield larger kinetic energies than CDBonn and Nijm1, which contain nonlocal terms. This is independent of the density considered.

A different point of view on nuclear correlations may be obtained from inspecting the relative wave functions for a correlated pair $|\psi_{ij}>$ defined in (10). Results for such correlated wave functions for a pair of nucleons in nuclear matter at empirical saturation density are displayed in Figs. 24 and 25. As an example we consider wave functions which "heal" at large relative distances to an uncorrelated two-nucleon wave function with momentum $q = 0.96$ fm^{-1}
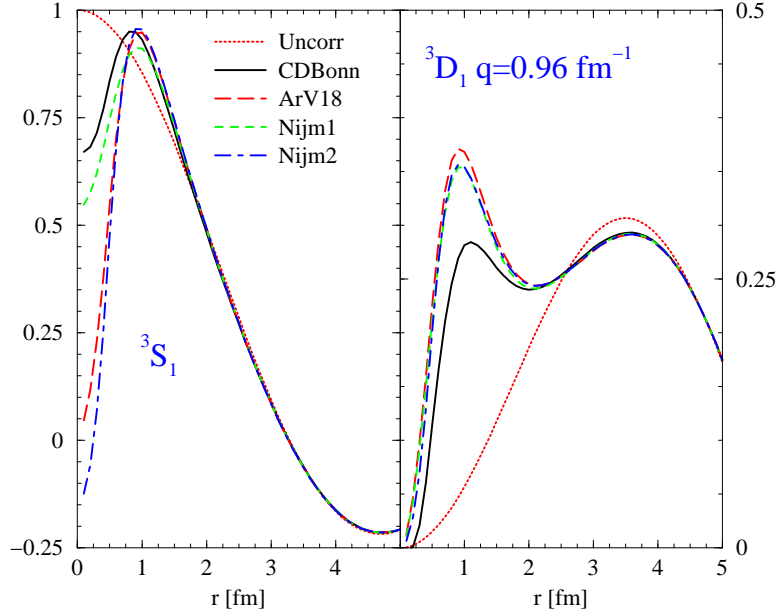
Figure 25: Correlated wave functions as a function of the relative distance for the $^3S_1$ and $^3D_1$ partial waves. Further details see Fig. 24.

calculated at a corresponding average value for the starting energy.

Fig. 24 shows relative wave functions for the partial wave $^1S_0$. One observes the typical features: a reduction of the amplitude as compared to the uncorrelated wave function for relative distances smaller than 0.5 fm, reflecting the repulsive core of the NN interaction, an enhancement for distances between ≈ 0.7 fm and 1.7 fm, which is due to the attractive components at medium range, and the healing to the uncorrelated wave function at large r. One finds that the reduction at short distances is much weaker for the interactions CDBonn and Nijm1 than for the other two. This is in agreement with the discussion of the kinetic energies and the difference between HF and BHF energies (see table 3). The nonlocal interactions CDBonn and Nijm1 are able to fit the NN scattering phase shifts with a softer central core than the local interactions.

Very similar features are also observed in the $^3S_1$ partial wave displayed in the left half of Fig. 25. For the $^3D_1$ partial wave, shown in the right part of Fig. 25, one observes a different behavior: All NN interactions yield an enhancement of the correlated wave function at $r \approx$ 1 fm. This enhancement is due to the tensor correlations, which couples the partial waves $^3S_1$ and $^3D_1$. This enhancement is stronger for the interactions ArV18, Nijm1 and Nijm2 than for the CDBonn potential. Note that the former potential contains a pure nonrelativistic, local one-pion-exchange term, while the CDBonn contains a relativistic, nonlocal pion-exchange contribution. See also the discussion of the wave function for the deuteron in the preceeding section 3.1 and Fig. 18.

These most recent parameterizations of the nucleon-nucleon interaction not only predict different saturation properties of symmetric nuclear matter. Also one can observe differences in the calculated symmetry energy at high densities[176]. The differences between the predictions derived from these modern potentials, however, are significantly smaller than those derived from older models of the NN interaction. All NN interactions now predict a steady increase of the symmetry energy with density. This may be considered as an improvement in the

parameterization of the NN interactions. Nevertheless the remaining differences lead to non-negligible differences in nuclear astrophysics, in the studies of neutron star matter[183, 184]. The CD Bonn potential predicts a slightly larger symmetry energy at high densities. This leads to a larger proton fraction in β-stable matter. As a consequence one finds that the so-called direct URCA process, a very efficient cooling mechanism for neutron stars by neutrino emission, may occur at densities around 0.88 fm^{-3}, 1.05 fm^{-3}, or 1.25 fm^{-3} according to the predictions of the CD Bonn, Argonne V_{18}, or Nijmegen I potential.

These modern NN interactions account for a breaking of isospin symmetry to reproduce pp and pn phase shifts accurately. Even after the electromagnetic effects have been removed, the strong interaction between two protons is in general less attractive than the pn interaction. If included in the calculation, these isospin symmetry breaking effects lead to differences in the predicted energy of the order of 0.3 MeV per nucleon[185]. Isospin symmetry breaking effects as well as charge-symmetry breaking effects (i.e. differences between proton-proton and neutron-neutron interactions which are partly due to the different masses of the nucleons) of these interactions have also been considered to explore their impact on the so-called Nolen-Schiffer anomaly[186].

Up to this point, we were mainly concerned with bulk properties of nuclear matter and correlations which are relevant for all nucleons in the Fermi sea. Special attention has also been paid to correlations around the Fermi level. This includes pairing correlations, which have been studied in the framework of the BCS approach by various groups[187, 188]. Traditionally, such studies concentrate on the $S = 0$, $T = 1$ pairing effects. Correlations, however, are even stronger for the $S = 1, T = 0$ channel and corresponding pairing effects have been studied within the framework of the Green's function approach[189, 190]. Instabilities of normal nuclear matter with respect to such pairing correlations are of particular importance at smaller densities, below the saturation density of nuclear matter.

We are now going to discuss the situation of many-body calculations based on realistic interactions for finite nuclei. On one hand such calculations are in general much more difficult to perform since one has to determine also the appropriate single-particle wave functions within the self-consistent calculations. In nuclear matter the basis of single-particle wave functions, the plane waves, is determined by the symmetry of the problem. This additional complication shows up in all the many-body approaches, which we consider. For the hole-line or Green' function approach this implies that one has to determine the basis, in which the single-particle self energy is diagonal. The same basis must the also be used to define quantities like the Pauli operator in the Bethe-Goldstone equation. One meets a very similar problem in the coupled cluster method, for which one has to determine also the amplitude S_1 in a self-consistent way. For variational calculations the additional complication shows up in the fact that one also has to determine the long-range part of the wave function, e.g. in terms of an appropriate mean field wave function Φ_{MF} in the trial wave function of Eq. (91) from the variational calculation.

On the other hand, however, the calculations for finite nuclei might lead to more reliable results as the average density is lower than for nuclear matter at saturation density. All the expansion techniques which we discussed should converge better for small densities, which means the results obtained at a given order might be more reliable for the finite system.

Some features discussed for the infinite systems should also hold for finite nuclei. This should be true in particular for short-range correlations. Such short range correlations should not be affected by the long-range behavior of the wave functions. To repeat the argument from a different point of view: Short-range correlations are described in terms of particle-hole excitations of such high energies that the shell structure of the single-particle spectrum of finite nuclei is not relevant. The information on such short-range correlations in finite nuclei might therefore be deduced from the corresponding information in nuclear matter by means of a
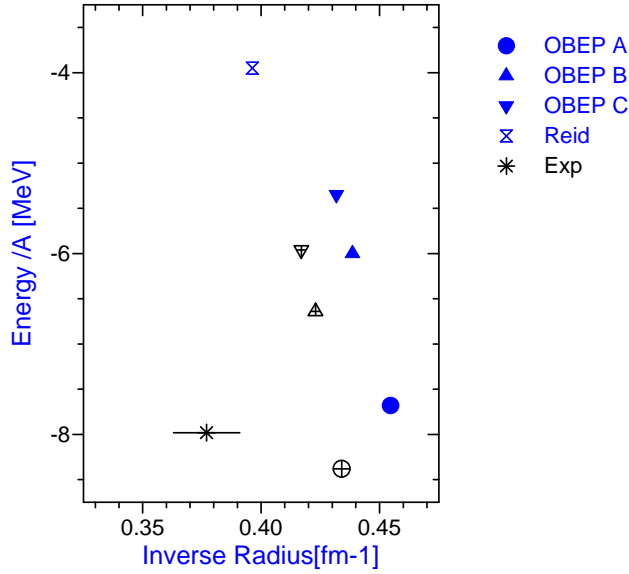
Figure 26: Ground state properties for ^{16}O as predicted in BHF calculations using different OBE potentials from [2]. In terms of open symbols we also present the results after corrections due to general ring diagrams are included.

local density approximation[191, 192, 193, 194]. The situation is different for the long-range correlations, which are built in terms of low energy configurations for which the shell structure is relevant. Such features of the correlations may also vary, depending on the specific nucleus under consideration.

Many-body calculations using the hole-line expansion, the coupled cluster method, the Green's function approach or variational calculations have been done for various different nuclei. In the following discussion we will mainly focus our attention to results on ^{16}O, since for this double magic nucleus results from the different approaches are available.

The complication in solving the BHF equations for finite nuclei have been discussed e.g. in [63], where also a computer program for solving the Bethe-Goldstone equations has been made available. Different techniques to solve the Bethe-Goldstone equation have been described by Barrett et al.[195] and Kuo and coworkers[196]. Also in BHF calculations for finite nuclei one has to choose the spectrum of the intermediate particle states in the Bethe-Goldstone equation. The standard choice is the same as for nuclear matter, use pure kinetic energies. Old studies of three-body terms in the coupled cluster method led to the suggestion that a shift of the kinetic energy spectrum by a value around -8 MeV, would minimize the effects of three-body correlations[197]. Such results indicate that the effects of three-body correlations may even be smaller than for nuclear matter (see the convergence argument given above), however, a systematic study of three-hole line contributions for various interactions should be performed and is still missing.

Results for the energy and the radius of the charge distribution of ^{16}O obtained from BHF calculations [198] using various meson exchange potentials are displayed in Fig. 26. The plot of the results in terms of the energy per nucleon versus the inverse of the radius of the charge distribution has been chosen to have a presentation of results which is similar to the plot of saturation point for nuclear matter in Fig. 22. The results for nuclear matter and finite nuclei are very similar in so far that also the calculated ground state properties for ^{16}O show

a behavior like the Coester band discussed for nuclear matter. There are interactions like the OBEP A (defined in Table A.1 of [2]), which yield about the correct binding energy per nucleon of -7.98 MeV but predict a radius of the charge distribution, which is much smaller than the experimental one. Therefore we also have in this case a density which is too large. Other OBE interaction, which show a larger D-state probability in the deuteron, like OBEP B and OBEB C, are "stiffer" and lead to slightly larger radii but less binding energy. Note that all these modern OBE potential yield more binding than the old Reid soft-core potential[177].

The BHF approximation can be considered as a very efficient tool to account for the effects of two-nucleon short range correlations. This approach, however, might be too simple to account for long-range correlations corresponding to low energy configurations in the nuclear shell-model. Therefore attempts have been made to consider a model space, in the sense as we introduced this term in the discussion around Eq. (5), in which these long range are treated explicitly, and use the lowest order hole-line expansion to account for the short-range correlations outside this model space. This is similar to the concept of model space for nuclear matter as it has been discussed by Kuo et al. [48, 68, 69]. One possible way along this line is to consider a solution of the Bethe-Goldstone equation (7) using a Pauli operator which restricts intermediate two-nucleon states to configurations which are outside the model-space considered. One may then use the resulting G-matrix in shell-model configuration mixing calculation, in which all nucleons are considered as active particles which are allowed to form all configurations within the model space. Such kind of no-core shell-model calculations have recently been done by Barrett and coworkers[199, 200]. Due to the dramatic increase of configurations with increasing number of active nucleons, however, such studies are restricted to very light nuclei.

For heavier nuclei one can consider a model space defined in terms of configurations in e.g. an oscillator basis and consider in a systematic way the effects of correlations defined within this model space. One important class of such long-range configurations are the RPA correlations represented by the so-called particle-hole ring diagrams. They correspond to an iteration of the particle-hole ladders to any order. Within such a limited model space the number of particle-particle configurations is of the same order as the number of hole-hole configurations. Therefore one may like to treat particle-particle and hole-hole ladders on the same footing as it is done in the Green's function formalism. This is achieved by summing the contribution of all particle-particle hole-hole ring diagrams. A technique has been developed which allows the consistent summation of all particle-hole and particle-particle hole-hole ring diagrams leading to a so-called Super RPA (SRPA)[70]. It is remarkable that the resulting SRPA equations yield a stable solution only if the self-energy, used to calculate the single-particle Green's function, is determined in a self-consistent way[201].

Such long-range correlations lead to an additional binding energy for closed shell nuclei like ^{16}O of around 1 MeV per nucleon. They might be characterized by the depletion of the hole-state occupation. Again for the example of ^{16}O, the SRPA correlations in a model space which includes the $1p0f$ oscillator states leads to an occupation probability for the $0p$ hole states which is of the order of 0.85. Note that this depletion of the hole state occupation due to the long-range correlations should be added to the depletion which is due to the short-range correlations (see discussion in the next subsection). The long-range correlations also have an effect on the calculated radii. The effects of these SRPA correlations on the ground-state properties of ^{16}O are also shown in Fig. 26 for the interactions OBEP A to C. The SRPA correlations yield a small improvement of the results obtained within the BHF approach. This improvement, however, is not sufficient to meet the experimental data.

Calculations for finite nuclei using the "Exp(S)" or Coupled Cluster Method have been performed already 25 years ago by Zabolitzky[67, 71]. Using the Reid soft-core potential he finds that the SUB2 approximation yields results which are very similar to those obtained

in the BHF approximation (see result for the Reid potential in Fig. 26) and that the effects of three-body correlations, included in the SUB3 approach, leads to an additional binding energy of around 0.5 MeV per nucleon connected with an enhancement of the wound integral or depletion of the hole-state occupation by around 0.05 percent. This indicates a very good convergence of the Coupled Cluster Method as well as the hole-line expansion.

More recent calculations using the language of the Coupled Cluster Approach have been reported by Heisenberg and Mihaila[73] for the Argonne V_{18} interaction[89]. The calculations are performed in a configuration space defined in terms of harmonic oscillator functions. They use a G-matrix approximation for the two-body interaction and calculate a mean field which they correct to account for 3p3h and 4p4h correlations. They obtain for the case of ^{16}O a binding energy of -5.9 MeV per nucleon and a radius of the charge distribution of 2.81 which is even larger than the experimental value. Unfortunately, there are no BHF calculations available for the same interaction. However, looking at the results obtained for nuclear matter, one would expect that BHF calculations for the V_{18} interaction might produce results with a binding energy around -6 MeV but a smaller radius. It is not clear whether these possible differences are due to the 3p3h and 4p4h corrections included in [73], due to the restricted oscillator space or due to a lack of self-consistency in solving the Bethe-Goldstone equation.

Variational calculations using the FHNC summation techniques which we discussed in section 2.4 have recently been performed for our reference nucleus ^{16}O as well[113]. As we have discussed before the techniques of these variational calculation restrict their applications to local interactions. In the work of Fabrocini et al. [113] various versions of the Argonne potentials V_{14} and V_8 have been used supplemented by three-nucleon potentials of the Urbana group. One of the main problems for such variational calculations for finite systems is to obtain a reliable description for the long range structure of the wave function, i.e. the shape of the single-particle wave functions which form the mean field part of the trial wave function (91). In ref. [113] two different models for these single-particle wave functions are considered: a harmonic oscillator model and a Woods Saxon parameterization. The optimal parameters are determined from the variational calculation. It turns out, however, that the functional exhibits a rather flat minimum as a function of the parameters characterizing the single-particle waves. This is mainly due to the balance between kinetic energy and potential energy. In particular for wave functions with small radii one observes a cancellation between these contributions, which is rather sensitive to the details of the variational form of the wave function.

In fact, one finds minima of the variational calculations, which are quite different for the two parameterization of the single-particle wave functions considered. Therefore also the expectation values of single-particle operators like the radius are rather model-dependent. The Woods Saxon parameterization yields a radius for ^{16}O, which is 0.2 fm smaller than the one derived from the harmonic oscillator parameterization. This certainly a drawback of variational calculations for finite systems. On the other hand, however, the variational calculation yield upper bounds for the energy of the order of -5.2 MeV per nucleon in the case of ^{16}O which is a very good benchmark for other many-body calculations. This is supported by the fact that the FHNC/SOC calculations yield results very close to corresponding Variational Monte-Carlo calculation in cases for which such a comparison is available[113].

Very extensive extensive Variational Monte Carlo (VMC) as well as Green's function Monte Carlo (GFMC) calculations have recently been performed for nuclei with particle number up to $A = 8$[134, 142]. Results of such calculations for the ground state of these nuclei are presented in table 4. The calculations leading to the results displayed in that figure used the Argonne V_{18} potential for the two-body interaction supplemented by the Urbana IX three-nucleon force. This version IX of the Urbana three nucleon forces has been adjusted to reproduce together with the V_{18} NN interaction the binding energy of ^{3}H and to give a reasonable saturation point

^AZ	Energy [MeV]			Radius [fm]	
	VMC	GFMC	Exp.	VMC	Exp.
^{3}H	-8.32	-8.47	-8.48	1.59	1.60
^{4}He	-27.78	-28.30	-28.30	1.47	1.47
^{6}He	-24.87	-27.64	-29.27	1.95	
^{6}Li	-28.09	-31.25	-31.99	2.46	2.43
^{7}He	-24.43	-25.16	-28.82		
^{7}Li	-32.78	-37.44	-39.24	2.26	2.27
^{8}He	-19.71	-25.77	-31.41		
^{8}Li	-29.70	-38.26	-41.28		
^{8}Be	-48.06	-54.66	-56.50		

Table 4: Results for ground state properties of nuclei with nucleon number up to $A = 8$ as obtained in VMC and GFMC calculations. These results for the total energy and rms radii for the protons have been obtained using the Argonne V_{18} for the two-body interaction supplemented by the Urbana IX three-nucleon force. The results displayed in this table have been copied from [134] and [142].

for nuclear matter. Because of these adjustments the calculated energies cannot directly be compared to the results which we discussed before in which no three-nucleon force has been employed. The expectation value of the three nucleon force alone yields a contribution to the energy of ^{7}Li of -8.9 MeV.

Despite the use of this adjusted three-nucleon force it is quite remarkable to see how well the GFMC calculations reproduce the experimental values for the binding energies. It is also very satisfactory to see that he variational calculations (VMC) yield predictions for the energies which are above those obtained in GFMC by values which are typically less than 1 MeV per nucleon. Here one must keep in mind, however, that for these very light nuclei more sophisticated shapes could be considered for the trial wave function than it was possible for heavier nuclei. In particular one does not start assuming a set of single-particle wave function in the mean field part of the trial function, but determines also the long range part of the radial shape in terms of correlation functions.

Also the results for the radii are in very good agreement with the empirical data. Again one should keep in mind, however, that this success is at least partly due to the use of the adjusted three-nucleon force, which has been determined to remove the problem of the Coester band in nuclear matter. This indicates that sophisticated variational calculations using a hamiltonian which has been adjusted to reproduce the saturation point in nuclear matter tend to give proper saturation mechanisms also for finite nuclei. This leads to the expectation that hamiltonians, which lead to a saturation of nuclear matter at a too high density shall predict radii for finite nuclei, which tend to be too small.

3.3   *Single Particle Properties in Nuclear Matter and Finite Nuclei*

Single particle properties are most conveniently described in terms of the Green's function which has been introduced in section 2.3. All single particle properties can be calculated from the single-particle Green's function, in the sense that the expectation value of any one-body
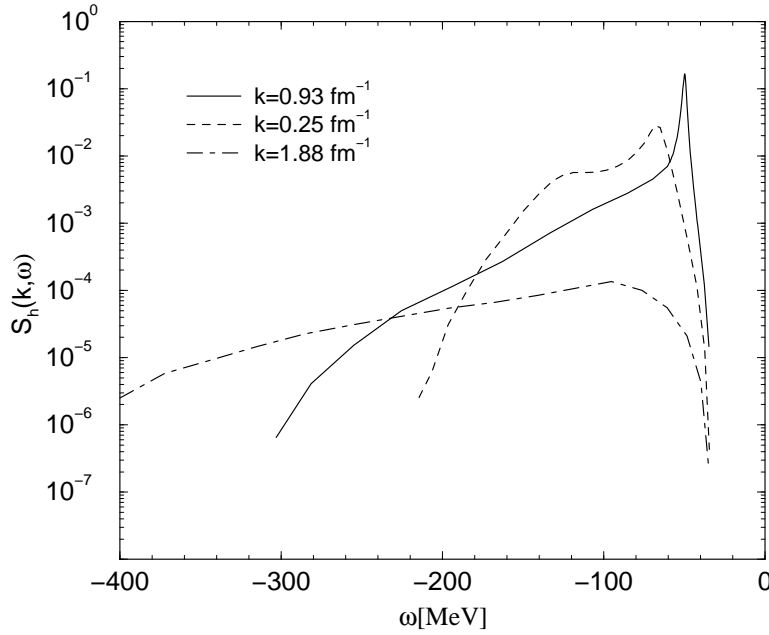
Figure 27: Hole spectral function (in MeV^{-1}) for three different momenta in nuclear matter at $k_F = 1.36 \text{ fm}^{-1}$.

operator can be obtained by using the hole spectral function (Eq. (75)). In this section we will mainly discuss the properties of the hole spectral function in finite nuclei. However, we will also present some results in nuclear matter which show some features of the spectral functions. A recent review on the effects of correlations in the independent particle motion in fermion systems, with special emphasis in the nuclear case, can be found in Ref. [202].

The physical meaning of the hole spectral function can be read from Eq. (72): it gives the probability of removing a particle with momentum **k** from the system of A particles leaving the resulting (A-1) system with an energy $E^{A-1} = E_0^A - \omega$, where E_0^A is the ground state energy of the A particle system. Analogously, the particle spectral function $S_p(k, \omega)$ is the probability of adding a particle with momentum k and leaving the resulting $(A+1)$-system with an energy $E^{A+1} = \omega + E_0^A$. (see also Fig. 12 and discussion in section 2.3

In the Self-Consistent Green's Function (SCGF) formalism, the self-energy is the key quantity to determine the one-body Green's function. The self-energy takes into account the strong interactions that a nucleon in the nuclear medium has with the other nucleons. Since the self-energy is determined from the two-body effective interaction between two dressed particles (Fig.(11)), and this requires in turn the knowledge of the propagator, one needs to deal with a coupled problem which must be solved self-consistently [14]. In the case of an infinite system, the self-energy is diagonal in k and the formal solution of the Dyson's equation (Eq.(78)) is particularly simple

$$g(k, \omega) = \frac{1}{\omega - \frac{k^2}{2m} - \Sigma(k, \omega)}. \tag{215}$$

By combining the Lehmann representation (71), which expresses the single particle propagator in terms of the spectral functions, with the Dyson equation (78), which relates the propagator to the self-energy, the following expressions for the spectral functions are obtained

:

$$S_{h(p)}(k,\omega) = \pm\frac{1}{\pi}\frac{Im\Sigma(k,\omega)}{(\omega - k^2/2m - Re\Sigma(k,\omega))^2 + (Im\Sigma(k,\omega))^2} \ , \ \text{for } \omega < \epsilon_F \ (\omega > \epsilon_F). \quad (216)$$

Due to the short range repulsion present in any realistic interaction, a meaningful approximation to the effective interaction, used in the calculation of the self-energy, should sum up ladder diagrams which in this approach include also hole-hole propagation, either to all orders [189, 14] or to a second order in the propagation of holes [203, 194]. The inclusion of hole-hole propagation is required since at the single particle level it yields the coupling to the excited states of the (A-1) particle system. The self-energy is used in the Dyson equation and the resulting single particle propagator is plugged again in the calculation of the effective interaction, until self-consistency is achieved. In the calculations presented here, self-consistency has been established only for the quasi-particle energies, i.e. at the level of the real on-shell part of the self-energy

$$\epsilon_{qp}(k) = \frac{k^2}{2m} + Re\Sigma(k, \epsilon_{qp}(k)). \quad (217)$$

When this self-consistency is achieved, the complete energy dependence of the self-energy can be studied [189]. The imaginary part of the self-energy is different from zero over a wide range of energies, being positive below ϵ_F and negative above. This yields a spreading of the single-particle strength, but for $k < k_F$ S_h will still contain a peak at the quasi-particle energy. Since S_p contains some fraction of the total strength the occupation probability (Eq. (74)) for $k < k_F$ will be depleted to a value below one.

The energy dependence of the hole spectral function is shown in Fig. 27 for several momenta. These spectral functions have been obtained for the Reid soft core potential at $k_F = 1.36$ fm^{-1} in the framework of SCGF[189]. The hole spectral function in nuclear matter has been also calculated for the Urbana V_{14} interaction [5] in the framework of CBF theory, by including one hole and 2h1p intermediate correlated states[204]. The agreement between both methods is rather satisfactory. For $k < k_F$ the hole spectral function shows a sharp peak (quasi-hole peak) located at the quasi-particle energy that concentrates most of the strength. When k approaches k_F the quasi-hole peak becomes sharper. In the limit $k = k_F$, the peak is just a δ-function, the strength of which defines the discontinuity of the momentum distribution at k_F. The typical occupation probability for $k < k_F$ is about 80%. Since the number of particles must be conserved, it is necessary to have partial occupation of states $k > k_F$, which were unoccupied in the mean field description. A smooth distribution of strength is observed for $k > k_F$ indicating the possibility to find a nucleon in a momentum that would be empty in absence of correlations.

A very important question concerns the location of the high momentum components in the nucleus as a function of the energy. To illustrate this point, Fig.28 shows the occupations for $k > k_F$ obtained by integrating $S_h(k,\omega)$ over excitation energies up to 100 Mev, 200 Mev and up to infinity. One concludes that it is necessary to integrate over high excitation energies of the $A-1$ system in order to catch the high-momentum components. As a result of correlations there are particles promoted above the Fermi sea and $n(k)$ is characterized by a depletion below k_F and a long tail (occupation above k_F) which gives $\approx$ a 62% of the total kinetic energy. The distribution, when the nuclear matter is considered as a normal Fermi fluid, is discontinuous at k_F and the discontinuity is given by Z_{k_F}. Basically all calculations, independently of the method and of the interaction used, provide rather similar results for the depletion. The result for the occupation at $k = 0$ using the Reid soft core at $k_F = 1.36$ fm^{-1} within SCGF is $n(0) = 0.83$ [189]. CBF gives the same result for Urbana V_{14}, however the calculation was performed at slightly smaller density $k_F = 1.33$ fm^{-1} [123]. The calculations in the framework of Green
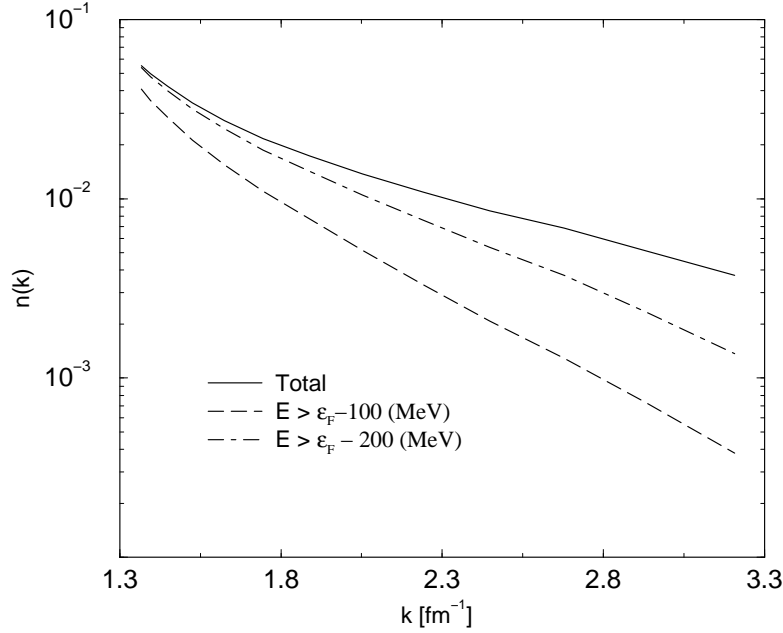
Figure 28: Momentum distribution for $k > k_F$ obtained with various energy cut-offs in the integration of the spectral functions.

function formalism but using a self-energy with up to second order in the propagation of holes, give also very similar results [194, 203]. However, the discontinuity at k_F is more sensitive to both the interaction and the method. Under the same conditions as before, $Z_{k_F} = 0.72$ for the Reid and 0.7 for the Urbana V_{14}. We will have further discussions on $n(k)$ in connection with the momentum distribution in ^{16}O.

The spectral function fulfils energy weighted sum-rules, which besides providing useful information on the spreading of the strength can also be used as a way to control the approximations employed in the calculation. The two lowest sum-rules have a simple expression. $m_0(k)$ is obtained by using the completeness relation in the energy integration of the spectral functions,

$$
\begin{aligned}
m_0(k) &= \int_{-\infty}^{\epsilon_F} d\omega S_h(k,\omega) + \int_{\epsilon}^{\infty} d\omega S_p(k,\omega) \\
&= \langle \Psi_0^A \mid \left\{ a_{\mathbf{k}}, a_{\mathbf{k}}^\dagger \right\} \mid \Psi_0^A \rangle = 1,
\end{aligned}
\tag{218}
$$

due to the fermion character of the nucleons, the anti-commutator $\left\{ a_{\mathbf{k}}, a_{\mathbf{k}}^\dagger \right\}$ is equal to the unit operator.

A similar procedure, leads to the first-order energy weighted sum rule $m_1(k)$:

$$
\begin{aligned}
m_1(k) &= \int_{-\infty}^{\epsilon_F} \omega S_h(k,\omega) d\omega + \int_{\epsilon_F}^{\infty} \omega S_p(k,\omega) d\omega \\
&= \langle \Psi_0^A \mid \left\{ [a_{\mathbf{k}}, H], a_{\mathbf{k}}^\dagger \right\} \mid \Psi_0^A \rangle.
\end{aligned}
\tag{219}
$$

In order to evaluate the right hand side of $m_1(k)$ it is necessary to assume a Hamiltonian, which in the present case is taken to be nonrelativistic and with only two-body forces. Under these assumptions,

$$
\langle \Psi_0^A \mid \left\{ [a_{\mathbf{k}}, H], a_{\mathbf{k}}^\dagger \right\} \mid \Psi_0^A \rangle = \frac{k^2}{2m} + \frac{1}{(2\pi)^3} \int d^3 k' n(k') \langle \mathbf{k}, \mathbf{k}' \mid V \mid \mathbf{k}, \mathbf{k}' \rangle_a,
\tag{220}
$$

where $\langle \mathbf{k}, \mathbf{k}' \mid V \mid \mathbf{k}, \mathbf{k}' \rangle_a$ is the anti-symmetrized two-body matrix element of the bare nucleon-nucleon interaction. The second term on the right hand side of Eq. (220) can be identified with
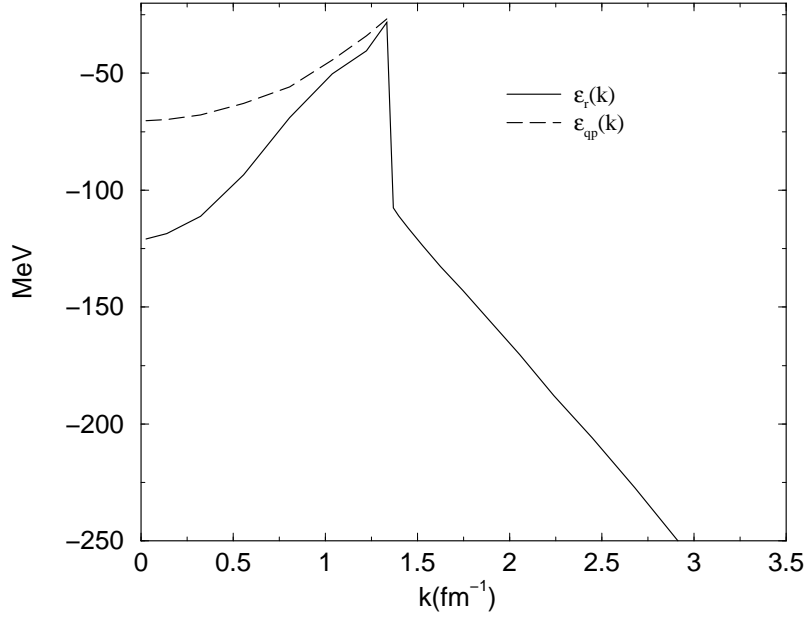
Figure 29: Momentum dependence of the removal energy and the quasi-particle energies, in nuclear matter at $k_F = 1.36$ fm^{-1}.

the energy independent part of the self-energy which is obtained as the high frequency limit of $\Sigma(k, \omega)$ [203]. These sum-rules have been investigated in Ref. [205]. There, it was found that the SCGF approach yields spectral functions that fulfil both sum-rules rather accurately. Due to the short range repulsion of the potential and to the positive character of the kinetic energy contribution, the right hand side of Eq.(220) is usually positive definite and rather large. For instance using the Reid potential it is around 300 MeV at saturation density for $k = 0$. For momenta below k_F, most of the strength ($\approx 80\%$) is below ϵ_F which is a negative quantity. Therefore the contribution of the hole part is negative and it must be the positive contribution of the high energy tail of the particle part of the spectral function which, besides compensating the negative contribution of the hole part, brings the left hand side to fulfil the equality. This confirms the need for the appearance of single-particle strength at very high energies.

Another useful check for the spectral functions is the density sum-rule

$$\rho = \frac{\text{deg}}{(2\pi)^3} \int d^3k \; n(k) = \frac{\text{deg}}{(2\pi)^3} \int d^3k \int_{-\infty}^{\epsilon_F} S_h(k, \omega) d\omega \,, \tag{221}$$

with deg denoting the degeneracy of the single-particle level, which is 4 for nuclear matter. This sum-rule is well respected by the different approaches. In the case of the SCGF formalism it is fulfilled within 1%. The integration up to k_F provides 81% of the sum-rule and one gets a 97% if the integration is carried up to $3k_F$.

In the case of two body interactions, the hole spectral function gives access, through the Koltun sum-rule (76), to the binding energy per particle,

$$e(\rho) = \frac{deg}{\rho(2\pi)^3} \int d^3k \int_{-\infty}^{\epsilon_F} \frac{1}{2} \left(\frac{k^2}{2m} + \omega \right) S_h(k, \omega) d\omega, \tag{222}$$

to the kinetic energy per particle,

$$t(\rho) = \frac{deg}{\rho(2\pi)^3} \int d^3k \frac{k^2}{2m} \int_{-\infty}^{\epsilon_F} d\omega S_h(k, \omega) = \frac{deg}{\rho(2\pi)^3} \int d^3k \frac{k^2}{2m} n(k) \tag{223}$$

and to the potential energy per particle $v(\rho) = e(\rho) - t(\rho)$. Introducing the removal energy $\epsilon_r(k)$,

$$\epsilon_r(k) = \frac{\int_{-\infty}^{\epsilon_F} d\omega \ \omega \ S_h(k,\omega)}{\int_{-\infty}^{\epsilon_F} d\omega S_h(k,\omega)} \tag{224}$$

one can express the binding energy as

$$e(\rho) = \frac{deg}{\rho(2\pi)^3} \int d^3k \frac{1}{2} \left(\frac{k^2}{2m} + \epsilon_r(k) \right) n(k). \tag{225}$$

In Brueckner-Hartree-Fock, $\epsilon_r(k) = k^2/2m + u(k)$, i.e. it coincides with the quasiparticle energy, and $n(k) = \theta(k_F - k)$, therefore

$$e_{BHF} = \frac{deg}{\rho(2\pi)^3} \int d^3k \left(\frac{k^2}{2m} + \frac{1}{2}u(k) \right). \tag{226}$$

Due to correlations, the spreading of the spectral function implies that $\epsilon_r(k) \neq \epsilon_{qp}(k)$. Obviously this comparison between $\epsilon_r(k)$ and ϵ_{QP} has sense only for $k \leq k_F$.

The momentum dependence of the removal energy is shown in Fig. 29 together with the quasi-particle energies (below k_F) for the Reid soft core within SCGF. $\epsilon_r(k)$ is an increasing function of k for $k < k_F$ and decreases quite fast for $k > k_F$ having a large discontinuity at k_F. For $k = 0.027$, $\epsilon_r = -121$ MeV, while $\epsilon_{QP} = -70.38$ MeV, and the occupation probability $n(0.027) = 0.83$.

Averaging (224) over all momenta one can define a mean removal energy, $\tilde{\epsilon}_r$, by

$$\tilde{\epsilon}_r = \frac{\int d^3k \int_{-\infty}^{\epsilon_F} d\omega \omega S_h(k,\omega)}{\int d^3k \int S_h(k,\omega)d\omega} = t(\rho) + 2v(\rho) \tag{227}$$

In the case that we are considering as an example, i.e. nuclear matter with the Reid soft core, at $k_F = 1.36$ fm^{-1} in the framework of SCGF, $\tilde{\epsilon}_r \approx -86$ MeV. On the other hand, the binding energy is ≈ -18MeV, which is too large. However, what we want to show here is the balance of kinetic and potential energy and the contribution to the Koltun sum-rule from momenta above k_F.

This binding energy is the result of a cancellation between a kinetic energy, $t(\rho) = 48.4$ MeV, and a potential energy ,$v(\rho) = -66.7$ MeV. The contributions to $t(\rho)$ and $v(\rho)$ of k's below k_F are the 38% and the 47% respectively. This supports the crucial role of the high momentum components also in the energetics of the system, when the kinetic and the potential energy are calculated separately. One should keep in mind that the contribution of the low momenta ($k < k_F$) to the density sum-rule was $\approx 80\%$ and their contribution to the total energy is around 70%. The details depend on the interaction used. Note that the expectation value for the kinetic energy obtained in SCGF agrees rather well with the result listed in table 3 for the Reid potential. The comparison in that table also shows that the non-local OBE interactions are softer than the Reid potential leading to smaller kinetic energies and smaller contributions from high momenta.

To carry on the full self-consistent scheme, and calculate the effective interaction with dressed particles, i.e. considering the spectral functions in the intermediate states in calculating the G-matrix is a very difficult task. There are however, recent attempts in that direction [206, 207] and also efforts to analyze the meaning of using dressed particles when one considers the scattering in the medium [208].

The calculation of the single particle spectral function for finite nuclei is much more compli-cated. Both the self-energy and the Green's function are not anymore diagonal in momentum

and furthermore, one should deal with discrete (bound) and continuum single particle basis states. Microscopic calculations have mainly been performed for very light nuclei [209]. For heavier nuclei, several procedures based on local density approximation have been devised [191, 192, 193]. Here we will pay more attention to the explicit calculations of the spectral function directly in finite nuclei. The calculations have been mainly dealing with the hole part of the spectral function for ^{16}O nucleus for which also systematic exclusive electron scattering measurements exist, which will be discussed in the next section. A convenient way to take advantage of the spherical symmetry is to introduce a partial wave decomposition of the spectral function and work in the single-particle basis characterized by the orbital angular momentum l, total angular momentum j, isospin third component τ and momentum k,

$$S_{lj\tau}(k,\omega) = \sum_n |\langle \Psi_n^{A-1} | a_{kl\tau} | \Psi_0^A \rangle |^2 \, \delta(\omega - (E_0^A - E_n^{A-1})) \qquad (228)$$

The momentum distribution

$$n_{lj\tau}(k) = \langle \Psi_0^A | a_{klj\tau}^\dagger a_{klj\tau} | \Psi_0^A \rangle = \sum_n |\langle \Psi_n^{A-1} | a_{klj\tau} | \Psi_0^A \rangle |^2, \qquad (229)$$

is obtained by integrating $S_{lj\tau}(k,\omega)$ over the excitation energies of the $A-1$ system. In the independent particle model (IPM), the sum in this equation is typically reduced to one term, if (l,j,τ) refer to a single-particle orbit occupied in Ψ_0^A. In that case, Eq.(229) yields the square of the momentum space wave function for this single particle state. The contribution $n_{lj\tau}(k)$ vanishes in the IPM if no state with this quantum numbers is occupied. If correlations are present beyond the IPM approach this simple picture is no longer true and one can study the effects of correlations on $n(k)$. Taking into account the degeneracy factors of each orbital one obtains the total momentum distribution

$$n(k) = \sum_{l,j,\tau}(2j+1)n_{lj\tau}(k). \qquad (230)$$

The spectral function for the various partial waves, $S_{lj\tau}(k,\omega)$ can be obtained from the imaginary part of the corresponding single-particle Green's function $g_{lj\tau}(k,\omega)$ which can be evaluated by solving the Dyson equation (Eq. (78))

$$g_{lj}(k_1,k_2;\omega) = g_{lj}^{(0)}(k_1,k_2;\omega) + \int dk_3 \int dk_4 g_{lj}^{(0)}(k_1,k_3;\omega)\Delta\Sigma_{lj}(k_3,k_4;\omega)g_{lj}(k_4,k_2;\omega), \qquad (231)$$

where $g^{(0)}$ refers to a Hartree-Fock propagator and $\Delta\Sigma_{lj}$ represents contributions to the real and imaginary part of the irreducible self-energy , which go beyond the Hartree-Fock approximation of the nucleon self-energy used to derive $g^{(0)}$. Notice that here and in the following we have dropped the isospin quantum number τ. Ignoring the Coulomb interaction between the protons the Green function are identical for $N = Z$ nuclei and therefore independent of the quantum number τ.

As in the nuclear matter case, the key point of this approach is the calculation of the self-energy, its calculation as well as the solution of the Dyson equation has been discussed in detail in Ref. [22]. However we include here a brief summary of the relevant aspects of the method.

The self-energy is evaluated in terms of a G matrix which is obtained as a solution of the Bethe-Goldstone equation for nuclear-matter. The Bethe-Goldstone equation is solved at a given density and starting energy. In the calculations reported here, the chosen interaction is the one-boson- exchange (OBE) potential B [2] for $k_F = 1.4 fm^{-1}$ and starting energy -10 MeV. These choices are rather arbitrary. It turns out, however, that the final result is not sensitive
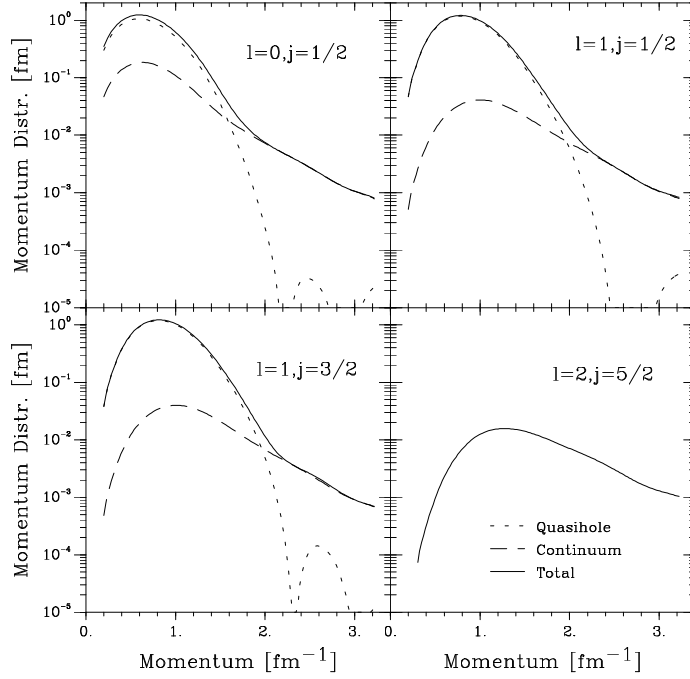
Figure 30: Momentum distribution (solid line) for different partial waves in ^{16}O. The momentum distribution is the sum of the quasihole contribution (short-dashed line) and the continuum contribution (long-dashed line).

to this choice. The self-energy contains a Hartree-Fock contribution plus terms of second order in G with intermediate two-particle-one-hole (2p1h) and two-hole-one-particle states, assuming harmonic oscillator states for the hole states and plane waves appropriately orthogonalized for the particle states. The techniques, which are needed to evaluate matrix elements in such a mixed representation are described in [22].

Using such matrix elements one can determine the imaginary part of the 2p1h and 2h1p contributions, W_{lj}^{2p1h} and W_{lj}^{2h1p} in a straightforward way.

The real parts of the self-energy are calculated by means of dispersion relations like,

$$V_{lj}^{2p1h}(k, k'; \omega) = \frac{\mathcal{P}}{\pi} \int_{-\infty}^{\infty} \frac{W_{lj}^{2p1h}(k, k'; \omega')}{\omega' - \omega} d\omega', \qquad (232)$$

where $\mathcal{P}$ indicates a principal value integral and k, k' refer to the modulus of the single-particle momentum k for the nucleon under consideration with angular momentum quantum numbers l and j. The imaginary part W^{2p1h} is different from zero only for positive energies. Since the diagonal matrix elements of W^{2p1h} are negative, the dispersion relation (Eq.(232)) implies that the diagonal elements of V^{2p1h} will be attractive for negative energies. They will decrease and change sign only for large positive values for the energy of the interacting nucleon.

Since the Hartree-Fock contribution Σ^{HF} is calculated in terms of a nuclear G-matrix, it already contains 2p1h terms. In order to avoid such an over-counting of particle-particle ladder terms, a correction term (V_c), which contains the 2p1h contribution calculated in nuclear matter with the same starting energy and Pauli operator as used in the Bethe-Goldstone equation, is subtracted from V^{2p1h}. A dispersion relation similar to Eq.(232) holds for V^{2h1p} and W^{2h1p}.

Summing up the different contributions, the self-energy is expressed as

$$\Sigma = \Sigma^{HF} + \Delta\Sigma = \Sigma^{HF} + (V^{2p1h} - V_c + V^{2h1p}) + i(W^{2p1h} + W^{2h1p}). \qquad (233)$$

The resulting self-energy is non-local and energy dependent. It represents a microscopic derivation of the optical potential which can be used to analyze the data of nucleon-nucleus scattering. Careful studies of the non-locality of this self-energy have been presented in Ref. [210]. In this reference, a parameterization of the self-energy, for both the real and the imaginary part, was given in terms of local energy dependent potential of the Woods-Saxon form.

Once the self-energy is calculated one must solve the Dyson equation (Eq. (231)) for the single particle propagator. To this aim, it is useful to discretize the integrals involved in this equation by considering a complete basis within a spherical box of a radius R_{box}. The calculated observables are independent of the choice of R_{box}, if it is chosen to be around 15 fm or larger. A complete and orthonormal set of regular basis functions within this box is given by

$$\Phi_{iljm}(\mathbf{r}) = \langle \mathbf{r} \mid k_i ljm \rangle = N_{il}j_l(k_i r)\mathcal{Y}_{ljm}(\theta, \phi). \tag{234}$$

In this equation $\mathcal{Y}_{ljm}$ represent the spherical harmonics including the spin degrees of freedom, N_{il} is a normalization constant and j_l denote the spherical Bessel functions for the discrete momenta k_i which fulfil

$$j_l(k_i R_{box}) = 0. \tag{235}$$

These basis functions, defined for discrete values of the momentum k_i within the box, differ from the plane wave states defined in the continuum with the same momenta just by the normalization constant, which is $\sqrt{2/\pi}$ for the latter.

As a first step, one constructs the Hartree-Fock approximation for the single-particle Green's function in the "box basis". To this end, the Hartree-Fock Hamiltonian is diagonalized,

$$\sum_{n=1}^{N_{max}} \langle k_i \mid \frac{k_i^2}{2m}\delta_{in} + \Sigma_{lj}^{HF} \mid k_n \rangle \langle k_n \mid \alpha \rangle_{lj} = \epsilon_{\alpha lj}^{HF} \langle k_i \mid \alpha \rangle_{lj}. \tag{236}$$

The set of basis states in the box is truncated by assuming an appropriate N_{max} (Usually $N_{max} = 20$ is enough). In the basis of Hartree-Fock states $\mid \alpha \rangle$, the Hartree-Fock propagator is diagonal and given by

$$g_{lj}^{(0)}(\alpha, \omega) = \frac{1}{\omega - \epsilon_{lj}^{HF} \pm i\eta}, \tag{237}$$

where the sign in front of the infinitesimal imaginary quantity $i\eta$ is positive (negative) if $\epsilon_{\alpha lj}^{HF}$ is above (below) the Fermi energy. With these ingredients one can solve the Dyson equation (Eq. (231)). An efficient procedure is to determine first the reducible self-energy,

$$\langle \alpha \mid \Sigma_{lj}^{red}(\omega) \mid \beta \rangle = \langle \alpha \mid \Delta\Sigma_{lj}(\omega) \mid \beta \rangle + \sum_{\gamma}\langle \alpha \mid \Delta\Sigma_{lj}(\omega) \mid \gamma \rangle \times g_{lj}^{(0)}(\gamma; \omega)\langle \gamma \mid \Sigma_{lj}^{red}(\omega) \mid \beta \rangle \tag{238}$$

and obtain the propagator from

$$g_{lj}(\alpha, \beta; \omega) = \delta_{\alpha\beta}g_{lj}^{(0)}(\alpha; \omega) + g_{lj}^{(0)}(\alpha; \omega)\langle \alpha \mid \Sigma_{lj}^{red}(\omega) \mid \beta \rangle g_{lj}^{(0)}(\beta; \omega). \tag{239}$$

Using this representation of the Green's function one can calculate the spectral function in the "box basis" from

$$\tilde{S}_{lj}^c(k_m, k_n; \omega) = \frac{1}{\pi}Im \left(\sum_{\alpha,\beta}\langle k_m \mid \alpha \rangle_{lj} g_{lj}(\alpha, \beta; \omega)\langle \beta \mid k_n \rangle_{lj} \right). \tag{240}$$

For energies below the lowest sp energy of a given Hartree-Fock state (with lj) this spectral function is different from zero only due to the imaginary part of Σ^{red}. This contribution involves the coupling to the continuum of 2h1p states and is therefore

$$\sum_{n=1}^{N_{max}} \langle k_i \mid \frac{k_i^2}{2m}\delta_{in} + \Sigma_{lj}^{HF} + \Delta\Sigma_{lj}(\omega = \epsilon_{\Upsilon lj}^{qh}) \mid k_n \rangle \langle k_n \mid \Upsilon \rangle_{lj} = \epsilon_{\Upsilon lj}^{qh}\langle k_i \mid \Upsilon \rangle_{lj}. \tag{241}$$
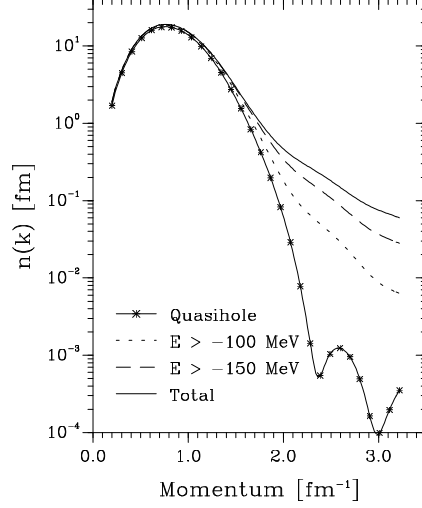
Figure 31: The total momentum distribution of ^{16}O. The quasihole contributions also shown together with the results obtained with various energy cutoffs in the integration of the spectral functions.

Since, in this approach $\Delta\Sigma$ contains a sizable imaginary part only for energies below ϵ_Υ^{qh}, the energies of the quasihole states are real and the continuum contribution is separated in energy from the quasihole contribution. The quasihole contribution to the hole spectral function is given by

$$\tilde{S}_{\Upsilon l j}^{qh}(k_m, k_n; \omega) = Z_{\Upsilon l j}\langle k_m \mid \Upsilon\rangle_{lj}\langle\Upsilon \mid k_n\rangle_{lj}\delta(\omega - \epsilon_{\Upsilon l j}^{qh}), \tag{242}$$

with the spectroscopic factor for the quasihole state given by

$$Z_{\Upsilon l j} = \left(1 - \frac{\partial\langle\Upsilon \mid \Delta\Sigma_{lj}(\omega) \mid \Upsilon\rangle}{\partial\omega} \mid \epsilon_{\Upsilon l j}^{qh}\right)^{-1}. \tag{243}$$

Finally, the continuum contribution of Eq. (240) and the quasihole parts of Eq. (243) can be added and renormalized to obtain the spectral function in the continuum representation at the momenta defined by Eq. (235):

$$S_{lj}(k_i, \omega) = \frac{2}{\pi}\frac{1}{N_{il}^2}\left(\tilde{S}_{lj}^c(k_i, \omega) + \sum_\Upsilon \tilde{S}_{\Upsilon l j}^{qh}(k_i, \omega)\right). \tag{244}$$

The quasi-hole states with a probability defined by the spectroscopic factor Z_{lj} (in this example 0.78, 0.91 and 0.90 in the case of $s_{1/2}$, $p_{3/2}$ and $p_{1/2}$) are located at the corresponding quasi-hole energies -34.30 MeV, -17.90 MeV and -14.14 MeV, respectively. Some strength has been moved to more negative values of ω in the (2h1p) continuum.

The momentum distribution $n_{lj}(k)$ is given by the energy-integrated spectral function. Here it is also convenient to separate the contribution in two pieces: the continuum and the quasi-hole part

$$n_{lj}(k) = \int_{-\infty}^{\epsilon_F} d\omega\left[\tilde{S}_{lj}^c(k, \omega) + \tilde{S}_{lj}^{qh}(k, \omega)\right]. \tag{245}$$

This separation into the two parts is displayed in Fig. 30 for various partial waves. This figure shows quite clearly that the momentum distribution at small momenta is dominated by the
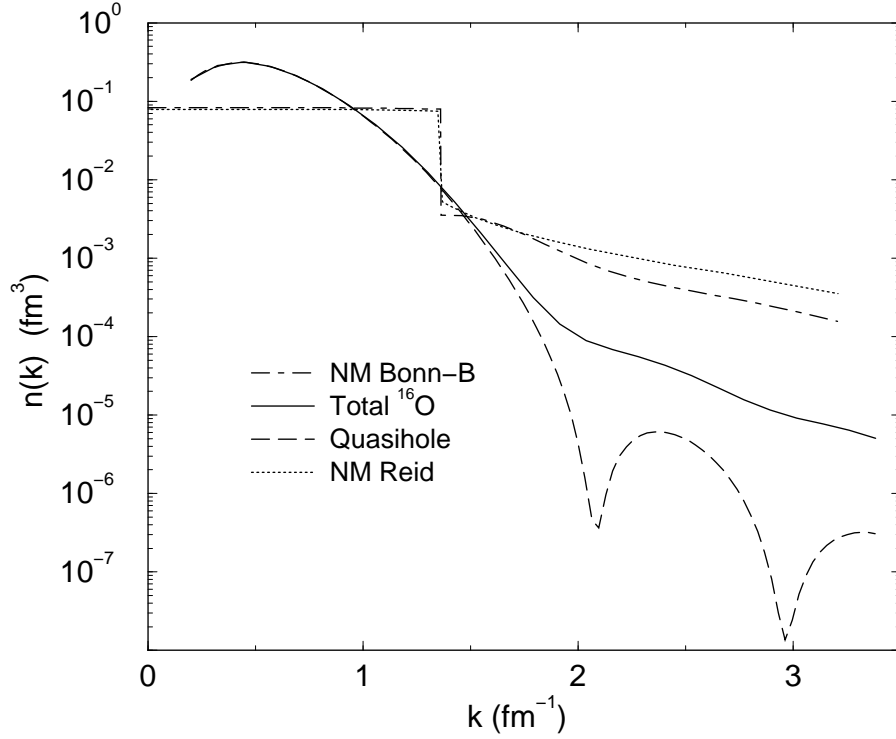
Figure 32: Momentum distribution of ^{16}O, obtained in the Green function approach employing the OBE potential, compared with $n(k)$ obtained in nuclear matter. Also reported are the $n(k)$ of nuclear matter within the SCGF approach for the Reid potential.

quasihole contribution (for those partial waves for which exists) whereas the high momentum components are given by the continuum part. In order to show the importance of the continuum part of the spectral functions as compared to the quasihole contribution, the particle numbers for each partial wave including the degeneracy of the states,

$$\tilde{n}_{ij} = 2(2j+1) \int_{-\infty}^{\epsilon_F} d\omega \int_0^\infty dk k^2 S_{lj}(k,\omega), \tag{246}$$

separating the quasihole and the continuum contributions are reported in Table 5. In this approach, there are only 14.025 out of 16 nucleons in the quasi-hole states. Another 1.13 "nucleons" are found in the $2h1p$ continuum with partial wave quantum numbers of the s and p shells, while an additional 0.79 "nucleons" are obtained from the continuum with orbital quantum numbers of the d,f and g shells. The quasi-hole strength can be identified with the experimental spectroscopic factor. In this approach, for the $p_{1/2}$ it turns to be 90% which is too large compared with the experimentally determined value, 63%. This discrepancy , can be associated to the fact that this approach is treating mainly the short-range correlations. Long-range (low-energy) correlations, will typically yield another 10% reduction of the quasihole strength [84, 211, 212]. Similar results are obtained with variational Monte Carlo techniques, calculating the overlap between a correlated ground state wave function for ^{16}O and the quasi-hole states of the $(A-1)$ residual system (^{15}N) [213]. However, an appropriate treatment of center of mass motion can enhance the spectroscopic factor by up to 7%[214] increasing again the discrepancy with the experimental data. The absolute value for the spectroscopic factors seems not to be understood yet.

lj	$\hat{n}^{qh}$	$\hat{n}^c$	$\hat{n}$
$s_{1/2}$	3.120	0.624	3.744
$p_{3/2}$	7.314	0.332	7.646
$p_{1/2}$	3.592	0.173	3.764
$d_{5/2}$	0.0	0.234	0.234
$d_{3/2}$	0.0	0.196	0.196
$f_{7/2}$	0.0	0.117	0.117
$f_{5/2}$	0.0	0.140	0.140
$g_{9/2}$	0.0	0.040	0.040
$g_{7/2}$	0.0	0.064	0.064
$\sum$	14.025	1.920	15.945

Table 5: Distribution of nucleons in ^{16}O. Listed are the total occupation number $\tilde{n}$ for various partial waves and also the contributions from the quasihole ($\tilde{n}^{qh}$) and the continuum part ($\tilde{n}^c$) of the spectral function separately. The last line gives the sum of particle numbers for all partial wave listed.

The sum of the particle numbers listed in Table 5 is slightly smaller (15.945) than the particle number corresponding to ^{16}O. There are several possible sources for this discrepancy: First of all the analysis only accounts for momenta below 3.3 fm^{-1} and the partial waves with $l > 4$ have not been considered. The restriction in k is determined by the choice of N_{max} in truncating the "box basis". Inspecting the decrease of the occupation numbers listed in Table 5 with increasing l one can expect that the "missing" nucleons may be found in partial waves with $l > 4$. Furthermore, however, one must also keep in mind that this approach to the single-particle Green function is not number conserving, as the Green functions used to evaluate the self-energy are not determined in a self-consistent way [14].

Similarly to Fig.28 for nuclear matter, the momentum distribution including the quasi-hole states obtained with various energy cutoffs is shown in Fig. 31. The quasihole part reflects the momentum components that one can detect in knock-out reactions with small energy transfer. As in the nuclear matter case, the high momentum components due to short-range correlations can be detected only for large excitation energies.

The total momentum distribution is displayed again in Fig.32 and compared to predictions for nuclear matter. In order to enable the comparison with nuclear matter results, the momentum distributions have been normalized such that $\int d^3k n(k)$ yields 1. In order to show the sensitivity of the calculated momentum distribution to the nucleon-nucleon interaction, the results obtained for Reid soft-core in SCGF are also shown[189]. The nuclear matter results for the OBE-B potential have been obtained by using a self-energy which contains only second order terms on the propagation of holes [194]. The OBE-B is consider to be softer than the older Reid potential. This is reflected by the fact that the momentum distribution obtained for the Reid potential yields larger occupation values for $k > k_F$ than those obtained for the OBE potential. The comparison between nuclear matter and finite nuclei seems to indicate that the enhancement of the momentum distribution predicted in this approach for high momenta is
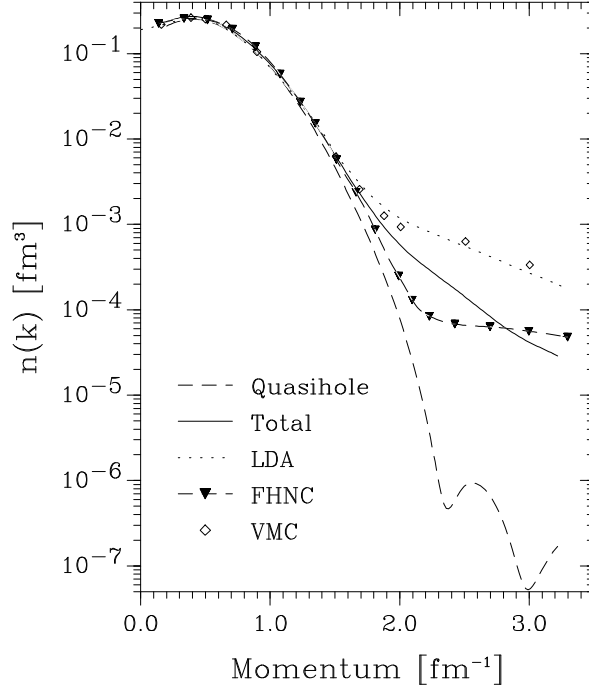
Figure 33: Comparison of different approaches to calculate the momentum distribution in ^{16}O. The results obtained from the spectral function are given separately including both the quasihole and the continuum part (total). The curve labeled LDA corresponds to the results from the local density approximation (LDA) obtained in Ref. [193], while the FHNC belongs to the Fermi hypernetted chain approach of Ref. [109] and VMC stands for the variational Monte Carlo calculation of Ref. [141].

below the corresponding prediction derived for nuclear matter. These problem has been clarified in Ref.[194] were an LDA estimation of the contribution to $n(k)$ of the partial wave not included in the calculation brought the tail of $n(k)$ in ^{16}O in close agreement with the nuclear matter results, when calculated with the same interaction.

In Fig. 33 we compare the $n(k)$ in ^{16}O obtained in different approaches. The results obtained in the Green function approach (total) are compared with those obtained in LDA from Ref. [193], which were obtained using the Urbana V_{14} interaction. Also shown are the results, obtained by a direct FHNC calculation of the expectation value of the number occupation operator in a correlated wave function of the ground state of ^{16}O, where the correlations were optimize by minimizing the ground state energy calculated with the semi-realistic Afnan and Tang interaction [109] and finally the variational Monte Carlo calculations of Ref.[141] obtained with a ground state wave function containing two- and three- operatorial correlations which minimize the ground state energy for the Argonne V_{14} interaction.

Now we want to illustrate the effects of correlations, which are taken into account in the Green's function approach beyond the BHF approximation, on the ground state properties of ^{16}O . To calculate these properties one needs also the non-diagonal part of the density matrix which is given by

$$\tilde{n}_{lj}(k_i, k_n) = \int_{-\infty}^{\epsilon_F} d\omega \frac{1}{\pi} Im \left(\sum_{\alpha,\beta} \langle k_i \mid \alpha \rangle_{lj} g_{lj}(\alpha, \beta; \omega) \langle \beta \mid k_n \rangle_{lj} \right). \tag{247}$$

and contains as in the case of the spectral function, a continuous contribution and a part originating from the quasihole states,

$$\tilde{n}_{lj}^{qh}(k_i, k_n) = \sum_{\Upsilon} Z_{\Upsilon lj} \langle k_i \mid \Upsilon \rangle_{lj} \langle \Upsilon \mid k_n \rangle_{lj}. \tag{248}$$

With this density matrix, the expectation value for the square of the radius can be calculated according to

$$\langle \Psi_0^A \mid r^2 \mid \Psi_0^A \rangle = \sum_{lj} 2(2j+1) \sum_{i,n=1}^{N_{max}} \langle k_i \mid r^2 \mid k_n \rangle_l n_{lj}(k_i, k_n). \tag{249}$$

The matrix elements of r^2 in the basis states are given by

$$\langle k_i \mid r^2 \mid k_n \rangle_l = N_{il} N_{nl} \int_0^{R_{max}} dr r^4 j_l(k_i r) j_l(k_n r). \tag{250}$$

The total energy of the ground state is obtained from the Koltun sum rule (76)

$$E_0^A = \sum_{lj} 2(2j+1) \sum_{i=1}^{N_{max}} \int_{-\infty}^{\epsilon_F} d\omega \frac{1}{2} \left(\frac{k_i^2}{2m} + \omega \right) \left(\tilde{S}_{lj}^c(k_i, \omega) + \sum_{\Upsilon} \tilde{S}_{\Upsilon lj}^{qh}(k_i, \omega) \right). \tag{251}$$

Using the previous equations we calculate the contributions of the different partial waves to the binding energy, the results are reported in Table 6. As a first step we consider the Hartree-Fock (HF) approximation. The resulting binding energy per nucleon (-1.93 MeV) is quite small. This is probably due to the use of a G matrix calculated at the saturation density of nuclear matter, which overestimates the Pauli effects as compared to a BHF calculation directly for ^{16}O.

The treatment of the Pauli operator is improved by adding the $2p1h$ part ,with the corresponding correction term, to the self-energy. This approximation can be considered as an approximation to a full BHF and we will labeled "BHF". This correction increases the binding energy to -4.01 MeV. This number is in reasonable agreement with self-consistent BHF calculations performed for ^{16}O using the same interaction [198]. However, as the single particle states are more bound than the single particle states obtained in the HF calculations, the gain in binding energy is accompanied by a reduction of the calculated radius of the nucleon distribution.

The inclusion of the 2h1p contributions to the self-energy reduces the absolute values of the quasi-hole energies. Despite of this reduction, the total binding energy is increased compared to BHF calculations. This increase of the binding energy is mainly due to the continuum part of the spectral function. Comparing the various contributions, one finds that only the 37 % of the total energy is due to the quasi-hole part in Eq. (251). The dominant part (63 %) results from the continuum part of the spectral functions although this continuum part only represents 11 % of the nucleons. The inclusion of $2h1p$ terms increases also the radius, moving the results for the ground state off the Coester band.

The relative importance of the various contribution to the single-particle strength can also be seen from inspecting Fig. 34 which shows the density profile of ^{16}O and some of its components. This figure also demonstrates that the strength located in single-particle states with $l > 1$, which would not be occupied in the mean field approach, provide a small but non-negligible contribution.

Another way of describing correlation effects in a single-particle basis is the representation of the single-particle density matrix in terms of natural orbits[215, 216, 217, 218].

lj	HF			BHF			Total		
	ϵ	t	ΔE	ϵ	t	ΔE	ϵ	t	ΔE
$s_{1/2}$ qh	-36.91	11.77	-50.28	-42.56	11.91	-61.30	-34.30	11.23	-35.98
$s_{1/2}$ c							-90.36	17.09	-22.89
$p_{3/2}$ qh	-15.35	17.62	9.08	-20.34	18.95	-5.59	-17.90	18.06	0.37
$p_{3/2}$ c							-95.19	35.19	-9.96
$p_{1/2}$ qh	-11.46	16.63	10.34	-17.07	18.46	2.76	-14.14	17.19	5.47
$p_{1/2}$ c							-103.62	35.94	-5.84
$l > 1$ c							-98.87	63.17	-12.27
E/A		-1.93			-4.01			-5.12	
$\langle r \rangle$		2.59			2.49			2.55	

Table 6: Groundstate properties of ^{16}O. Listed are the energies ϵ and kinetic energies t of the quasihole states (qh) and the corresponding mean values for the continuum contribution (c), normalized to 1, for the various partial waves. Multiplying the sum: $1/2(t+\epsilon)$ of these mean values with the corresponding particle numbers of Tab.I, one obtains the contribution ΔE to the energy of the ground state. Results are presented for the Hartree-Fock (HF), Brueckner-Hartree-Fock (BHF) and the Green function approach (Total). The particle numbers for the qh states in HF and BHF are equal to the degeneracy of the states, all other occupation numbers are zero. The results for the radii are given in fm, all other entries in MeV.
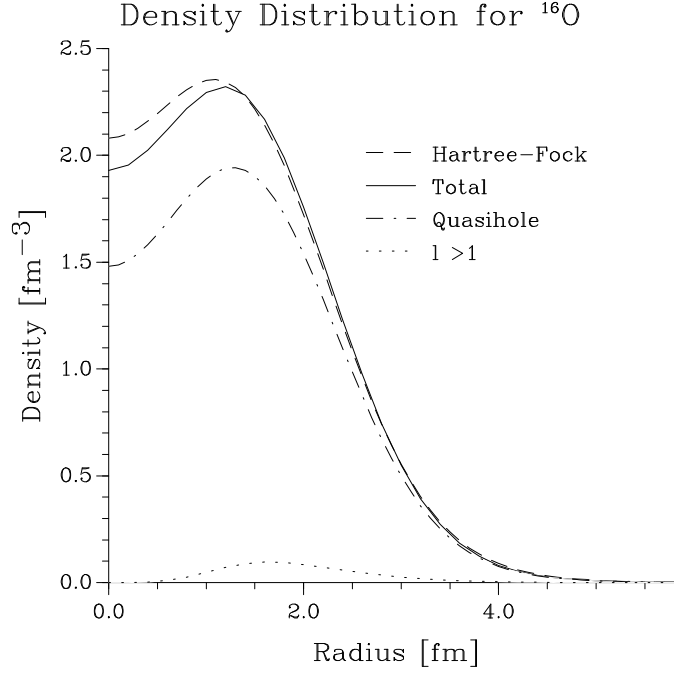
Figure 34: Density distribution of nucleons in ^{16}O as a function of the distance from the center of the nucleus.

3.4 *Correlations in Nucleon Knock-Out Experiments*

The uncorrelated Hartree-Fock state of nuclear matter is given as a Slater determinant of plane waves, in which all states with momenta k smaller than the Fermi momentum k_F are occupied, while all others are completely unoccupied. Correlations in the wave function beyond the mean field approach will lead to occupation of states with k larger than k_F. Therefore correlations should be reflected in an enhancement of the momentum distribution at high momenta. Indeed, as we have already discussed above, microscopic calculations exhibit such an enhancement for nuclear matter as well as for finite nuclei[194, 22]. At first sight one feels encouraged to measure this momentum distribution by means of exclusive $(e, e'p)$ reactions at low missing energies, such that residual nucleus remains in the ground state or other well defined bound state. From the momentum transfer q of the scattered electron and the momentum p of the outgoing nucleon one can calculate the momentum of the nucleus before the absorption of the photon and therefore obtain direct information on the momentum distribution of the nucleons inside the nucleus.

This idea, however, suffers from a little inaccuracy. In such exclusive $(e, e'p)$ experiments one does not measure the whole momentum distribution but rather the spectral function, at the energy which correspond to the specific final state. As we have seen in the discussion of the preceeding section the spectral function at low energies does not show this enhancement of the high momentum components, which shows up only if one integrates the spectral function up to high excitation energies (see Fig. 31 and discussion there). A general review on nucleon knock-out by means of electromagnetic probes is presented in the book of Boffi et al.[219]

A second problem is related to the fact that the nucleon, which is knocked out in such an $(e, e'p)$ process, feels the interaction with the remaining nucleus. It will be retarded and might also get reabsorbed. These effects of the final state interaction (FSI) can be taken into account
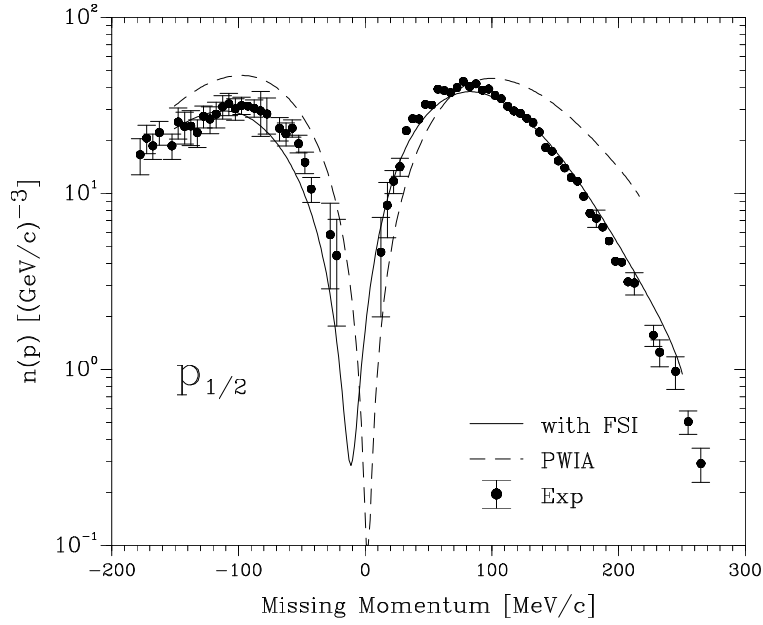
Figure 35: Reduced cross section for the $^{16}O(e, e'p)^{15}N_{gs}$ reaction in parallel kinematics. Results from [24] with and without (plane wave impulse approximation, PWIA) inclusion of FSI are compared to experimental data taken by Leuschner et al.[220]

by means of an optical potential. As an example for the importance of FSI effects we show in Fig. 35 the reduced cross section for the $^{16}O(e, e'p)^{15}N_{gs}$ reaction with and without inclusion of FSI effects. The reduced cross section is defined as the cross section divided by the elementary electron - nucleon cross section times a kinematical factor. Data were taken [220] in so-called parallel kinematics. This means that the missing momentum of the proton, the momentum of emerging proton minus the momentum transfer is parallel or antiparallel (negative values) to the momentum transfer. Note that the missing momentum roughly corresponds to the momentum of the nucleon before absorption of the virtual photon. The retardation effects yield a reduction of the momentum for the outgoing proton. Therefore FSI effects lead to a shift of the cross section to smaller missing momenta, which can nicely be seen from Fig. 35.

The data displayed in Fig. 35 exhibit results only up to moderate values of the missing momenta. Experiments trying to explore high missing momenta were performed at MAMI in Mainz[221] and NIKHEF in Amsterdam [222]. These data can be well reproduced over a range of missing momenta going up to 600 MeV/c by calculations which account for the FSI using a relativistic model for the optical potential[223]. The shape of the calculated cross section, however, is rather insensitive to the use of spectral functions, which are derived either from mean field or more general single-particle Green's function (see Fig. 36). The only difference is the global spectroscopic factor which is adjusted to reproduce the total cross section.

This demonstrates that exclusive one-nucleon knock-out experiments only yield limited information on NN correlations. Therefore one tries to investigate exclusive $(e, e'NN)$ reactions, i.e. triple coincidence experiments in which the energies of the two outgoing nucleons and the energy of the scattered electron guarantee that the rest of the target nucleus remains in the ground state or a well defined excited state. The idea is that processes in which the virtual photon, produced by the scattered electron, is absorbed by a pair of nucleons should be sensitive to the correlations between these two nucleons.

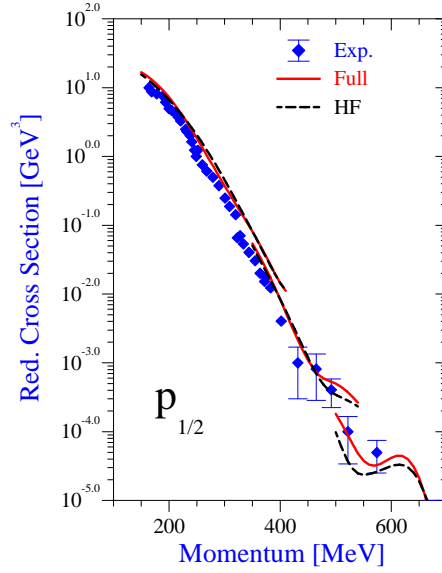Unfortunately, however, this process which is represented by the diagram in Fig. 37a, com-

Figure 36: Reduced cross section for the ^{16}O$(e, e'p)^{15}$N reaction leading to the ground state $(1/2^-)$ of ^{15}N in the kinematical conditions considered in the experiment at MAMI (Mainz) [21]. Results for the mean-field description (HF) and the correlated spectral function (Full) are presented.

petes with the other processes described by the diagrams of Fig. 37b and c. These last two diagrams refer to the effects of final-state-interaction (FSI) and contributions of two-body currents. Here we denote by final state interaction not just the feature that each of the outgoing nucleons feels the remaining nucleus in terms of an optical potential. Here we call FSI the effect, that one of the nucleons absorbs the photon, propagates (on or off-shell) and then shares the momentum end energy of the photon by interacting with the second nucleon which is also knocked out of the target. The processes described in Figs. 37a and 37b, correlations and FSI, are rather similar, they differ only by the time ordering of NN interaction and photon absorption. Therefore it seems evident that one must consider both effects in an equivalent way. Nevertheless, most studies up to now have ignored this equivalency but just included the correlation effects in terms of a correlated two-body wave function. For the sake of consistency one should assume the same interaction to be responsible for the correlations and this two-body FSI. Correlations can be evaluated in terms of the Brueckner G-matrix while the T-matrix derived from the very same interaction should be used to determine FSI.

The nine-fold differential cross section of such an $(e, e'2N)$ reaction can be written as a product of a matrix element of the leptonic current j_μ times the matrix elements of the corresponding hadronic current $< J^\mu >$ calculated between the initial and final nuclear state

$$\frac{\mathrm{d}^9\sigma}{\mathrm{d}\tilde{E}_1\mathrm{d}\tilde{\Omega}_1\mathrm{d}\tilde{E}_2\mathrm{d}\tilde{\Omega}_2\mathrm{d}E'_e\mathrm{d}\Omega'_e} = K|j_\mu < J^\mu > |^2 \tag{252}$$

with K a kinematical factor. This expression can be rewritten into the form [224, 225]

$$\frac{\mathrm{d}^9\sigma}{\mathrm{d}\tilde{E}_1\mathrm{d}\tilde{\Omega}_1\mathrm{d}\tilde{E}_2\mathrm{d}\tilde{\Omega}_2\mathrm{d}E'_e\mathrm{d}\Omega'_e} = \frac{1}{4}\frac{1}{(2\pi)^9}\tilde{p}_1\,\tilde{p}_2\,\tilde{E}_1\,\tilde{E}_2\,\sigma_{\mathrm{Mott}}\left\{v_C W_L + v_T W_T + v_S W_{TT} + v_I W_{LT}\right\}$$
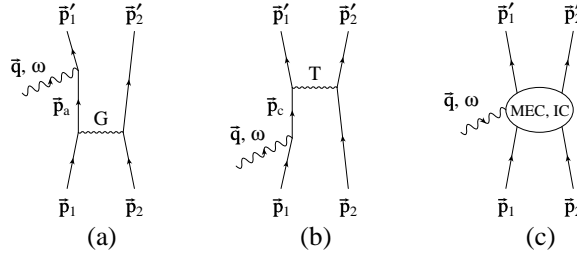$$\times (2\pi)\,\delta(E_f - E_i) \tag{253}$$

Figure 37: Diagrams for the different processes contributing to the $(e, e'2N)$ reaction. Diagram (a) and (b) show the absorption of the photon by a single nucleon. The nucleon-nucleon correlations are described by the G matrix. Diagram (c) depicts photon absorption via meson exchange (MEC) or isobaric currents (IC)

where $\tilde{E}_1, \tilde{E}_2$ and $\tilde{p}_1, \tilde{p}_2$ denote the energies and momenta of the outgoing nucleons, respectively. The virtual photon created in the electron scattering process carries a transfered momentum $\vec{q}$ and energy ω. The leptonic structure functions v_i $(i = C, T, S, I)$ are defined by

$$
\begin{aligned}
v_C &= \left(\frac{q_\mu q^\mu}{\vec{q}^2}\right)^2 \\
v_T &= \tan^2\frac{\theta_e}{2} - \frac{1}{2}\left(\frac{q_\mu q^\mu}{\vec{q}^2}\right) \\
v_I &= \frac{q_\mu q^\mu}{\sqrt{2}|\vec{q}|^3}(E_e + E_e')\tan\frac{\theta_e}{2} \\
v_S &= \frac{q_\mu q^\mu}{2\vec{q}^2}
\end{aligned}
\tag{254}
$$

Here, θ_e is the angle of the scattered electron with respect to the incident electron beam and E_e, E_e' are the energies of the incident and the scattered electron, respectively. The nuclear structure functions W_i $(i = L, T, TT, LT$ stands for longitudinal, transverse, etc.) contain the matrix elements of the nuclear current operator for a given photon polarization λ. These matrix elements have to be calculated for the various processes displayed in Fig. 37.

The relative importance of the various contributions under different kinematical setups, can be explored in calculations of the structure function W_i for nuclear matter at saturation density[226]. As a first example we consider the longitudinal structure function for the knockout of a proton-proton pair. In this case one can ignore the effects of meson-exchange currents (MEC) and isobar currents (IC) displayed in Fig. 37, since two protons do not exchange charged mesons. One of the protons is assumed to be emitted parallel to the momentum of the virtual photon with an energy of $T_{p,1} = 156\,\text{MeV}$, while the second is emitted antiparallel to the photon momentum with an energy of $T_{p,2} = 33\,\text{MeV}$ (see left part of Fig. 38). This is called the 'super-parallel kinematic', which should be appropriate for a separation of longitudinal and transverse structure functions. In this situation the dominant contribution to the longitudinal response function is due to correlation effects (dashed line). But also the FSI effects contribute in a non-negligible way to the cross section (curve with circle symbols), although the two protons are emitted in opposite directions. The effects of FSI are much more important, if we request that the two protons are emitted in a more symmetric way. As an example we show the longitudinal structure function for $(e, e'pp)$, requesting that each of the protons carries away an energy of 70 MeV and is emitted with an angle of 30º or −30º with respect to the momentum transfer q of the virtual photon. Corresponding results are displayed in in the right part of Fig. 38. For this
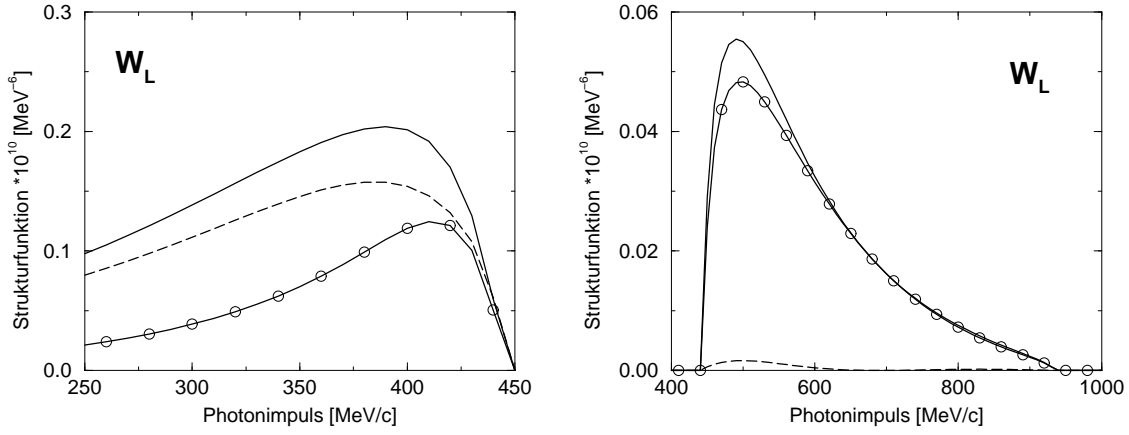
Figure 38:   Longitudinal structure function for the knockout of a proton-proton pair as a function of the photon momentum q, keeping the photon energy constant at $\omega = 215\,\text{MeV}$. The left figure shows results for a 'super parallel' kinematical situation with angles $\theta'_{p,1} = 0^\text{o}$ and $\theta'_{p,2} = 180^\text{o}$ of the two protons with respect to the direction of the photon momentum, while the figure on the right-hand side displays results assuming $\theta_{p_i} = \pm 30^\text{o}$. The dashed line represents the contribution from correlations, the line with circles those of the FSI and the solid line the coherent sum of these two

kinematical situation the FSI contribution is much more important than the correlation effect.

The situation is even more complicated in the case of the $(e, e'pn)$ reaction, since in this case also MEC effects need to be considered. Results for the longitudinal structure function for $(e, e'pn)$ assuming the same kinematical setup as in the right part of Fig. 38 are displayed in Fig. 39. The resulting structure function for $(e, e'pn)$ is almost an order of magnitude larger than for the corresponding $(e, e'pp)$ case. The dominating contribution to the longitudinal response is again the correlation part. Comparison with Fig. 4 demonstrates that the pn correlations are significantly larger than those for the pp pairs. This supports our conclusion from discussing the results of table 3 that the pionic or tensor correlations which are different for isospin $T = 0$ and $T = 1$ pairs play an important role and are even more important than the central correlations, which are independent of the isospin. Note that the MEC contribution for this 'superparallel kinematic' is smaller than the correlation effect. This is due to a strong cancellation between the pion seagull and the pion in flight contributions to the MEC. In fact, the dominant MEC contribution in this kinematical setup is due to the coupling of the photon to the ρ meson. This does not hold for other situations, in which the pion contributions to MEC are dominant.

The calculation of $(e, e'NN)$ reactions for finite nuclei typically account for the FSI effects only on the level of the mean field approximation. This means one considers an optical potential for the outgoing nucleons but ignores the FSI effects which are due to the residual interaction between the two ejected nucleons. As a typical example we will consider again the closed shell nucleus ^{16}O as the target nucleus. For an exclusive experiment leading to a discrete final state of the daughter nucleus with well defined angular momentum J and isospin T the initial state Φ_i, for which the matrix elements $< J^\mu >$ (see Eq. (252) of the current operator have to be calculated can be expanded in terms of correlated two-hole wave functions

$$\Phi_i^{JT}(\vec{r}_1, \vec{r}_2) = \sum_{\nu_1 \nu_2} a_{\nu_1 \nu_2}^{JT} < \vec{r}_1, \vec{r}_2 | \Psi_2 | \nu_1 \nu_2 JT > \tag{255}$$

where we have used the nomenclature of the coupled cluster method introduced in subsection 2.2. The expansion coefficients $a_{\nu_1 \nu_2}^{JT}$ are determined from a configuration mixing calcu-
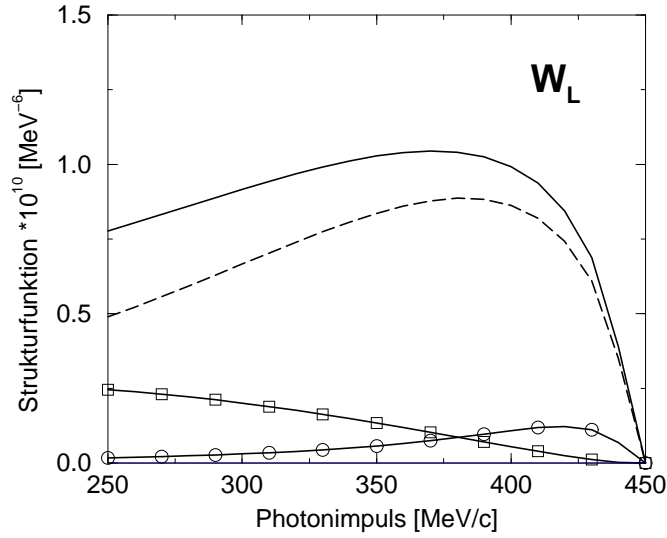
92

Figure 39: Longitudinal structure function for $(e, e'pn)$ for the kinematical condition as displayed in the right part of Fig. 38. The contribution of MEC is shown by the solid line with box symbol

lation of the two-hole states in ^{16}O, which can be coupled to the angular momentum and parity of the requested state within the model space considered for the treatment of long range correlations[227].

As an example, exhibiting the effects of correlations, we display in Fig. 40 the two-body densities, resulting from the knock-out of two nucleons from the $p_{1/2}$ shell in ^{16}O. In Fig. 40 such two-body densities are displayed for a fixed $\vec{r}_1 = (x_1 = 0, y_1 = 0, z_1 = 2 \text{ fm})$ as a function of $\vec{r}_2$, restricting the presentation to the x_2, z_2 half-plane with $(x_2 > 0, y_2 = 0)$. The upper left part of this figure displays the two-body density without correlations ($\hat{S}_2 = 0$). One observes that the two-body density, displayed as a function of the position of the second particle $\vec{r}_2$ is not affected by the position of the first one $\vec{r}_1$. Actually, the two-body density displayed is equivalent to the one-body density. This just reflects the feature of independent particle motion. If correlation effects are included, as it is done in the upper right part of Fig. 40, one finds a drastic reduction of the two-body density at $\vec{r}_2 = \vec{r}_1$ accompanied by a slight enhancement at medium separation between $\vec{r}_1$ and $\vec{r}_2$.

In order to amplify the effect of correlations, the lower part of Fig. 40 displays the corresponding correlation densities (i.e. the corresponding amplitudes $\hat{S}_2$ squared). While the left part shows the correlation density for the removal of a proton-proton pair, the corresponding density for a proton-neutron pair is displayed in the right part. Comparing these figures one sees that that the pn correlations are significantly stronger than the pp correlations. This is mainly due to the presence of pionic or tensor correlations in the case of the pn pair. This part of Fig. 40 also exhibits quite nicely the range of the correlations. This range is short compared to the size of the nucleus even in the case of the pn correlations. All results displayed in this figure have been obtained using the Argonne V14 potential for the NN interaction[4].

Results for the cross section of exclusive $(e, e'pn)$ reactions on ^{16}O leading to the ground state of ^{14}N are displayed in Fig. 41. The calculations have been performed in the super-parallel kinematic, which we already introduced before. The kinematical parameters correspond to those adopted in a recent ^{16}O(e,e'pp)^{14}C experiment at MAMI [228]. In order to allow a direct comparison of $(e, e'pp)$ with $(e, e'pn)$ experiments, the same setup has been proposed for the
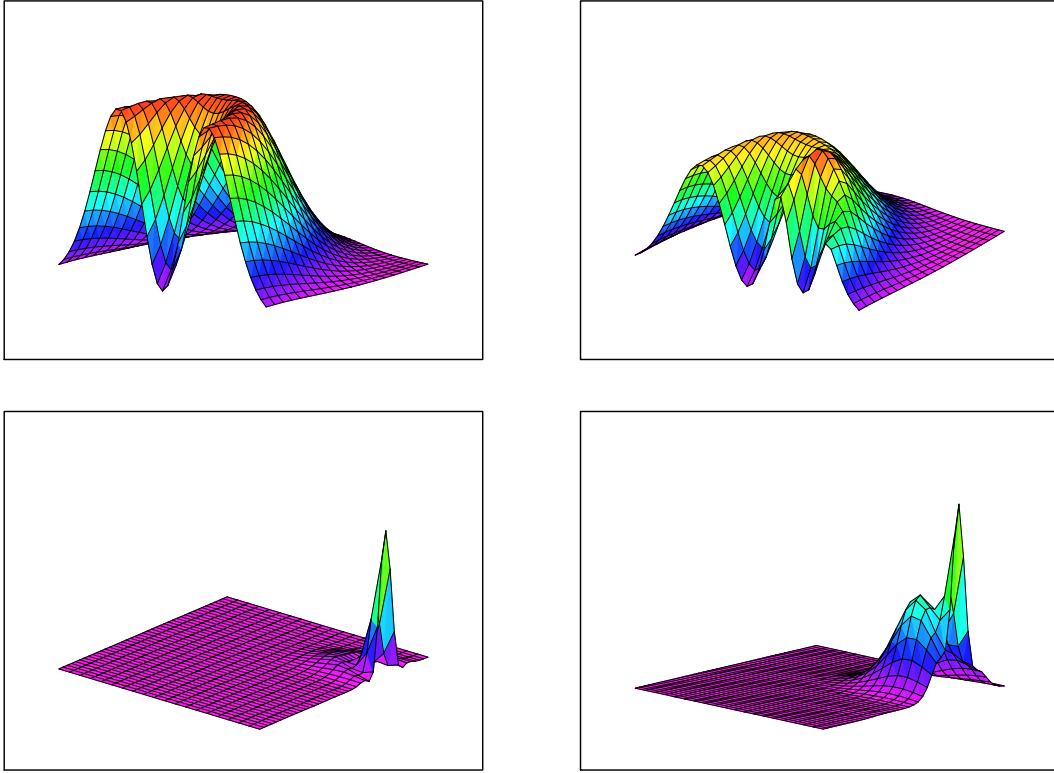
Figure 40: Two-body density for the removal of two nucleons from $p_{1/2}$ shell in ^{16}O. The upper part displays the results for the total density Ψ_2^2 without (left) and with inclusion (right) of NN correlations. The lower part shows the defect function squared for pp (left) and pn knock-out (right). See text for further description.

first experimental study of the ^{16}O(e,e'pn)^{14}N reaction [229]. This means that we assume an energy of the incoming electron $E_0 = 855$ MeV, electron scattering angle $\theta = 18º$, $\omega = 215$ MeV and $q = 316$ MeV/c. The proton is emitted parallel and the neutron antiparallel to the momentum transfer $\vec{q}$.

Separate contributions of the different terms of the nuclear current are shown in the figure and compared with the total cross section[227]. The contribution of the one-body current, entirely due to correlations, is large. It is of the same size as that of the pion seagull current. The contribution of the Δ-current is much smaller at lower values of p_B, whereas for values of p_B larger than 100 MeV/c it becomes comparable with that of the other components. It is worth noting the the total cross section is about an order of magnitude larger than the one evaluated for the corresponding $(e, e'pp)$ experiment[230]. This confirms our finding about the relative cross sections for pp and pn knock out, which we have discussed above for the study in nuclear matter.

The right-hand part of Fig. 41 shows the quantities as the left part but calculated with the simpler prescription of correlations, i.e. by the product of the pair function of the shell model, described for 1_1^+ as a pure $(p_{1/2})^{-2}$ hole, and of a Jastrow type central and state independent correlation function. The large differences between the cross sections in the two parts of Fig. 41 indicate that a refined description of the two-nucleon overlap, involving a careful treatment of both aspects related to nuclear structure and NN correlations, is needed to give reliable predictions of the size and the shape of the $(e, e'pn)$ cross section.
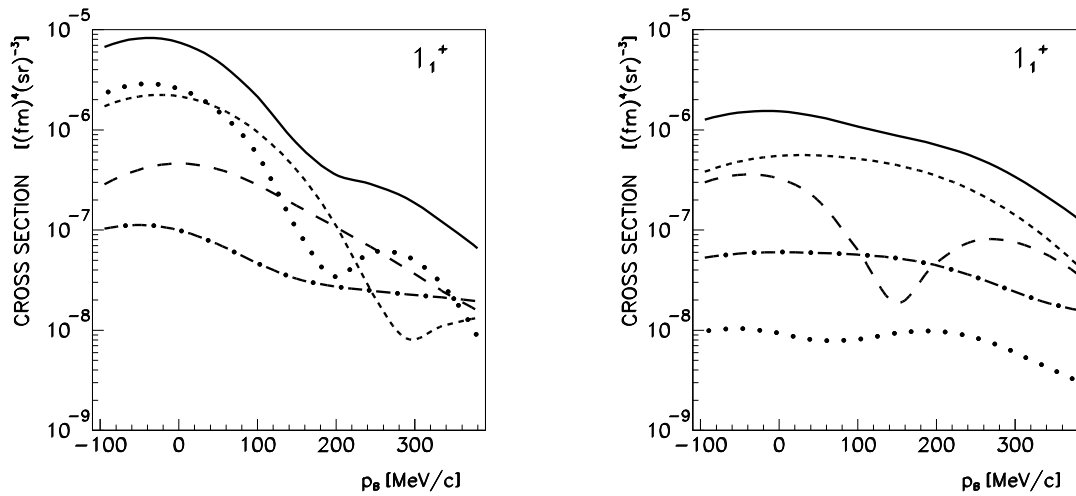
Figure 41: The differential cross section of the ^{16}O(e,e'pn) reaction as a function of the recoil momentum p_B for the transition to the 1_1^+ ground state of ^{14}N ($E_{2m} = 22.96$ MeV), in the super-parallel kinematics with $E_0 = 855$ MeV, and $\omega = 215$ MeV $q = 316$ MeV/c. The recoil-momentum distribution is obtained changing the kinetic energies of the outgoing nucleons. Separate contributions of the one-body, seagull, pion-in-flight and Δ-current are shown by the dotted, short-dashed, dot-dashed and long-dashed lines, respectively. Positive (negative) values of p_B refer to situations where $\boldsymbol{p}_B$ is parallel (antiparallel) to $\boldsymbol{q}$. The calculations leading to the left part used correlated wave functions calculated in the frameworkof the CCM, while for the right part a simple Jastrow correlation function has been considered.

4 Conclusion

The main aim of this review has been to demonstrate that nuclear systems are very intriguing many-body systems. They are non-trivial systems in the sense that they require the treatment of correlations beyond the mean field or Hartree-Fock approximation. Therefore, from the point of view of many-body theory, they can be compared to other quantum many-body systems like liquid He, electron gas, clusters of atoms etc. A huge amount of experimental data is available for real nuclei with finite number of particles as well as for the infinite limit of nuclear matter or the matter of a neutron star.

It is a challenge for theoretical physics to develop many-body theories for a description of these data, which are based on a realistic model for the NN interaction and yield predictions of the many-body data which are free of any parameters. A lot of progress has been made during the last years to develop such tools of many-body theory as the Brueckner hole-line expansion, the coupled cluster or "exponential S" method, the self-consistent calculation of Green's function and variational calculations, which are based on cluster expansion techniques as well as Monte Carlo methods. These techniques are very useful for the study of nuclear structure but are also used in investigationis of other quantum-many-body sytems.

The different techniques yield predictions for the bulk properties of nuclear systems at normal densities which tend to agree with each other. This is certainly true for the treatment of short-range correlations. Additional effort may be required for a reliable treatment of long-range correlations in finite nuclei. Those correlations are related to the low energy configurations within a shell-model basis. Shell-model configuration mixing calculations using Monte-Carlo

techniques[231] or other sophisticated methods to deal with nuclear structure calculations in large model spaces[232] might be appropriate and should be combined with the formalisms to handle short-range correlations.

Many-body theories have reached a level of sophistication that their predictions can be considered as a reliable test of models for the NN interaction. Characteristic differences can be observed if either a complete meson exchange model is used, which leads to a non-local NN interaction, or if the local approximation is considered. In any case, however, one finds that a two-nucleon interaction alone does not lead to the empirical saturation point of nuclear matter and also fails to reproduce binding energy and density of finite nuclei. The calculations tend to predict binding energies which are too small and/or densities which are too large.

This can be corrected by introducing empirical three-nucleon forces. It is not clear, however, whether such three-nucleon forces simulate sub-nucleonic degrees of freedom (Δ excitations of the nucleons) or relativistic features as they are contained in the Walecka model[30]. Further studies are needed to clarify this point. One must try to inspect special observables like e.g. the spin-orbit splitting in the single-particle potential, the energy dependence of the optical potential or the response functions for $(e, e'p)$ experiments[233, 234], which are sensitive to the relativistic features.

There is also a challenge for a cooperation between experimental and theoretical physics to search for observables, which test the significance of the short-range NN correlations and thereby the short-range structure of the underlying NN interaction. The study of exclusive $(e, e'NN)$ experiments seems to be an appropriate tool to explore the proton-proton and proton-neutron correlations.

Acknowledgments

References

[1] A. Valcarce, A. Buchmann, F. Fernández, and Amand Faessler, *Phys. Rev.* C 51 (1995) 1480

[2] R. Machleidt, *Adv. Nucl. Phys.* 19 (1989) 189

[3] M.M. Nagels, T.A. Rijken, and J.J. de Swart, *Phys. Rev.* D 17 (1978) 768

[4] R.B. Wiringa, R.A. Smith, and T.L. Ainsworth, *Phys. Rev.* C 29 (1984) 1207

[5] I.E. Lagaris and V.R. Pandharipande, *Nucl. Phys.* A 359 (1981) 331

[6] M. Brack, C. Guet, and H.-B, Hakansson, *Phys. Rep.* 123 (1985) 275

[7] H. Müther and A. Polls, *Phys. Rev.* C (1999) in press , preprint nucl-th/9908002.

[8] T. Hamada and I.D. Johnston, *Nucl. Phys.* 34 (1962) 382

[9] K.A. Brueckner, *Phys. Rev.* 97 (1955) 1353

[10] H.A. Bethe, *Ann. Rev. Nucl. Sci.* 21 (1971) 93

[11] J.P. Jeukenne, A. Legeunne, and C. Mahaux, *Phys. Rep.* 25 (1976) 83

[12] H. Kümmel, K. H. Lührmann, and J. G. Zabolitzky, *Phys. Rep.* 36 (1978) 1

[13] R. F. Bishop, in *Microscopic Quantum Many-Body Theories and Their Applications*, eds. J. Navarro and A. Polls (Springer 1998)

[14] W.H. Dickhoff and H. Müther, *Reports on Progress in Physics* 11 (1992) 1947

[15] R.B. Wiringa, V. Fiks, and A. Fabrocini, *Phys. Rev.* C 38 (1988) 1010

[16] A. Akmal and V.R. Pandharipande, *Phys. Rev.* C 56 (1997) 2261

[17] S. Fantoni and A. Fabrocini, in *Microscopic Quantum Many-Body Theories and Their Applications*, eds. J. Navarro and A. Polls (Springer 1998)

[18] K.E. Schmidt and D.M. Ceperley, in *Monte Carlo Methods III*, ed. K. Binder (Springer 1991)

[19] D.M. Ceperley, *Rev. Mod. Phys.* 67 (1995) 279

[20] I. Bobeldijk et al., *Phys. Rev. Lett.* 73 (1994) 2684

[21] K.I. Blomqvist *et al.*, *Phys. Lett.* B 344 (1995) 85

[22] H. Müther, A. Polls, and W.H. Dickhoff, *Phys. Rev.* C 51 (1995) 3040

[23] H. Müther and W.H. Dickhoff, *Phys. Rev.* C 49 (1994) R17

[24] A. Polls, M. Radici, S. Boffi, W.H. Dickhoff, and H. Müther, *Phys. Rev.* C 55 (1997) 810

[25] C. J. G. Onderwater *et al.*, *Phys. Rev. Lett.* 81 (1998) 2213

[26] G. Rosner, Proc. on *"Perspectives in Hadron Physics"*, eds. S. Boffi, C. Cioffi degli Atti and M. Giannini, (World Scientific 1998).

[27] R. Vinh Mau in *Mesons in Nuclei* Vol. I (North-Holland, Amsterdam, 1979)

[28] J.W. Durso, M. Saarela, G.E. Brown, and A.D. Jackson *Nucl. Phys.* A 278 (1977) 445

[29] J.D. Walecka, *Ann. Phys. (N.Y.)* 83 (1974) 491

[30] B.D. Serot and J.D. Walecka, *Adv. Nucl. Phys.* 16 (1986) 1

[31] M.R. Anastasio, L.S. Celenza, W.S. Pong, and C.M. Shakin, *Phys. Rep.* 100 (1983) 327

[32] R. Brockmann and R. Machleidt, *Phys. Rev.* C 42 (1990) 1965

[33] B. Ter Haar and R. Malfliet, *Phys. Rep.* 149 (1987) 207

[34] H. Huber, F. Weber, and M.K. Weigel, *Phys. Lett.* B317 (1993) 485

[35] H. Müther, R. Machleidt, and R. Brockmann, *Phys. Lett.* B 202 (1988) 483

[36] R. Fritz, H. Müther, and R. Machleidt, *Phys. Rev. Lett.* 71 (1993) 46

[37] R. Fritz and H. Müther, *Phys. Rev.* C 49 (1994) 633

[38] F. Boersma and R. Malfliet, *Phys. Rev.* C 49 (1994) 233

[39] R. Machleidt, K. Holinde, and Ch. Elster, *Phys. Rep.* 149 (1987) 1

[40] H. Müther, *Prog. Part. Nucl. Phys.* 14 (1985) 123

[41] F. Osterfeld, *Rev. Mod. Phys.* 64 (1992) 491

[42] R. Rapp, R. Machleidt, J.W. Durso, and G.E. Brown, *Phys. Rev. Lett.* 82 (1999) 1827

[43] R. Rapp, J.W. Durso, Z. Aouissat, G. Chanfray, O. Krehl, P. Schuck, J. Speth, J. Wambach, *Phys. Rev.* C 59 (1999) R1237

[44] T. Hatsuda, T. Kunihiro, H. Shimzu, *Phys. Rev. Lett.* 82 (1999) 2840

[45] R.B. Wiringa, R.A. Smith, and T.L. Ainsworth, *Phys. Rev.* C 29 (1987) 1207

[46] H. Riffert, H. Müther, H. Herold, and H. Ruder: *Matter at High Densities in Astrophysics*, Springer Tracts in Modern Physics 133, (Springer Verlag, 1996)

[47] P.J. Brussard and P.W.M. Glaudemans: *Shell model applications in nuclear spectroscopy* (North-Holland, Amsterdam, 1977)

[48] T.T.S. Kuo, Z.Y. Ma, and R. Vinh Mau, *Phys. Rev.* C 33 (1986) 717

[49] H. Feshbach, *Ann. Phys. (N.Y.)* 19 (1962) 287

[50] C. Bloch and H. Horowitz, *Nucl. Phys.* 8 (1958) 51

[51] B.H. Brandow, *Rev. Mod. Phys.* 39 (1967) 771

[52] T.T.S. Kuo, S.Y. Lee, and K.F. Ratcliff, *Nucl. Phys.* A 176 (1971) 65

[53] M. Hjorth-Jensen, T.T.S. Kuo, and E. Osnes, *Phys. Rep.* 261 (1995) 125

[54] S.Y. Lee and K. Suzuki, *Phys. Lett.* B 91 (1980) 79

[55] H. Müther, A. Polls and T.T.S. Kuo, *Nucl. Phys.* A 435 (1985) 548

[56] H.A. Bethe, B.H. Brandow and A.G. Petschek, *Phys. Rev.* 129 (1962) 225

[57] J.D. Jeukenne, A. Lejeune and C. Mahaux, *Phys. Rep.* 25 (1971) 83

[58] R. Rajarman and H.A. Bethe, *Rev. Mod. Phys.* 39 (1967) 745

[59] B.D. Day, *Phys. Rev.* C 24 (1981) 1203

[60] H.Q. Song, M. Baldo, U. Lombardo, and G. Giansiracusa, *Phys. Lett.* B 411 (1997) 237

[61] H.Q. Song, M. Baldo, G. Giansiracusa, annd U. Lombardo, *Phys. Rev. Lett.* 81 (1998) 1584

[62] M.I. Haftel and F. Tabakin, *Nucl. Phys.* A 158 (1970) 1

[63] H. Müther and P. U. Sauer, *Computational Nuclear Physics 2*, eds. K. Langanke, J. A. Maruhn and S. E. Koonin (Springer Verlag 1992)

[64] F. Coester, *Nucl. Phys.* 7 (1958) 421

[65] F. Coester and H. Kümmel, *Nucl. Phys.* 17 (1960) 477

[66] D.J. Thouless, *Nucl. Phys.* 21 (1960) 225

[67] J.G. Zabolitzky, *Nucl. Phys.* A 228 (1974) 272

[68] H.Q. Song, S.D. Yang, and T.T.S. Kuo *Nucl. Phys.* A 462 (1987) 491

[69] M.F. Jiang, T.T.S. Kuo, and H. Müther, *Phys. Rev.* C 38 (1988) 2408

[70] H.A. Mavromatis, P. Ellis, and H. Müther, *Nucl. Phys.* A 530 (1991) 251

[71] J.G. Zabolitzky, *Nucl. Phys.* A 228 (1974) 285

[72] M. Stauf, "Diplomarbeit" (University T"ubingen, 1998)

[73] J.H. Heisenberg and B. Mihaila, *Phys. Rev.* C 59 (1999) 1440

[74] K. Emrich, J.G. Zabolitzky, and K.H. Lührmann, *Phys. Rev.* C 16 (1977) 1650

[75] A.L. Fetter and J.D. Walecka, *Quantum Theory of Many Particle Systems* (McGraw-Hill New York, 1971)

[76] J. Negele and H. Orland *Quantum Many-Particle Systems* (Addison-Wesley Redwood City. 1988)

[77] R.D. Mattuck, *A Guide to Feynman Diagrams in the Many-Body Problem* (McGraw-Hill New York, 1976)

[78] C. Mahaux and R. Sartor, *Adv. Nucl. Phys.* 20 (1991) 1

[79] M. Gell-Mann and F.E. Low, *Phys. Rev.* 84 (1951) 350

[80] G.C. Wick, *Phys. Rev.* 80 (1950) 268

[81] H. Lehmann, *Nuovo Cimento* A 11 (1954) 342

[82] H. Müther and L.D. Skouras, *Nucl. Phys.* A 555 (1993) 541

[83] G. Baym and L.P. Kadanov, *Phys. Rev.* 124 (1961) 287

[84] H. Müther and L.D. Skouras, *Nucl. Phys.* A 581 (1995) 247

[85] H. Müther, T. Taigel and T.T.S. Kuo, *Nucl. Phys.* A 482 (1988) 601

[86] D. Van Neck, M. Waroquier, and J. Ryckebusch, *Nucl. Phys.* A 530 (1991) 347

[87] J. Carlson, V. R. Pandharipande, and R.B. Wiringa, *Nucl. Phys.* A 401 (1983) 59

[88] R. Schiavilla, V. R. Pandharipande and R. B. Wiringa, *Nucl. Phys.* A 449 (1986) 219

[89] R.B. Wiringa, V. G. J. Stoks, and R. Schiavilla, *Phys. Rev.* C 51 (1995) 38

[90] R. Jastrow, *Phys. Rev.* 98 (1955) 1479

[91] E. Feenberg, it Theory of Quantum Fluids (Academic, New York,1969)

[92] J.W. Clark, *Prog. Part. Nucl. Phys.* 2 (1979) 89

[93] A. Fabrocini and S. Fantoni, in *Advances in Quantum Many-Body Theories*, Vol. 2, eds. R.F. Bishop and N.R. Wilets, (World Scientific, Singapore ,1999).

[94] F. Iwamoto and M. Yamada, *Prog. Theor. Phys.* 17 (1957) 543

[95] J. W. Clark and P. Westhaus, *J. Math. Phys.* 9 (1968) 131

[96] R. Guardiola and A. Polls, *Nucl. Phys.* A 342 (1980) 385

[97] M. Gaudin, J. Gillespie, and G. Ripka, *Nucl. Phys.* A 176 (1971) 237

[98] S. Fantoni and S. Rosati, *Nuovo Cimento* A 20 (1974) 179

[99] S. Fantoni and S. Rosati, *Nuovo Cimento* A 25 (1975) 593

[100] E. Krotscheck and M.L. Ristig, *Nucl. Phys.* A 242 (1975) 389

[101] J.M.J. van Leeuwen, J. Groeneveld, and J. de Boer, *Physica* 25 (1959) 792

[102] S.W. Lovesey, *Theory of Neutron Scattering from Condensed Matter*, Vol. 1, (Clarendon Press, Oxford, 1986)

[103] G. Ripka, *Phys. Rep.* 56 (1979) 1

[104] V.R. Pandharipande and R.B. Wiringa, *Rev. Mod. Phys.* 51 (1979) 821

[105] R.B. Wiringa, *Nucl. Phys.* A 338 (1980) 57

[106] J.W. Clark, in it The Many-Body Problem, Jastrow Correlations Versus Brueckner Theory, eds. R. Guardiola and J. Ros, Lectures Notes in Physics, Vol. 138. (Springer-Verlag, Heidelberg, 1980)

[107] R. Guardiola, A. Faessler, H. Müther, and A. Polls, *Nucl. Phys.* A 371 (1981) 79

[108] G. Co', A. Fabrocini, S. Fantoni, and I. Lagaris, *Nucl. Phys.* A 549 (1992) 439

[109] G. Co', A. Fabrocini, and S. Fantoni, *Nucl. Phys.* A 568 (1994) 73

[110] F. Arias de Saavedra, G. Co', A. Fabrocini, and S. Fantoni, *Nucl. Phys.* A 605 (1996) 359

[111] I. R. Afnan and Y. C. Tang, *Phys. Rev.* 175 (1968) 1337

[112] A. Fabrocini, F. Arias de Saavedra, G. Co', and P. Folgarait, *Phys. Rev.* C 57 (1998) 1668

[113] A. Fabrocini, F. Arias de Saavedra, and G. Co', Preprint IFUP-TH 57/99.

[114] A. Akmal, V.R. Pandhariapnde, and D.G. Ravenhall, *Phys. Rev.* C 58 (1998) 1804

[115] J.W. Clark and E. Feenberg, *Phys. Rev.* 113 (1959) 388

[116] A. Fabrocini and S. Fantoni, in *First International Course on Condensed Matter, ACIF series*, Vol. 8, eds. D. Prosperi, S. Rosati and S. Violini, (World Scientific, Singapore, 1987)

[117] P.M. Morse and H. Feshbach, in *Methods of Theoretical Physics*,(Addison-Wesley,1991)

[118] S. Fantoni, *Phys. Rev.* B 29 (1984) 2544

[119] E. Krotscheck, R.A. Smith and A.D. Jackson, *Phys. Lett.* B 104 (1981) 421

[120] S. Fantoni and V.R. Pandharipande, *Nucl. Phys.* A 427 (1984) 473

[121] S. Fantoni and V.R. Pandhariapnde, *Phys. Rev.* C 37 (1988) 1697

[122] P.O. Löwdin, *J. Chem. Phys.* 18 (1950) 365

[123] O. Benhar, A. Fabrocini and S. Fantoni, *Phys. Rev.* C 41 (1990) R24

[124] O. Benhar, A. Fabrocini and S. Fantoni, *Nucl. Phys.* A 550 (1992) 201

[125] S. Fantoni and V.R. Pandharipande, *Nucl. Phys.* A 473 (1987) 234

[126] A. Fabrocini and S. Fantoni, *Nucl. Phys.* A 503 (1989) 375

[127] A. Fabrocini, *Phys. Rev.* C 55 (1997) 338

[128] D. M. Ceperley and M.H. Kalos, in *Monte Carlo Methods in Statistical Physics*, ed. K. Binder, (Springer Verlag, Berlin, 1979).

[129] K. Schmidt and M. H. Kalos, in *Applications of the Monte Carlo Methods in Statistical Physics*, ed. K. Binder, (Springer-Verlag, Berlin, 1984).

[130] S. Caracciolo and A. Fabrocini Eds., *Monte Carlo Methods in Theoretical Physics*, (ETS Editrice, Pisa, 1991).

[131] R. Guardiola in *Microscopic Quantum Many-Body Theories and Their Applications*, eds. J. Navarro and A. Polls (Springer 1998)

[132] R. Guardiola *First International Course on Condensed Matter, ACIF series*, Vol. 8, eds. D. Prosperi, S. Rosati and S. Violini, (World Scientific, Singapore, 1987)

[133] J. A. Carlson and R. B. Wiringa in *Computational Nuclear Physics 1*, eds. K. Langanke, J.A. Marhun and S.E. Koonin, (Springer-Verlag, 1991).

[134] S.C. Pieper in in *Microscopic Quantum Many-Body Theories and Their Applications*, eds. J. Navarro and A. Polls (Springer 1998)

[135] N. Metropolis, A. Rosenbluth, M. Rosenbluth, A. Teller, and E. Teller, *J. Chem. Phys.* 21 (1955) 1087

[136] D. Ceperley, G.V. Chester and M.H. Kalos, *Phys. Rev.* B 16 (1977) 3081

[137] K.E. Schmidt and S. Fantoni, *Phys. Lett.* B 446 (1999) 99

[138] J. Lomnitz-Adler, V.R. Pandhariapnde and R.A. Smith, *Nucl. Phys.* A 361 (1981) 399

[139] J. Carlson and M.H. Kalos, *Phys. Rev.* C 32 (1999) 2105

[140] S.C. Pieper, R.B. Wiringa and V.R. Pandharipande, *Phys. Rev. Lett.* 64 (1990) 364

[141] S. C. Pieper, R.B. Wiringa and V.R. Pandharipande, *Phys. Rev.* C 46 (1992) 1741

[142] B. S. Pudliner, V.R. Pandharipande, J. Carlson, S.Pieper and R.B. Wiringa, *Phys. Rev.* C 56 (1997) 1720

[143] S. Moroni, S. Fantoni and G. Senatore, *Phys. Rev.* B 52 (1995) 13547

[144] J. Boronat and J. Casulleras, in *Proceedings of the MBX, Advances in Quantum Many-Body Theory*, Vol. 3. (World Scientific, Singapore, 2000).

[145] H.M. Müller, S.E. Koonin, R. Seki, U. van Kolck, nucl-th/9910038.

[146] N. Isgur and G. Karl, *Phys. Rev.* D 18 (1978) 4187

[147] K. Yazaki, *Prog. Part. Nucl. Phys.* 24 (1990) 353

[148] K. Bräuer, A. Faessler, F. Fernandez, and K. Shimizu, *Nucl. Phys.* A 507 (1990) 599

[149] G. T'Hooft, *Nucl. Phys.* B 75 (1974) 461

[150] E. Witten, *Nucl. Phys.* B 160 (1979) 57

[151] K. Erkelenz, *Phys. Rep.* 13 (1974) 191

[152] K. Holinde, *Phys. Rep.* 68 (1981) 121

[153] G.E. Brown and A.D. Jackson, *The Nucleon-Nucleon Interaction* (North-Holland Pub. Comp. Amsterdam, 1976)

[154] H. Yukawa, *Proc. Phys. Math. Soc. Jpn* 17 (1935) 48

[155] J.D. Bjorken and S.D. Drell, *Relativistic Quantum Mechanics*, (McGraw-Hill New York, 1964)

[156] C. Itzykson and J.-B. Zuber, *Quantum Field Theory* (McGraw-Hill New York, 1980)

[157] R. Blankenbecler and R. Sugar, *Phys. Rev.* 142 (1966) 1051

[158] V.G. Kadychevsky, *Nucl. Phys.* B 6 (1968) 125

[159] F. Gross, *Phys. Rev.* 186 (1969) 1448

[160] R.H. Thompson, *Phys. Rev.* D 1 (1970) 110

[161] G. Schierholz, *Nucl. Phys.* B 40 (1972) 335

[162] Particle Data Group, *Phys. Rev.* D 50 (1994) 1173

[163] G. Höhler and E. Pietarinen, *Nucl. Phys.* B 95 (1975) 210

[164] K. Holinde, R. Machleidt, M. Anastasio, A. Faessler, and H. Müther, *Phys. Rev.* C 18 (1978) 780

[165] M. Lacombe, B. Loiseau, J.M. Richard, R. Vinh Mau, J. Cote, P. Pires, and R. de Tourreil, *Phys. Rev.* C 21 (1980) 861

[166] V.G.J. Stoks et al. *Phys. Rev.* C 48 (1993) 792

[167] V.G.J. Stoks, R.A.M. Klomp, C.P.F. Terheggen, and J.J. de Swart, *Phys. Rev.* C 49 (1994) 2950

[168] R. Machleidt, F. Sammarruca, and Y. Song, *Phys. Rev.* C 53 (1995) R1483

[169] A. Polls, H. Müther, R. Machleidt, and M. Hjorth-Jensen, *Phys. Lett.* B 432 (1998) 1

[170] M. Anastasio, H. Müther, A. Faessler, K. Holinde, and R. Machleidt, *Phys. Rev.* C 18 (1978) 2916

[171] J. Fujita and H. Miyazawa, *Prog. Theor. Phys.* 17 (1957) 360

[172] K.A. Brueckner and J.L. Gammel, *Phys. Rev.* 109 (1958) 1023

[173] K. Suzuki, R. Okamoto, M. Kohno, and S. Nagata, *Nucl. Phys.* A (1999) in press , nucl-th9907050

[174] E. Schiller, H. Müther, and P. Czerski, *Phys. Rev.* C 59 (1999) 2934 , Erratum *Phys. Rev.* C 60 (1999) 059901

[175] J.G. Zabolitzky, *Phys. Rev.* A 16 (1977) 1258

[176] L. Engvik, M. Hjorth-Jensen, R. Machleidt, H. Müther, and A. Polls, *Nucl. Phys.* A 627 (1997) 85

[177] R. Reid, *Ann. Phys. (N.Y.)* 50 (1968) 411

[178] F. Coester, S. Cohen, B. D. Day and C. M. Vincent *Phys. Rev.* C 1 (1970) 769

[179] H. Müther and A. Polls, *Phys. Rev.* C (2000) in print , preprint nucl-th/9908002

[180] A.B. Migdal, *Rev. Mod. Phys.* 50 (1978) 10

[181] G.E. Brown and W. Weise, *Phys. Rep.* 27 (1976) 1

[182] W.H. Dickhoff, A. Faessler, J. Meyer-ter-Vehn, and H. Müther, *Phys. Rev.* C 23 (1981) 1154

[183] M. Prakash, *Phys. Rep.* 242 (1994) 191

[184] H. Heiselberg and M. Hjorth-Jensen, *Phys. Rep.* to be published (1999) ; preprint nucl-th/9902033

[185] H. Müther, A. Polls, and R. Machleidt, *Phys. Lett.* B 445 (1999) 259

[186] C. Harzer, H. Müther, and R. Machleidt, *Phys. Lett.* B 459 (1999) 1

[187] M. Baldo, J. Cugnon, A. Lejeune, and U. Lombardo, *Nucl. Phys.* A 515 (1990) 409

[188] Ø. Elgaroy and M. Hjorth-Jensen, *Phys. Rev.* C 57 (1998) 1174

[189] B.E. Vonderfecht, W.H. Dickhoff, A. Polls, and A. Ramos, *Nucl. Phys.* A 555 (1993) 1

[190] A. Schnell, G. Röpke, and P. Schuck, *Phys. Rev. Lett.* 83 (1999) 1926

[191] S. Stringari, M. Traini, and O. Bohigas, *Nucl. Phys.* A 516 (1990) 33

[192] D. van Neck, L. Dieperink, and E. Moya de Guerra, *Phys. Rev.* C 51 (1995) 1800

[193] O. Benhar, A. Fabrocini, S. Fantoni, and I. Sick, *Nucl. Phys.* A 579 (1994) 493

[194] H. Müther, G. Knehr, and A. Polls, *Phys. Rev.* C 52 (1995) 2955

[195] B.R. Barrett, R.G.L. Hewitt, and R.J. McCarthy, *Phys. Rev.* C 3 (1971) 1137

[196] E.W. Krenciglowa, C.L. Kung, T.T.S. Kuo, and E. Osnes, *Ann. Phys. (N.Y.)* 101 (1976) 154

[197] J.G. Zabolitzky, *Phys. Lett.* B 47 (1973) 487

[198] K.W. Schmid, H. Müther, and R. Machleidt, *Nucl. Phys.* A 530 (14) 1991

[199] D.C. Zheng, B.R. Barrett, J.P. Vary, W.C. Haxton, and C.L. Song, *Phys. Rev.* C 52 (1995) 2488

[200] P. Navratil and B.R. Barrett, *Phys. Rev.* C 57 (1998) 3119

[201] E. Heinz, H. Müther, and H.A. Mavromatis, *Nucl. Phys.* A 587 (1995) 77

[202] V. R. Pandharipande, I. Sick, and P. K. A. deWitt Huberts, *Rev. Mod. Phys.* 69 (1997) 981

[203] M. Baldo, I. Bombaci, G. Giansiracusa, U. Lombardo, C. Mahaux, and, R. Sartor, *Nucl. Phys.* A 545 (1992) 741

[204] O. Benhar, A. Fabrocini and S. Fantoni *Nucl. Phys.* A 505 (1989) 267

[205] A. Polls, A. Ramos, J. Ventura, S. Amari, and W.H. Dickhoff, *Phys. Rev.* C 49 (1994) 3050

[206] C.C. Gearhart, W.H. Dickhoff, A. Polls, and A. Ramos, *Int. J. Mod. Phys.* E 5 (1996) 261

[207] P. Bozek, *Phys. Rev.* C 59 (1999) 2619

[208] W.H. Dickhoff, *Phys. Rev.* C 58 (1998) 2807

[209] J. Carlson and R. Schiavilla, *Rev. Mod. Phys.* 70 (1998) 743

[210] M. Borromeo, D. Bonatsos, H. Müther, and A. Polls, *Nucl. Phys.* A 539 (1992) 189

[211] K. Amir Azimi Nili, H. Müther, L.D. Skouras, and A. Polls, *Nucl. Phys.* A 604 (1996) 245

[212] W.J.W. Geurts, K. Allaart, W.H. Dickhoff, and H. Müther, *Phys. Rev.* C 53 (1996) 2207

[213] M. Radici, S. Boffi, S.C. Peiper, and V. R. Pandharipande, *Phys. Rev.* C 50 (1994) 3010

[214] D. Van Neck, M. Waroquier, A.E.L. Dieperink, S.C. Pieper, and V.R. Pandharipande, *Phys. Rev.* C 57 (1998) 2308

[215] A. Polls, H. Müther, and W. H. Dickhoff, *Nucl. Phys.* A 594 (1995) 117

[216] P.-O. Löwdin, *Phys. Rev.* 97 (1955) 1474

[217] M. V. Stoitsov, A.N. Antonov and S.S. Dimitrova, *Phys. Rev.* C 48 (1994) 74

[218] D. Van Neck, M. Waroquier and K. Heyde, *Phys. Lett.* B 314 (1993) 255

[219] S. Boffi, C. Giusti, F.D. Pacati, and M. Radici, *Electromagnetic Response of Atomic Nuclei* (Oxford University Press, Oxford 1996)

[220] M. Leuschner et al., *Phys. Rev.* C 49 (1994) 955

[221] K.I. Blomqvist et al., *Phys. Lett.* B 344 (1995) 85

[222] I. Bobeldijk et al., *Phys. Rev. Lett.* 73 (1994) 2684

[223] K. Amir-Azimi-Nili, J.M. Udias, H. Müther, L.D. Skouras, and A.Polls, *Nucl. Phys.* A 625 (1997) 633

[224] C. Giusti and F. D. Pacati, *Nucl. Phys.* A 535 (1991) 573

[225] J. Ryckebusch, M. Vanderhaeghen, K. Heyde, and M. Waroquier, *Phys. Lett.* B 350 (1995) 1

[226] D. Knödler, H. Müther, and P. Czerski, preprint nucl-th9909051

[227] C. Giusti, H. Müther, F. D. Pacati, and M. Stauf, *Phys. Rev.* C 60 (1999) 054608

[228] G. Rosner, *Proceedings of the 10th Mini-Conference on Studies of Few-Body Systems with High Duty-Factor Electron Beams*, NIKHEF, Amsterdam 1999, in press

[229] J. R. M. Annand, P. Bartsch, D. Baumann, J. Becker, R. Böhm, D. Branford, S. Derber, M. Ding, I. Ewald, K. Föhl, J. Friedrich, J. M. Friedrich, P. Grabmayr (spokesperson), T. Hehl, D. G. Ireland, P. Jennewein, M. Kahrau, D. Knödler, K. W. Krygier, A. Liesenfeld, I. J. D. MacGregor, H. Merkel, K. Merle, P. Merle, U. Müller, H. Müther, A. Natter, R. Neuhausen, Th. Pospischil, G. Rosner (spokesperson), H. Schmieden, A. Wagner, G. J. Wagner, Th. Walcher, M. Weis, S. Wolf, MAMI proposal Nr: A1/5-98.

[230] C. Giusti, F. D. Pacati, K. Allaart, W. J. W. Geurts, W. H. Dickhoff, and H. Müther, *Phys. Rev.* C 57 (1998) 1691

[231] S.E. Koonin, D.J. Dean, and K. Langanke, *Phys. Rep.* 278 (1997) 1

[232] E. Hammaren, K.W. Schmid, and A. Faessler, *Eur. Phys. J. A* 2 (1998) 371

[233] S. Ulrych and H. Müther, *Nucl. Phys.* A 641 (1998) 499

[234] William Bertozzi, Contribution to the Workshop on 'Electromagnetically induced two-hadron emission', Granada 99